Theoretical and experimental analysis of supercritical carbon dioxide cooling

PM Harris

20551843

Dissertation submitted in fulfilment of the requirements for the degree *Magister in Mechanical Engineering* at the Potchefstroom Campus of the North-West University

Supervisor: Dr M van Eldik

Co supervisor Mr W Kaiser

May 2014

It all starts here ™

NORTH-WEST UNIVERSITY
YUNIBESITI YA BOKONE-BOPHIRIMA
NOORDWES-UNIVERSITEIT
®

Acknowledgements

I would like to express special thanks to the following people who played a significant role in the completion of this study over the past two years:

- My supervisor, Dr. Martin van Eldik for his insight, commitment and exceptional leadership in this project.
- My co-supervisor, Mr. Werner Kaiser for his contribution in making project related decisions and giving guidance.
- I would like to thank Dr. Martin van Eldik, the North West University and the NRF for the financial support making it possible to study full-time.
- My parents, Paul and Elize Harris. Thank you for the day-to-day motivation and for believing in me. Your guidance, prayers and wisdom have carried me throughout this study.
- To my wife, Esmé, a special thank you for your unconditional love, support and positivity throughout this study. You made the completion of this study possible.

I am above all grateful to my Heavenly Father, to whom I wish to give praise for the talents, guidance and wisdom that enabled me to complete this study.

Soli Deo Gloria

Abstract

Title: Theoretical and experimental analysis of supercritical carbon dioxide cooling
Author: Paul Marius Harris
Supervisor: Dr. Martin van Eldik
Co-supervisor: Mr. Werner Kaiser
School: School of Mechanical and Nuclear Engineering, North West University
Degree: Magister Engineering (M.Eng)

With on-going developments in the field of trans-critical carbon dioxide (R-744) vapour compression cycles, a need to effectively describe the heat transfer of supercritical carbon dioxide for application in larger diameter tube-in-tube heat exchangers was identified. This study focuses on the in-tube cooling of supercritical carbon dioxide for application in the gas cooler of a trans-critical heat pump.

A literature study has revealed Nusselt number correlations specifically developed for the cooling of supercritical carbon dioxide. These correlations were proven to be accurate only for certain operating conditions and tube geometries. A shortcoming identified in the reviewed literature was a generic heat transfer correlation that can be applied over a wide range of fluid conditions for supercritical carbon dioxide cooling.

The objective of this study was to compare experimental data obtained from a trans-critical heat pump with different Nusselt number correlations available in literature. The experimental tube diameter used for this study (16mm), was considerably larger than the validated tube diameters used by the researchers who developed Nusselt number correlations specifically for the supercritical cooling of carbon dioxide. The experimental Reynolds number (*Re)* ranges (350’000 - 680’000) were very high compared to the studies found in the literature (< 300’000), due to the test section from this study forming part of a complete heat pump cycle.

Experimental results showed that correlations specifically developed for supercritical carbon dioxide cooling generally over-predicts experimental Nusselt numbers (Nu_{exp}) with an average relative error of 62% to 458% and subsequently also over-predicts the convection heat transfer coefficient.

Furthermore, generic heat transfer correlations were compared to the experimental results which over-predicted the Nu_{exp} with an average relative error between 20% and 45% over the entire *Re* number range. More specifically, the correlation by Dittus & Boelter (1985) correlated with an average relative error of 9% for 350’000 < *Re* < 550’000.

From the results of this study it was concluded that cooling heat transfer of supercritical carbon dioxide in larger tube diameters at higher *Re* numbers is more accurately predicted by the generic Dittus & Boelter (1985) and Gnielinski (1975) correlations mainly due to the absence of thermo-physical property ratios as seen in the CO_2-specific correlations.

Keywords: gas cooler, CO2, R-744, trans-critical, heat pump

Uittreksel

Titel:	‘n Teoretiese en eksperimentele analise van die afkoeling van superkritiese koolstofdioksied
Outeur:	Paul Marius Harris
Studieleier:	Dr. Martin van Eldik
Mede studieleier:	Mnr. Werner Kaiser
Skool:	Skool vir Meganiese en Kern Ingenieurswese, Noord-Wes Universiteit
Graad:	Magister in Ingenieurswese (M.Ing)

Met die deurlopende ontwikkelinge wat tans op transkritiese koolstofdioksied (R-744) damp samedrukkingsiklusse plaasvind, is daar ‘n leemte geïdentifiseer om die hitte-oordrag van superkritiese koolstofdioksied te beskryf vir groter diameter, pyp-in-pyp hitteruiler opstellings. Hierdie studie fokus op die binne-buis afkoeling van superkritiese koolstofdioksied vir die toepassing in die gas-verkoeler van ‘n transkritiese koolstofdioksied hittepomp.

‘n Literatuurstudie het aan die lig gebring dat daar talle Nusselt getal korrelasies bestaan wat spesifiek ontwikkel is vir superkritiese afkoeling van koolstof dioksied. Hierdie korrelasies is egter slegs geldig bewys vir sekere vloeikondisies en pyp geometrieë. ‘n Generiese hitte-oordrag korrelasie wat toegepas kan word oor ‘n wye reeks vloeikondisies vir die afkoeling van superkritiese koolstofdioksied, is geïdentifiseer as ‘n tekortkoming in die literatuur.

Die doel van hierdie studie was om eksperimentele data van ‘n transkritiese hittepomp opstelling te vergelyk met verskillende Nusselt korrelasies beskikbaar in die literatuur. Die eksperimentele pyp diameter wat in hierdie studie gebruik is (16mm), was aansienlik groter as dié wat deur ander navorsers gebruik is in die ontwikkeling van Nusselt getal korrelasies spesifiek vir die superkritiese afkoeling van koolstof dioksied. Die eksperimentele Reynolds getalle (*Re*) het wyer gestrek in vergelyking met die studies in die literatuur as gevolg van die toets seksie wat deel uitmaak van ‘n hittepomp siklus.

Eksperimentele resultate het gewys dat die korrelasies wat spesifiek ontwikkel is vir die afkoeling van superkritiese koolstofdioksied daartoe neig om Nusselt getalle te oorvoorspel, met ‘n gemiddelde relatiewe fout van 62% tot 458%. Die hitte-oordragkoëffisiënt is vervolgens ook oorvoorspel.

Verder is daar ook generiese hitte-oordrag korrelasies vergelyk met die eksperimentele resultate. Die generiese korrelasies het die hitte-oordragkoëffisiënte oor-voorspel met ‘n gemiddelde relatiewe fout van 20% tot 45% oor die hele *Re* getal interval. Meer spesifiek korreleer die korrelasie van Dittus & Boelter (1985) met a gemiddelde relatiewe fout van 9% vir 350’000 < *Re* < 550’000.

Vanuit die eindresultate van hierdie studie, kon die afleiding gemaak word dat die afkoeling van superkritiese koolstofdioksied in groter diameter pype en by hoër *Re* getalle, die beste voorspel word deur die generiese

Dittus & Boelter (1985) en die Gnielinski (1975) korrelasies weens die afwesigheid van termo-fiesiese eienskap verhoudings - soos daar gevind word in die korrelasies spesifiek ontwikkel vir CO_2 afkoeling.

Table of Contents

List of Figures

List of Tables

Nomenclature

A	Area	m^2
A_{ff}	Face flow area	m^2
c_p	Specific heat capacity at constant pressure	J/Kg-K
$c_{p,b}$	c_p at the bulk fluid temperature	J/Kg-K
$c_{p,w}$	c_p at the tube wall temperature	J/Kg-K
$\tilde{c}_p$	Integrated specific heat capacity at constant pressure	J/Kg-K
$\bar{c}_p$	Mean specific heat capacity at constant pressure	J/Kg-K
D	Diameter	m
$D_{i,i}$	Inner tube, inside diameter	m
$D_{i,o}$	Inner tube, outside diameter	m
D_H	Hydraulic diameter	m
f	Friction factor	-
f_f	Filonenko friction factor	-
$f_{f,f}$	Filonenko friction factor at the film temperature	-
f_B	Blasius friction factor	-
Gr	Grashof number	-
g	Gravitational acceleration	m/s^2
h	Enthalpy	J/kg
h_i	Enthalpy at the inlet	J/kg
h_e	Enthalpy at the outlet	J/kg
h_c	Convection heat transfer coefficient	W/m^2-
k	Conduction heat transfer coefficient	W/m-K
k_b	Conduction heat transfer coefficient of the bulk fluid	W/m-K
k_w	Conduction heat transfer coefficient at the wall temperature	W/m-K
k_f	Conduction heat transfer coefficient at the film temperature	W/m-K
L	Length	m

$LMTD$	Logarithmic mean temperature difference	K
$\dot{m}$	Mass flow rate	kg/s
$\dot{m}_i$	Mass flow rate at the inlet	kg/s
$\dot{m}_e$	Mass flow rate at the outlet	kg/s
Nu	Nusselt number	-
Nu_{DB}	Nusselt number with the Dittus & Boelter (1985) correlation	-
Nu_G	Nusselt number with the Gnielinski (1975) correlation	-
$Nu_{G,M}$	Nusselt number with the modified Gnielinski (1976) correlation	-
Nu_P	Nusselt number with the Pitla *et.al.* (2002) correlation	-
$Nu_{D\&H}$	Nusselt number with the Dang & Hihara (2004) correlation	-
$Nu_{S\&P}$	Nusselt number with the Son & Park (2006) correlation	-
$Nu_{O\&S}$	Nusselt number with the Oh & Son (2010) correlation	-
Nu_Y	Nusselt number with the Yoon *et.al.* (2003) correlation	-
$Nu_{Z\&J}$	Nusselt number with the Zhao & Jiang (2011) correlation	-
p	Pressure	Pa
p_i	Pressure at the inlet	Pa
p_e	Pressure at the outlet	Pa
Pr	Prandtl number	-
Pr_b	Prandtl number at the bulk fluid temperature	-
Pr_w	Prandtl number at the wall temperature	-
$\dot{Q}$	Heat transfer rate	W
r	Radius	m
$r_{i,i}$	Inner tube, inside radius	m
$r_{i,o}$	Inner tube, outside radius	m
$r_{o,i}$	Outer tube, inside radius	m
Re	Reynolds number	-
Re_b	Reynolds number of the bulk fluid	-
Re_w	Reynolds number at the wall	-

Re_f	Reynolds number at the film temperature	-
t	Time	s
T	Temperature	K
T_b	Bulk fluid temperature	K
T_w	Wall temperature	K
T_f	Film temperature	K
T_{pc}	Pseudo-critical temperature	K
U	Overall heat transfer coefficient	W/m^2-
v	Momentum diffusivity	m^2/s
V	Velocity	m/s
V_b	Bulk fluid velocity	m/s
V_{avg}	Average fluid velocity	m/s
$\forbidden{V}$	Volume	m^3
$\dot{W}$	Rate of work	W
z	Elevation height	m
z_i	Elevation height at the inlet	m
z_e	Elevation height at the outlet	m

Greek symbols

Δp_L	Pressure loss over the entire length	Pa
ΔT	Temperature difference	K
α	Thermal diffusivity	m^2/s
ρ	Density	kg/m^3
ρ_b	Density of the bulk fluid	kg/m^3
ρ_w	Density at the tube wall	kg/m^3
ρ_{pc}	Density at the pseudo-critical point	kg/m^3
σ	Standard deviation	-
μ	Viscosity	Ns/m^2

μ_b	Viscosity of the bulk fluid	Ns/m^2
μ_w	Viscosity at the tube wall	Ns/m^2
μ_f	Viscosity at film temperature	Ns/m^2

Chapter 1 INTRODUCTION

1.1 Background

In the Heating, Ventilation, Air Conditioning and Refrigeration (HVAC&R) industry, working fluids (or refrigerants) are continuously changing due to the ever growing demand of the industry. Over the last decade, the trend in the industry was towards refrigerants that has a low Global Warming Potential (GWP) and are not ozone depleting. Most synthetic refrigerants are fluorine - and/or chlorine based substances that have a negative impact on climate change (Kim *et al.*, 2004). Carbon dioxide gained renewed interest as a refrigerant in recent years. Being a non-toxic, inexpensive, natural gas that has a zero net impact on global warming, it is readily accepted as a good alternative by many governments and environmentalists (Calm, 2008).

Carbon dioxide (CO_2), or R-744 as it is known in the HVAC&R industry, has certain interesting properties that make it very unique among refrigerants. The low critical temperature of 31.1 °C at a high pressure of 7.29MPa poses challenges when used in a vapour compression cycle (Kim *et al.*, 2004). Heat pump cycles using carbon dioxide as refrigerant must operate in a trans-critical fashion to be efficient and competitive (Austin & Sumathy, 2011). Heat rejection cannot take place at supercritical temperatures by condensation and thus a gas cooler, for supercritical cooling, is used to replace the condenser of the traditional cycle. Very high gas temperatures and pressures are typical of trans-critical carbon dioxide heat pump cycles.

In order to successfully design a trans-critical heat pump with carbon dioxide as refrigerant, accurate Nusselt number (*Nu*) correlations describing the heat transfer must be acquired. Recent studies have been conducted to measure experimental *Nu* numbers and compare them with theoretical *Nu* values in order to predict the heat transfer when cooling supercritical carbon dioxide (Cheng *et al.*, 2008). The main shortcomings with these correlations are the narrow operating conditions[1] and geometry to which they can be applied.

[1] Inlet temperature, inlet pressure and mass flux.

These available correlations can be classified into two main geometry classes, namely macro-tubes (D_h > 3mm) and micro-tubes (D_h < 3mm). Table 1 below summarizes the studies done on cooling of supercritical CO_2 for application in a vapour compression cycle. From these studies, there appears to be no generalised correlation for heat transfer when cooling supercritical carbon dioxide. Only six of these studies (Yoon *et al*, 2003, Pitla *et al.*, 2001, Dang & Hihara, 2004, Son & Park 2006, Oh & Son, 2010 and Zhao & Jiang, 2011) considered macro-scale channel geometry for their experiments (Cheng *et al.*, 2008). All six of these researchers came forth with new heat transfer correlations for super critical cooling of carbon dioxide as deliverables from their studies. All of these correlations are based on generic *Nu* correlations which were modified to fit experimental data.

Table 1: A summary of experimental studies done on cooling of supercritical CO_2 (Cheng *et al.*, 2008).

Author	Tube diameter (mm)	Inlet Temperature range (°C)	Inlet Pressure range (MPa)
Yoon *et al. (2003)*	7.73	50-80	7.5-8.8
Pettersen (2000)	0.79	15-70	8.1-10.1
Pitla *et al.* (2001)	4.72	120	8 - 12
Dang & Hihara (2004)	1-6	30-70	8-10
Mori *et al.* (2003)	6	20-70	9.5
Huai *et al.*(2005)	1.31	22-53	7.4-8.5
Son & Park (2006)	7.75	90-100	7.5-10
Dang *et al.* (2007)	1,2,4,6	20-70	8-10
Oh & Son (2010)	4.55, 7.75	90-100	90-100
Zhao & Jiang (2011)	4.01	80-140	4.5-5.5

As seen in Table 1, numerous studies were conducted on cooling of supercritical carbon dioxide, but none of these entail experiments for tube diameters larger than 7.75mm. The existing experimental heat pump test-bench setup at the North-West University (NWU) utilizes tubing with an inner diameter of 16mm in a tube-in-tube heat transfer configuration for the gas cooling process. This tube diameter was chosen to satisfy the design philosophy to construct a heat pump test-bench using standardised construction materials which are commercially available.

The absence of approved *Nu* correlations to describe heat transfer for a system with larger geometry tubing used in the heat transfer process creates a window of opportunity for contribution to the existing field of knowledge by conducting research in this field.

1.2 Problem statement

The main purpose of the proposed research is to compare existing *Nu* correlations for heat transfer against experimental data for the cooling of supercritical carbon dioxide in larger diameter flow channels.

1.3 Research objectives

The main research objectives for this study are:

- To analyse the cooling of supercritical carbon dioxide.

- To apply different *Nu* correlations for heat transfer in an analysis model.
- To upgrade and commission a trans-critical heat pump test bench with R-744 as refrigerant.
- To capture useable data for a spectrum of operating conditions using the experimental trans-critical heat pump.
- To compare theoretical and experimental data at various operating conditions.
- To make relevant conclusions with regards to the usability of existing correlations for cooling of supercritical carbon dioxide.

1.4 Research Methodology

To acquire an in depth understanding of recent development in this field of research, a literature survey was conducted. In this survey, suitable correlations for use on macro-scale flow channels were identified.

An analysis model was set up from fundamental principles[2] to effectively compare the selected *Nu* correlations with experimental *Nu* values.

The software package "Engineering Equation Solver" (EES) was used to program the system in order to verify the chosen correlations.

The experimental test facility was expanded in order to capture useable data. The expansion of the experimental facility comprised of the following:

- Temperature transducers which are directly in contact with the working fluid were installed at frequent intervals on the gas cooler.
- Pressure transducers were installed at frequent intervals over the gas cooler.
- Mass flow meters were installed on both the water and gas side of the concentric tube-in-tube gas cooling heat exchanger.
- A Variable Frequency Drive (VFD) was integrated into the system to vary mass flow through the system by controlling the compressor frequency.
- Data logging equipment was installed to keep record of all the experimental data during tests.

Experimental results were compared with theoretical results by plotting certain parameters against relevant flow conditions.

A conclusion will be drawn with regards to the applicability of the identified correlations used in the analysis model.

1.5 Contribution of this study

The contribution of this study is twofold. Firstly, the broad spectrum impact of contributing to the development of environmentally friendly refrigeration systems, and secondly contributing to the research done

[2] Conservation of mass, energy and momentum.

on trans-critical carbon dioxide systems. Broad spectrum contributions include:

- The favourable environmental impact of the working fluid compared to that of conventional heat pump refrigerants.
- New application areas and opportunities arising from the development of refrigeration systems using carbon dioxide as refrigerant.

Contributing factors within the scope of this heat pump research project includes:

- Ability to accurately describe cooling heat transfer of supercritical carbon dioxide.
- Ability to effectively design a supercritical carbon dioxide gas cooler.

Chapter 2 LITERATURE STUDY

A brief introduction of carbon dioxide as refrigerant was given in Chapter 1. This chapter will focus on:

- The history of carbon dioxide as refrigerant.
- An overview of the unique thermodynamic properties of the supercritical state.
- A review of relevant experimental studies done on carbon dioxide as refrigerant.

2.1 History of CO_2 as refrigerant

The first vapour compression cycle machine was built and patented by Jacob Perkins in 1834. Perkins' design proposed the use of ethyl ether as refrigerant in his vapour compression machine although the first test was done using *caoutchoucine*, an industrial solvent which Perkins had available at his printing business (Pearson, 2005). Many experts in refrigeration refer to vapour compression cycles as the Perkins-cycle due to his landmark contribution in this field of study.

In the years to follow the use of different refrigerants were explored. These refrigerants were chosen on a "what worked" and "what were available" basis. Ethers, carbon dioxide, ammonia, methyl chloride and sulphur dioxide were marked as the main refrigerants of the 19th century (Calm, 2008). All these refrigerants were hazardous to some extent: they were either flammable (various ethers, ammonia, methyl chloride), noxious (sulphur dioxide, ammonia, ethers) or required high pressures (carbon dioxide).

In the late 1800's, carbon dioxide was the most popular refrigerant in the industry. Although higher pressures were difficult to obtain, being a non-toxic and non-flammable alternative made carbon dioxide the preferred choice over dangerous ammonia systems (Pearson, 2005).

With improved manufacturing techniques in the early 1900's, ammonia's safety record began to improve. This allowed the commercialization of ammonia refrigeration systems and consequently the decline and fall of carbon dioxide systems (Pearson, 2005).

Due to the industrial demand for better performing refrigeration systems, General Motors (GM) researched the development of synthetic refrigerants in the late 1920's (Pearson, 2005). The research, led by Thomas Midgeley, was aimed at the development of a stable, non-toxic, non-flammable refrigerant with operating pressure correlating well to that of ammonia. Dichlorodifluoromethane (CCl_2F_2) or more specifically R-12 was produced. In the years to follow other synthetic refrigerants in the chlorofluorocarbon (CFC) and hydro chlorofluorocarbon (HCFC) group were introduced to the market (Pearson, 2005).

In the 1980's, scientists linked ozone depletion and consequent climate change to the use of synthetic refrigerants in the CFC and HCFC group. The extent to which each refrigerant can deplete ozone has been quantified in an Ozone Depleting Potential (ODP) value[3]. The ODP values of a few typical refrigerants are given in Table 2. The acceptance of the Montreal Protocol on Substances That Deplete the Ozone (Montreal Protocol, 1987), has lead the way to decrease the use and phase out CFC's and HCFC's due to their ozone depleting properties (Calm, 2008). The quest to find a refrigerant which is a non-ozone depleting substance gave rise to the development of haloalkane refrigerants such as tetrafluoroethane or more commonly known as R-134a (Pearson, 2005).

Table 2: ODP values of refrigerants (Calm, 2008).

Refrigerant	Ozone Depletion Potential (ODP)
R-12 Dichlorodifluoromethane	1.0
R13 B1 Bromotrifluoromethane	10
R-22 Chlorodifluoromethane	0.05
R-134a Tetrafluoroethane	0
R-744 Carbon Dioxide	0

In recent years research has shown that some non-ozone depleting refrigerants are potent greenhouse gasses (GHG) which can contribute largely to climate change (Calm, 2008). The Kyoto Protocol (1997) sets binding targets on the emission of GHG's based on the equivalent GHG effect of carbon dioxide. Global Warming Potential (GWP) values were introduced to quantify this measure, assigning carbon dioxide a GWP = 1. The phasing out of substances with a high GWP was agreed upon in the Kyoto Protocol. This decision marked the beginning of a decrease in all synthetic refrigerants with high GWP like R-134a (GWP = 1300).

Carbon dioxide, or R-744 as referred to in the refrigeration industry, has received renewed attention as a natural refrigerant with low environmental risks (ODP = 0, GWP = 1). In the section to follow, it will become clear that carbon dioxide is not only a viable and sustainable choice as a refrigerant but also holds promise to revolutionise the heating industry.

2.2 Thermodynamic properties of the supercritical state

Significant property variations are observed when a supercritical fluid approaches the transition temperature.

[3] An ODP value of 1.0 has been assigned to trichlorofluoromethane (R-11) as a reference point.

The transition temperature marks the transition point where a supercritical fluid behaves in a gas-like manner when above this temperature and like a liquid when below this temperature (Andresen, 2006). This transition temperature differs for each pressure line and is referred to as the pseudo-critical (*PC*) temperature (Aldana *et al.*, 2002). Property variations relevant to this study include specific heat capacity at a constant pressure (C_p), density (ρ), viscosity (μ) and thermal conductivity (k). Figure 1 shows these variations graphically. As the pressure approaches the critical pressure of 7.29MPa, the fluid properties becomes more volatile (Andresen, 2006). Due to the high C_p values when the supercritical fluid approaches pseudo-critical temperature, a high convection heat transfer coefficient is achieved. The difference in maximum amplitude between higher and lower pressures also impacts on the heat transfer coefficient as the fluctuations are less severe at higher pressures. The fluctuation of the convection heat transfer coefficient has significant implications when deriving a correlation to predict heat transfer in the supercritical region.

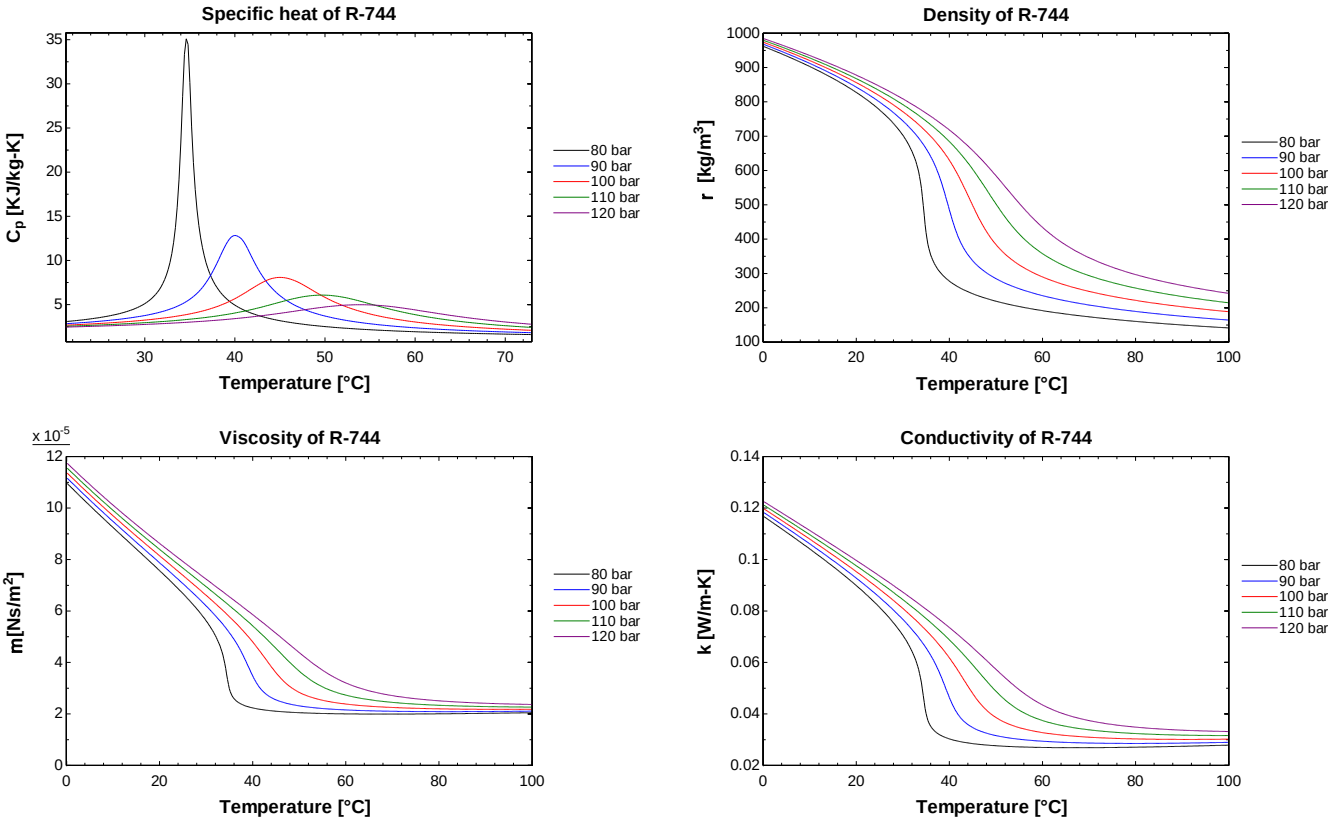

Figure 1: Various properties of R-744 at different pressures plotted against temperature.

2.3 Overview of previous studies

Plenty of researchers have investigated the accuracy of heat transfer correlations for supercritical carbon dioxide in the past century. The first correlation to predict supercritical heat transfer for CO_2 was done by Petukhov *et al.* (1961) and was later modified by Gnielinski in 1976 (Aldana *et al.*, 2002). These correlations did not take thermo-physical property variations into account when calculating *Nu*.

In the supercritical cooling of carbon dioxide, it may happen that the bulk fluid temperature is above the

pseudo-critical point, when the wall temperature is already below this point, due to the temperature gradient in the gas cooler. As shown in Figure 1, vast property variations can take place near the pseudo-critical region. Due to this phenomenon, the under prediction of the heat transfer coefficient was identified as a shortcoming of the constant property correlations (Krasnoshchekov *et al.*, 1970, Hiroaki *et al.*, 1971, Shitsman, 1963). In the cooling process of the fluid, Krasnoshchekov *et al.* (1970) noticed that the thermal conductivity would be higher near the wall, where the wall temperature approaches the pseudo-critical temperature, and the fluid resembles a liquid-like state. If heating takes place, the opposite is also true when a supercritical condition exist near the wall, while the bulk fluid is still below the pseudo-critical point. The gas-like fluid above the pseudo-critical point will have a lower heat transfer coefficient due to the lower thermal conductivity at this condition (Venter, 2010). The dissimilarity of wall and bulk temperatures provoked the need for property corrections to be introduced in heat transfer correlations (Andresen, 2006, Mitra, 2005). This statement will be assessed in this study by also testing correlations at flow conditions where the wall temperatures are closer to bulk temperature due to high turbulence in the system. According to Andresen (2006), in most of the studies done on supercritical heat transfer, emphasis was placed on the heating process where the bulk fluid temperature is below the wall temperature. Andresen (2006) also stated that these heating correlations are insufficient to use when predicting cooling heat transfer of supercritical carbon dioxide.

In the following sections, an overview of recent and relevant studies done on the supercritical cooling of carbon dioxide will be briefly discussed.

2.3.1 Study by Pitla *et.al.* (1998)

In 1998 Pitla *et al.* (1998) conducted a critical review of the heat transfer correlations available at the time. Pitla (1998) distinguished between correlations for heating and cooling purposes. The authors compared existing correlations from Krasnoshchekov *et al.* (1970), Baskov *et al.* (1977), Petrov & Popov (1985) and the text-book Petukhov-Popov-Kirilov (1974) correlation. These correlations were not developed for implementation on carbon dioxide as a refrigerant. Consequently these studies were focussed on heating applications rather than cooling (Pitla *et al.*, 1998). From these available correlations Pitla *et al.* (1998) observed the large impact of fluid temperature on the heat transfer coefficient. Pitla *et al.* (1998) concluded that the heat transfer correlations available at the time were inconsistent and that further accurate experimental studies are needed. It was also noted that the effect of turbulence on the heat transfer coefficient is not fully understood.

In 2002 Pitla *et al.* (2002) conducted an experimental study for supercritical cooling of carbon dioxide. The fluid was cooled in 4.72mm inner diameter tubes from 120°C to 25°C with pressures ranging from 8MPa to 12MPa. Reynolds (*Re*) numbers ranged from 95’000 < *Re* < 415’000. The authors published a newly developed heat transfer correlation for the supercritical cooling of carbon dioxide (Pitla *et al.*, 2002). Experimental data were captured and analysed in a numerical model to develop a new correlation. This correlation is based on a corrected mean Nusselt (*Nu*) number as evaluated at the wall and in the centre of the tube where the *Nu* numbers were calculated with the Gnielinski (1975) correlation. The newly developed

correlation was claimed to predict *Nu* accurately with less than 20% deviation from the experimental data for up to 85% of the collected data.

2.3.2 Study by Yoon *et al.* (2003)

Yoon *et al.* (2003) reported experimental data of in-tube cooling of supercritical carbon dioxide. The heat transfer and pressure drop characteristics were measured in tubes with an inner diameter of 7.73mm, while mass flux was controlled and the inlet pressures varied from 7.5MPa to 8.8MPa. Inlet temperature of carbon dioxide ranged from 50°C to 80°C and *Re* ranged from 60'000 < *Re* < 170'000. Yoon *et al.* (2003) compared the experimental data obtained in their experiments to the correlations of Krasnoshchekov *et al.* (1970), Baskov *et al.* (1977), Petrov & Popov (1985) and Pitla *et al.* (1998). Due to the variations found between existing correlations and experimental data, the authors of this article also proposed a new heat transfer correlation based on the Dittus & Boelter (1985) equation, by taking thermo-physical property variations into account. Yoon *et al.* (2003) made the following conclusions:

- In the supercritical gas cooling process, heat transfer reaches a maximum value and then decreases as the gas temperature falls below the pseudo-critical temperature.
- At higher pressures, the maximum value of the heat transfer coefficient decreases. This stands in agreement with the specific heat's maximum value as illustrated in Figure 1.
- The increase in mass flux resulted in an increased heat transfer coefficient for all pressures.
- The pressure drop measured correlated well with the Blasius correlation for pressure drop with a root mean square (RMS) deviation of 5.9%. This correlation was recommended for further use by the authors.
- Existing correlations for the supercritical region generally under predicts the heat transfer coefficients.
- The newly proposed correlation has an absolute average deviation of 12.7% when compared to the experimental data.

2.3.3 Study by Dang & Hihara (2004)

Dang & Hihara (2004) investigated the heat transfer of supercritical cooling of carbon dioxide in circular tubes. These researchers focussed on the effect of mass flux, inlet pressure and heat flux on heat transfer coefficients. In the experimental setup, they measured fluid conditions in four horizontal cooling tubes with diameters ranging from 1mm to 6mm (Dang & Hihara, 2004). The fluid was cooled from 70°C to 30°C with gas pressures ranging from 8MPa to 10MPa. The *Re* numbers ranged from 4000 < Re < 80'000. The authors compared the captured experimental data with the proposed correlations of Gnielinski (1975), Petrov & Popov (1985), Pitla *et al.* (1998), Liao & Zhao (2002) and Yoon *et al.* (2003). According to Dang & Hihara (2004), the following conclusions were made:

- Heat transfer coefficient increase is proportional to mass flux increase.
- The effect of pressure on the heat transfer coefficient depends on property variations in the flow direction.

- The effect of heat flux and tube diameter on heat transfer coefficient depends on the property variations in the radial direction.
- Pressure drop increases with increase in mass flux.
- In the supercritical state pressure drop decreases with increase in inlet pressure.

From the comparison between experimental data and predicted values, the authors proposed a modification of the Gnielinski (1975) correlation for further use in predicting heat transfer coefficients. This newly developed correlation takes variations in thermo-physical properties into account (Dang & Hihara, 2004). The authors claimed their correlation to predict *Nu* numbers accurately with less than 20% deviation from experimental data.

2.3.4 Study by Son & Park (2006)

Heat transfer and pressure drop were investigated by means of an experimental apparatus by Son & Park (2006). In the experimental setup, supercritical carbon dioxide was cooled in a stainless steel tube-in-tube heat exchanger with inner diameter of 7.75mm. Supercritical carbon dioxide was cooled from 100°C to approximately 25°C with gas pressure ranging from 7.5MPa to 10.0MPa. The *Re* numbers ranged from 50’000 < Re < 150’000. The findings of the article published by the authors can be summarized as follows:

- Due to the maximum value of specific heat near the pseudo-critical temperature, the heat transfer coefficient reaches a maximum value as this temperature is approached. This maximum value exist somewhere in the middle of the gas cooler.
- Ascribed to the density variations of the supercritical fluid, pressure drop during the cooling process decreases when inlet pressure is increased. The Blasius correlation predicts this fairly accurate and was chosen as the preferred pressure drop correlation.
- Experimental data were compared with the correlations of Baskov *et al.* (1977), Bringer & Smith (1957), Ghajar & Asadi (1986), Gnielinski (1975), Krasnoshchekov *et al.* (1970), Krasnoshcekov & Protopopov (1966), Petrov & Popov (1985), Petukhov *et al.* (1961) and Pitla *et al.* (1998). It was reported that the Bringer & Smith (1957) correlation showed the best agreement to experimental data with a mean deviation of 23.6% compared to the experimental data. The correlation by Pitla *et al.* (2002) had a mean deviation of 36.4%.

Based on the Dittus & Boelter (1985) correlation, Son & Park (2006) proposed a newly developed correlation which was claimed to be more accurate than any other correlation used in the study with a mean deviation of 17.62% with regards to the experimental data. This correlation takes the density and specific heat ratio determined at wall and mean bulk temperature into account.

2.3.5 Study by Zhao & Jiang (2011)

A comprehensive study on supercritical cooling of carbon dioxide was done by Chinese researchers Zhao & Jiang (2011). Stainless steel tubes with an inner diameter of 4.01mm were used in their experimental setup. Inlet temperatures varied from 80°C to 140°C with pressures ranging from 4.5MPa to 5.5MPa. The *Re*

numbers ranged from 4000 < Re < 80’000. Experimental test results were compared to the correlations developed by Gnielinski (1975), Pitla *et al.* (1998), Yoon *et al.* (2003) and Dang & Hihara (2004). It was reported by the authors that the correlation of Yoon *et al.* (2003) generally over predicts heat transfer as opposed to the correlation by Pitla *et al.* (1998) that generally under predicts the experimental data when the bulk fluid temperature is in the vicinity of the pseudo-critical temperature. It was further reported that the Gnielinski (1975) correlation slightly under predicts experimental data where the Pitla *et al.* (1998) correlation and Dang & Hihara (2004) correlation slightly over predicts heat transfer when the bulk fluid temperature is above the pseudo-critical point. According to the authors, over corrected thermo-physical property variations explains the deviations between measured data and estimated values from previous correlations.

Zhao & Jiang (2011) concluded the following:

- At supercritical pressures the heat transfer coefficient reaches a maximum when the pseudo-critical temperature is approached.
- The heat transfer coefficient will increase with the increase of mass flux.
- When the bulk temperature is well below the pseudo-critical point, pressure has an insignificant effect on the heat transfer coefficient. However, with the bulk temperature above the pseudo-critical point, heat transfer is affected with change in pressure.
- The Gnielinski (1975) correlation most accurately predicts heat transfer amongst the chosen correlations of previous studies deviating less than 25% from the experimental data.
- The Petrov & Popov (1985) correlation for frictional pressure drop correlated the best with the pressure drop measurements.

Zhao & Jiang (2011) proposed a newly developed correlation based on the modified Gnielinski (1975) correlation. The authors claim that the newly developed correlation predicts *Nu* numbers accurately within 15% of the experimental data for 90% of the collected data.

2.3.6 Study by Oh & Son (2010)

The in-tube cooling of supercritical carbon dioxide was experimentally investigated by Oh & Son (2010). Carbon dioxide was cooled at supercritical pressures in tubes with inner diameters of 4.55mm and 7.75mm. Inlet temperatures ranged from 90°C to 100°C with pressures ranging from 7.5MPa to 10.0MPa. The *Re* numbers ranged from 40’000 < *Re* < 210’000. Oh & Son (2010) focussed their study on the effect that gas pressure, tube diameter, mass flux and fluid temperature have on the heat transfer coefficient.

Test results were compared with the correlations from Petuhkov *et al.* (1961), Krasnoshchekov & Protopopov (1966), Baskov *et al.* (1977), Petrov & Popov (1985), Ghajar & Asadi (1986), Gnielinski (1975), Pitla *et al.* (1998), Fang *et al.* (2001) and Yoon *et al.* (2003).

Conclusions made from this study entail the following:

- The heat transfer coefficient decreases with an increase in gas pressure.

- The heat transfer coefficient would increase with an increase in mass flux. These two findings stand in agreement with the study of Yoon *et al.* (2003).
- An increase of 8% to 35.6% in heat transfer coefficient was measured in the smaller tube diameter as opposed to the larger tube diameter.
- The comparison of experimental data with predictions from existing correlations, showed significant deviations. The authors argued that existing correlations might not be valid for predicting cooling heat transfer in larger, macro scale tube diameters.

Density ratio (to account for the effect of density gradient and buoyancy) as well as specific heat ratio (representing the variations of specific heat in the cross section of the tube) was brought into consideration in developing the new correlation. A study by Du *et.al.* (2010) also analysed the effect of buoyancy forces in supercritical carbon dioxide. The authors came to the conclusion that free convection is the dominant heat transfer mechanism. This observation was based on the statement that free convection is dominant when $Re/Gr^2 > 0.01$. There was no reference made by the authors to verify this value. However numerous other sources (Cheng *et al*, 1994; Incropera *et al.*, 2011 & Jing *et al.*, 2012) indicated that the Re/Gr^2 relation should in fact be larger than 0.1 when considering free convection as noteworthy a heat transfer mechanism.

A newly developed correlation based on the Dittus & Boelter (1985) equation was proposed by Oh & Son (2010). This correlation predicted experimental data with a mean deviation of 14.1%.

2.3.7 Summary

In the studies reviewed, some strong agreements came forth. The following summary can be made when considering the facts stated in the literature:

- The heat transfer coefficient will reach a maximum value when the gas temperature approaches the pseudo-critical point.
- The heat transfer coefficient will decrease with an increase in pressure.
- An increase in mass flux leads to an increase in heat transfer.
- Thermo-physical property variations around the pseudo-critical region remain a challenge in the development of heat transfer correlations.
- Correlations developed for a specific tube diameter may not be accurate for other diameters.
- All of the proposed correlations were modifications of either the Dittus & Boelter (1985) correlation, or the Gnielinski (1975) correlation.
- Fair agreement amongst researchers exists that the Blasius correlation predicts pressure drop of supercritical carbon dioxide with sufficient accuracy.

For this study an inner tube diameter of 16mm was investigated. Although the fluid conditions tested by the authors of above articles differ quite significantly from the tube diameters used in the current study, the findings of these researchers give a baseline of data to work from. The findings of Oh & Son (2010), Yoon *et al* (2003) and Son & Park (2006) are particularly relevant to this study due to the larger tube diameters

(>7.7mm) used in their experimental tests.

The following chapter focuses on the relevant theoretical background to fully comprehend this study. Selected correlations as identified in the literature will also be discussed in detail.

Chapter 3 THEORETICAL BACKGROUND

This chapter presents an overview of the theory that is required to accurately simulate the heat transfer process between the supercritical carbon dioxide and water. The conservation laws, concepts used in heat transfer analysis and different Nusselt number correlations as identified in Chapter 2 will be discussed. Furthermore, theoretical background regarding uncertainty propagation analysis and non-linear regression are shown.

The theory discussed in sections 3.1 and 3.2 is based on the work of Rousseau (2011), Incropera *et al.* (2011), Van Wylen & Sonntag (2003) and Munson *et al.* (1999).

3.1 Conservation laws

The conservation laws of physics serve as the basis on which modern science is built. All the thermal fluid equations used in this field of study is governed by these basic conservation laws. It is therefore relevant to review the foundations on which the concepts that follow later in this chapter are built upon.

3.1.1 Conservation of mass

The differential form of the conservation of mass for a fluid in a control volume is given by:

$$\forall \frac{\partial \rho}{\partial t} + \dot{m}_e + \dot{m}_i = 0 \qquad (3.1)$$

where $\forall$ denotes the volume, ρ the density, t the time and $\dot{m}$ the mass flow rate[4].

If a steady state condition is assumed, the first term reduces to zero, and the equation simplifies to the following:

$$\dot{m} = \dot{m}_e = \dot{m}_i \qquad (3.2)$$

[4] For this study subscripts "i" and "e" refers to the inlet and outlet conditions. Refer to $\dot{m}_i$ and $\dot{m}_e$ in eq (3.2).

In the analysis model developed for this study, conservation of mass is applied in the form of equation (3.2).

3.1.2 Conservation of energy

The differential form of the conservation of energy equation for a finite control volume is given by:

$$\dot{Q} + \dot{W} = \forall \frac{\partial}{\partial t}(\rho h_0 - p) + \dot{m}_e h_{0e} - \dot{m}_i h_{0i} + \dot{m}_e g z_e + \dot{m}_i g z_i \qquad (3.3)$$

where $\dot{Q}$ denotes the heat transfer rate to the fluid, $\dot{W}$ the rate of work done on the fluid and h_0 the total enthalpy of the fluid.

For horizontal flow under steady state conditions, no work is performed on the liquid, the change in elevation is zero and $\frac{\partial}{\partial t}(\rho h - p) = 0$.

The use of total enthalpy may also be reduced to static enthalpy as $h_0 = h + \frac{1}{2}V^2$ and $(V_e^2 - V_i^2)$ may be assumed to stay constant over a small enough control volume, and with no work done on the fluid simplifying equation (3.3) to the following:

$$\dot{Q} = \dot{m}(h_e - h_i) \qquad (3.4)$$

where *h* is the static enthalpy at the evaluated point in the control volume.

3.2 Thermal fluid concepts

This section discusses some basic thermal flow concepts frequently used when setting up a thermal fluid model.

3.2.1 Mass flow rate

The following equation is used in the generic form to calculate mass flow:

$$\dot{m} = \rho V A_{ff} \qquad (3.5)$$

where A_{ff} denotes the free flow area or the cross sectional area perpendicular to the flow. For this study heat transfer is obtained through a cylindrical tube-in-tube heat exchange configuration. For this configuration there are two areas to be calculated namely: the cross sectional area of the inner tube and that of the annulus between the inner and the outer tube. For the inner tube the following equation is valid:

$$A_{ff} = \pi r_{i,i}^2 \qquad (3.6)$$

where $r_{i,i}$ denotes the inner radius of the inner tube.

For the annular area it is written as:

$$A_{ff} = \pi\left(r_{o,i}^2 - r_{i,o}^2\right) \qquad (3.7)$$

where $r_{o,i}$ denotes the inner radius of the outer tube and $r_{i,o}$ is the outer radius of the inner tube.

3.2.2 Heat transfer

Heat transfer is thermal energy in transit due to spatial temperature difference (Incropera *et al.*, 2011). Heat transfer can take place by three different processes namely conduction, convection or radiation. In this study the radiation heat transfer is of negligible importance and thus focus is placed on conduction and convection.

When thermal energy is transferred from or to a fluid, the rate of heat transfer can be calculated by equation (3.4) by evaluating the enthalpy change between the inlet and the outlet. This method is only applied when evaluating one single fluid at two conditions. To understand the heat transfer between two fluids in a tube-in-tube configuration conduction and convection must be calculated.

Conduction heat transfer

In a tube-in-tube configuration conduction takes place through the wall of the inner tube. For a radial system the following equation may be used:

$$\dot{Q} = 2\pi Lk \frac{\Delta T}{\ln\left(D_{i,o} / D_{i,i}\right)} \tag{3.8}$$

where k denotes the conduction heat transfer coefficient of the associated wall material.

Convection heat transfer

Convection takes place between the wall and the fluid. The following equation is used when calculating convective heat transfer in a tube:

$$\dot{Q} = \pi DLh_c \Delta T \tag{3.9}$$

where h_c denotes the convection heat transfer coefficient and ΔT the temperature difference between the wall and the mean bulk fluid temperature.

The value of k is obtained from the associated materials property table as a function of temperature. The convection heat transfer coefficient (h_c) is not so easily obtained. h_c is a function of the Nusselt (Nu) number which in turn is a function of the non-dimensional Reynolds (Re) and Prandtl (Pr) numbers. These non-dimensional parameters are functions of other thermo-physical properties such as velocity, temperature, pressure, density, viscosity, the flow channel geometry and orientation. The correlations for Nu numbers (section 3.3) will relate all these properties to predict the value for h_c.

3.2.3 Non-dimensional parameters

In the field of fluid mechanics it is common to employ dimensionless parameters to describe convective heat transfer. These parameters typically are ratios of mechanisms used to describe convective heat transfer.

This section discusses the three non-dimensional parameters needed to calculate the heat transfer coefficient.

Prandtl number

The Prandtl (Pr) number can be defined as the ratio of the ability to transport momentum versus the ability to

transport energy through diffusion in the velocity and thermal boundary layers respectively (Rousseau, 2011). This ratio is defined by:

$$Pr = \frac{c_p \mu}{k} = \frac{\nu}{\alpha} \tag{3.10}$$

where c_p denotes the specific heat capacity at constant pressure and μ the viscosity.

The ratio which the Prandtl number represents can be explained by the second part of equation (3.10) by:

$$\nu = \frac{\mu}{\rho} \tag{3.11}$$

and

$$\alpha = \frac{k}{\rho c_p} \tag{3.12}$$

where ν denotes the momentum diffusivity and α the thermal diffusivity.

Reynolds number

The Reynolds number (*Re)* represents the ratio of inertia forces to viscous forces in the velocity boundary layer (Incropera *et al.*, 2011). This ratio also defines the flow regime present like laminar flow at low *Re* with dominant viscous forces *vs.* turbulent flow at high *Re* where inertial forces are dominant. For internal flow the *Re* number is defined by:

$$Re = \frac{\rho V_b D_H}{\mu} \tag{3.13}$$

where V_b denotes the bulk fluid velocity and D_H the hydraulic diameter of the flow channel.

Furthermore it is important to note that the product of the Reynolds and Prandtl numbers shows the relative importance of thermal energy transport through the mechanism of diffusion versus convection. If *RePr* is a large value, convection plays a larger role in thermal energy transport in the thermal boundary layer of the fluid and vice versa (Rousseau, 2011). For this study it is relevant to explain the meaning of this value due to its occurrence in most of the *Nu* correlations discussed in section 3.3.

Grashof number

The Grashof number (*Gr)*, provides a measure of the ratio of buoyancy forces to viscous forces acting on the fluid. It plays the same role in free convection that the *Re* number plays in forced convection (Incropera *et.al*, 2011). The *Gr* number can be calculated as follows:

$$Gr = \frac{g\beta(T_s - T_b)D^3}{\nu^2} \tag{3.14}$$

where g denotes the local acceleration due to gravity, β the volumetric thermal expansion coefficient, T_s the

surface temperature, T_∞ the bulk fluid temperature, *D* the tube diameter and *v* the kinematic viscosity of the fluid.

Nusselt number

The *Nu* number (*Nu)* is a non-dimensional parameter that provides a measure of the convective heat transfer occurring at the surface. For flow within a tube the *Nu* value can be calculated by:

$$Nu = \frac{h_c D_H}{k_b} \tag{3.15}$$

For laminar flow the *Nu* number is a constant value which is defined for each fluid under heating or cooling conditions respectively. For turbulent flow however it varies. It was mentioned in section 3.2.2 that h_c is a function of *Nu*. It is therefore necessary to obtain an equation without h_c as an input parameter to solve the *Nu* number. This equation must be a function of available fluid properties to solve. From the previous section it is not surprising to see that $Nu = f(x^*, Re_L, Pr)$ where *x** represents a spatial variable. This function is known as a Nusselt correlation and is discussed in more detail in section 3.3.

In order to present experimental results from various flow conditions in a thoughtful way, non-dimensional parameters can also be put to good use. A dimensionless parameter may be used as a dependent variable (such as *Re* and *Pr*) to compare an independent variable (such as *Nu*) from various experimental tests over a wide range of test conditions.

3.3 Nusselt number correlations

For this study heat transfer must be calculated for both the water and the supercritical carbon dioxide sides of the heat exchanger. This allows the verification of results from an energy balance perspective. The well-known Dittus & Boelter *Nu* number correlation will be used on the water side. For the gas side several correlations (including the Dittus & Boelter correlation) will be evaluated against the experimental data. In this section these correlations are discussed.

3.3.1 The correlation by Dittus & Boelter (1985)

The Dittus & Boelter (1985) correlation is very suitable to use with water as fluid, although it can also be applied to various gasses with great accuracy. The correlation[5] is defined by:

$$Nu_{DB} = 0.023 Re_b^{0.8} Pr_b^n \tag{3.16}$$

$$n = \begin{cases} 0.4 \text{ if } \frac{T_w}{T_b} > 1 \\ 0.3 \text{ if } \frac{T_w}{T_b} < 1 \end{cases}$$

[5] For this study subscripts “b” refers to the property of the bulk fluid and subscript “w” refers to the property evaluated at the wall.

This correlation has been confirmed experimentally for the following range of conditions:

$$\begin{bmatrix} 0.6 \le \mathrm{Pr} \le 160 \\ \mathrm{Re} \ge 10000 \\ \frac{L}{D} \ge 10 \end{bmatrix}$$

3.3.2 The correlations by Gnielinski (1975)

Gnielinski developed a *Nu* correlation to predict the supercritical heat transfer of carbon dioxide. The correlation is defined by:

$$Nu_G = \frac{f_f}{8}\left(Re_b - 1000\right)Pr_b\left[1.07 + 12.7\sqrt{\frac{f_f}{8}}\left(Pr_b^{2/3} - 1\right)\right]^{-1} \qquad (3.17)$$

Gnielinski modified the above equation in order to achieve greater accuracy and published the following correlation a year later:

$$Nu_{G,M} = \frac{\frac{f_f}{8}\left(Re_b - 1000\right)Pr_b}{1.07 + 12.7\sqrt{\frac{f_f}{8}}\left(Pr_b^{2/3} - 1\right)}\left[1 + \left(\frac{D_H}{L}\right)^{2/3}\right] \qquad (3.18)$$

where f_f denotes the Filonenko friction factor defined by:

$$f_f = \left(1.82\log Re_b - 1.64\right)^{-2} \qquad (3.19)$$

This correlation has been confirmed experimentally for the following range of conditions:

$$\begin{bmatrix} 0.5 \le \mathrm{Pr} \le 2000 \\ 3000 \le \mathrm{Re} \le 5\times10^6 \end{bmatrix}$$

Although neither the Dittus & Boelter (1985) correlation nor the Gnielinski (1975) correlations were developed for predicting cooling of supercritical carbon dioxide, they serve as the foundation for most of the newly developed correlations. In the following sections (3.3.3 - 3.3.7) the correlations developed in more recent years are discussed.

3.3.3 The correlation by Pitla *et al.* (2002)

The correlation by Pitla *et al.* is based on a mean Nu_P number and is defined by:

$$Nu_P = \left(\frac{Nu_w + Nu_b}{2}\right)\frac{k_w}{k_b} \qquad (3.20)$$

where Nu_w and Nu_b are Nusselt numbers calculated with the Gnielinski (1975) correlation (3.17) using thermo-physical properties evaluated at the bulk temperature and wall temperature respectively.

In the calculation of the Reynolds number, Pitla *et al.*(2002) used the inlet velocity of the test section to calculate the Nu_w and used the mean velocity (3.21) of each increment to calculate Nu_b:

$$V_{avg} = \frac{\dot{m}}{A\rho_b} \tag{3.21}$$

3.3.4 The correlation by Yoon *et al.* (2003)

The equation developed by Yoon *et al.* (2003) is based on the Dittus & Boelter (1985) equation. Yoon *et al.* (2003) accounted for a variance in the density ratio between bulk and pseudo-critical temperatures. The correlation is defined by:

$$Nu_Y = 0.14 Re_b^{0.69} Pr_b^{0.66} \tag{3.22}$$

if $T_b > T_{pc}$

and

$$Nu_Y = 0.013 Re_b Pr_b^{-0.05} \left(\frac{\rho_{pc}}{\rho_b} \right)^{1.6} \tag{3.23}$$

if $T_b \le T_{pc}$

where T_{pc} denotes the pseudo-critical[6] temperature and ρ_{pc} the density at the pseudo-critical temperature.

3.3.5 The correlation by Dang & Hihara (2004)

The correlation developed by Dang & Hihara (2004) is based on the Gnielinski (1975) correlation. Dang & Hihara (2004) took into account the property variations as evaluated at the bulk, film and wall temperatures. This correlation is defined by:

$$Nu_{D\&H} = \frac{f_{f,f}}{8}\left(Re_b - 1000\right) Pr \left[1.07 + 12.7 \sqrt{\frac{f_{f,f}}{8}} \left(Pr^{2/3} - 1 \right) \right]^{-1} \tag{3.24}$$

$$Pr = \begin{cases} c_{p_b}\mu_b / k_b, & \text{for } c_{p_b} > \tilde{c}_p \\ \tilde{c}_p \mu_b / k_b, & \text{for } c_{p_b} < \tilde{c}_p \text{ and } \mu_b/\mathrm{k}_b \ge \mu_f/\mathrm{k}_f \\ \tilde{c}_p \mu_f / k_f, & \text{for } c_{p_b} < \tilde{c}_p \text{ and } \mu_b/\mathrm{k}_b < \mu_f/\mathrm{k}_f \end{cases}$$

$$\tilde{c}_p = \left(h_b - h_w\right) / \left(T_b - T_w\right)$$

$$f_{f,f} = \left(1.82 \log Re_f - 1.64\right)^{-2}$$

$$\tilde{c}_p = \left(h_b - h_w\right) / \left(T_b - T_w\right) \tag{3.25}$$

$$f_{f,f} = \left(1.82 \log Re_f - 1.64\right)^{-2} \tag{3.26}$$

[6] For this study the subscript "pc" refers to the property evaluated at the pseudo-critical temperature.

where $\tilde{c}_p$ denotes an integrated specific heat in the radial direction and $f_{f,f}$ the Filonenko friction factor evaluated at the film[7] temperature (T_f) which is calculated by:

$$T_f = \frac{(T_b + T_w)}{2} \tag{3.27}$$

3.3.6 The correlation by Son & Park (2006)

The correlation developed by Son & Park is based on the correlation by Dittus & Boelter. Modifications were made to account for a variance in specific heat ratio and the density ratio evaluated at the bulk and wall temperatures respectively. This correlation is defined by:

$$Nu_{S\&P} = Re_b^{0.55} Pr_b^{0.23} \left(\frac{c_{p_b}}{c_{p_w}} \right)^{0.15} \quad \text{for } \frac{T_b}{T_{pc}} > 1 \tag{3.28}$$

and

$$Nu_{S\&P} = Re_b^{0.35} Pr_b^{1.9} \left(\frac{\rho_b}{\rho_w} \right)^{-1.6} \left(\frac{c_{p_b}}{c_{p_w}} \right)^{-3.4} \quad \text{for } \frac{T_b}{T_{pc}} \leq 1 \tag{3.29}$$

3.3.7 The correlation by Oh & Son (2010)

The correlation developed by Oh & Son (2010) is in the form of the Dittus & Boelter (1985) correlation (3.16). This correlation takes into account the effect of density gradient as well as the effect of variable specific heat along the radial direction within the tube. The correlation is defined by:

$$\begin{aligned} Nu_{O\&S} &= 0.023 Re_b^{0.7} Pr_b^{2.5} \left(\frac{c_{p_b}}{c_{p_w}} \right)^{-3.5} \quad \text{for } \frac{T_b}{T_{pc}} > 1 \\ Nu_{O\&S} &= 0.023 Re_b^{0.6} Pr_b^{3.2} \left(\frac{\rho_b}{\rho_w} \right)^{3.7} \left(\frac{c_{p_b}}{c_{p_w}} \right)^{-4.6} \quad \text{for } \frac{T_b}{T_{pc}} \leq 1 \end{aligned} \tag{3.30}$$

$$Nu_{O\&S} = 0.023 Re_b^{0.6} Pr_b^{3.2} \left(\frac{\rho_b}{\rho_w} \right)^{3.7} \left(\frac{c_{p_b}}{c_{p_w}} \right)^{-4.6} \quad \text{for } \frac{T_b}{T_{pc}} \leq 1 \tag{3.31}$$

3.3.8 The correlation by Zhao & Jiang (2011)

Zhao & Jiang (2011) introduced a correlation based on the modified Gnielinski (1975) correlation (3.18). Zhao & Jiang (2011) accounted for the variance in specific heat ratio evaluated at the bulk fluid temperature at a specific point versus the average specific heat of the entire test section. This correlation also accounts for variance of properties in the radial direction by evaluating wall and bulk fluid temperatures respectively. The correlation is defined by:

[7] For this study the subscript "f" refers to the property evaluated at the average film temperature of the thermal boundary layer.

$$Nu_{Z\&J} = \frac{\frac{f_f}{8}\left(Re_b - 1000\right)Pr_b}{1.07 + 12.7\sqrt{\frac{f_f}{8}}\left(Pr_b^{2/3} - 1\right)}\left[1 + \left(\frac{D_H}{L}\right)^{2/3}\right]C_{vp} \qquad (3.32)$$

with

$$C_{vp} = \begin{cases} 0.93\left(\frac{Pr_w}{Pr_b}\right)^{-0.11}\left(\frac{\bar{c}_p}{c_{p_b}}\right)^{0.96}\left(\frac{\rho_w}{\rho_b}\right)^{1.06} & \text{for } \frac{T_b}{T_{pc}} \le 1 \\ 1.07\left(\frac{T_w}{T_b}\right)^{-0.45}\left(\frac{\bar{c}_p}{c_{p_b}}\right)^{0.61}\left(\frac{\rho_w}{\rho_b}\right)^{-0.18} & \text{for } \frac{T_b}{T_{pc}} > 1 \end{cases}$$

$$\bar{c}_p = \frac{h_i - h_e}{T_i - T_e}$$

where C_{vp} denotes the property variation coefficient and $\bar{c}_p$ the mean value of specific heat calculated over the entire length of the test section.

3.4 Uncertainty analysis[8]

Any experimental measurement of a variable contains inaccuracies. There is no such thing as a perfect measurement. In an experimental analysis it is therefore necessary to quantify the uncertainties of the measured values and, consequently, their effect on further calculations.

3.4.1 Total standard uncertainties

Total experimental uncertainty can consist of several components of uncertainty originating from different mechanisms in the data capturing procedure. These components may include uncertainties due to instrument uncertainty, instrument drift over time, statistical uncertainty and uncertainty due to scattered data when applying a regression model to data. When experimental uncertainty propagation is analysed, it is important to combine all experimental uncertainties into one value of total experimental uncertainty as seen in equation (3.33).

$$u_{total}(y_i) = \sqrt{(u_{stat}(y_i))^2 + (u_{instr}(y_i))^2 + (u_{drift}(y_i))^2} \qquad (3.33)$$

where $u_{stat}(y_i)$ denotes the statistical uncertainty of the *i*-th measurement , $u_{instr}(y_i)$ denotes the instrument uncertainty of the *i*-th measurement and $u_{drift}(y_i)$ denotes the uncertainty associated with the difference in calibration values before and after data were collected.

[8] Uncertainty concepts used in this study are based on the work of Coleman & Steele (2009) and Rousseau *et.al.* (2012).

The standard statistical uncertainty of measured data is equivalent to the standard deviation and is calculated by:

$$u_{stat}(y_i) = \sqrt{\frac{1}{N}\sum_{i=1}^{N}\left(x_i - \bar{x}\right)^2} \tag{3.34}$$

For calculation of instrument uncertainty $(u_{instr}(y_i))$, it is assumed that the distribution form of errors is rectangular (Coleman & Steele, 2009) . This means that an equal probability exists for a measurement to be anywhere between the bound limits stated by the manufacturer. To convert this stated uncertainty to standard uncertainty, it is divided by $\sqrt{3}$ for a rectangular distribution.

Drift uncertainty is determined by calculating the change in the gradient and intercept of calibration curves before and after measurements were taken as follows:

$$u_{drift} = \frac{\left|(m_1 - m_2) - (c_1 - c_2)\right|}{2} \tag{3.35}$$

where m_x denotes the gradient of the linear calibration curve and c_x denotes the intercept of the calibration curves (Rousseau *et.al*., 2012).

3.4.2 Propagation of uncertainty

In order to analyse the propagation of uncertainty from measured parameters $(x_1, x_2, ..., x_n)$ to a derived parameter (y), the total standard uncertainty must first be calculated as per equation (3.33). To calculate the combined standard uncertainties the following is valid:

$$u\left(y(x_1, x_2, ..., x_n)\right) = \sqrt{\sum_{i=1}^{n}\left(c_{x_i} u(x_i)\right)^2} \tag{3.36}$$

with

$$c_{x_i} = \frac{\partial y}{\partial x_i} \tag{3.37}$$

the sensitivity coefficients.

In some cases no analytical relationship exists between two parameters, e.g. between viscosity and temperature obtained from a property table. In such cases the partial derivative to determine the sensitivity coefficients can be calculated by a numerical approximation method. Using a forward-differencing finite-difference approach, we can write

$$\frac{\partial y}{\partial x_i} \approx \frac{y(x_i + \delta) - y(x_i - \delta)}{2\delta} \tag{3.38}$$

with $\delta = 0.01 \cdot x_i$, a small fraction of x_i as an initial guess value of δ.The numerical derivative is calculated

with this first perturbation. A second derivative is calculated with a perturbation of one half of the first perturbation. These two derivative values are compared for convergence, and the process is repeated if necessary.

By applying equation (3.36) for each calculation step in a heat transfer problem, the propagation of experimental uncertainties can be tracked and a combined standard uncertainty can be quoted in a final answer such as a *Nu* number value as seen in this study.

3.5 Statistical concepts[9]

Statistical concepts used in this study include mean and average error. The concepts explained here are used in the data reduction procedure to quantify the accuracy (or inaccuracy) of evaluated data.

3.5.1 Mean

The mean or average is defined by the summation, $\bar{x}$, of all observations, divided by the number of observations:

$$\bar{x} = \frac{1}{n}\sum_{i=1}^{n} x_i \tag{3.39}$$

where $\bar{x}$ denotes any numerical value.

3.5.2 Average error

The average error, or average deviation, is defined by the difference in observed and expected values, divided by the expected value:

$$\text{Average error} = \left| \frac{x_{\text{expected}} - x_{\text{observed}}}{x_{\text{expected}}} \right| \cdot 100 \tag{3.40}$$

3.5.3 Standard deviation

The standard deviation is the measure of the dispersion of data from the mean value. The more spread apart the data is, the higher the standard deviation. The following equation is used to calculate the standard deviation

$$\sigma = \sqrt{\frac{1}{N}\sum_{i=1}^{N}\left(x_i - \bar{x}\right)^2} \tag{3.41}$$

where σ denotes the standard deviation.

3.6 Non-linear regression

Non-linear regression is employed when it is suspected that data sets have an underlying relationship defined by a non-linear model such as an m^{th} order polynomial.

[9] Statistical concepts used in this study are based on the work of Rice (2007).

For the purpose of this study[10], m^{th} order polynomial regression was applied to obtain a smooth temperature profile curve through *n* data points as will be shown in section 5.1.2. A function in the following form

$$T(x) = c_0 + c_1 x + c_2 x^2 + ... + c_m x^m \tag{3.42}$$

must be found.

Let $\bar{c} = [c_0 \quad c_1 \quad c_2 \quad ... \quad c_m]$ be the vector containing the coefficients of the polynomial and $\bar{\beta} = [\beta_0 \quad \beta_1 \quad \beta_2 \quad ... \quad \beta_m]$ with

$$\beta_k = \sum_{i=1}^{n} T_i x_i^k \tag{3.43}$$

where *n* denotes the number of data points in the set. Furthermore, let $\bar{\alpha}$ be the matrix

$$\bar{\alpha} = \begin{bmatrix} \alpha_{0,0} & \alpha_{0,1} & \alpha_{0,2} & ... & \alpha_{0,m} \\ \alpha_{1,0} & \alpha_{1,1} & \alpha_{1,2} & ... & \alpha_{1,m} \\ \alpha_{2,0} & \alpha_{2,1} & \alpha_{2,2} & ... & \alpha_{2,m} \\ ... & ... & ... & ... & ... \\ \alpha_{m,0} & \alpha_{m,1} & \alpha_{m,2} & ... & \alpha_{m,m} \end{bmatrix} \tag{3.44}$$

with

$$\alpha_{j,k} = \sum_{i=1}^{n} (x_i^j x_i^k) \tag{3.45}$$

The coefficients can then be calculated as

$$\bar{c} = \bar{\varepsilon}\bar{\beta} \tag{3.46}$$

with $\bar{\varepsilon} = \bar{\alpha}^{-1}$ the inverse of $\bar{\alpha}$. Following this, equation (3.42) may be re-written as

$$T(x) = \bar{\beta}\bar{\varepsilon}\bar{x} \tag{3.47}$$

with $\bar{x}$ defined as $\bar{x} = \begin{bmatrix} x^0 & x^1 & x^2 & ... & x^m \end{bmatrix}$.

When calculating the uncertainty associated with a curve fit, the total uncertainty (instrument, statistical and drift uncertainty) is incorporated in the calculation of the curve fit uncertainty. This can be shown by

$$u_{y(x)}(x) = \sqrt{\sum_{i=1}^{n} \left(\frac{\partial}{\partial y_i} \big(y(x) \big) u_{total}(y_i) \right)^2} \tag{3.48}$$

where $y(x)$ denotes the value calculated by the polynomial curve fit with *n* data points (y_i) and $u_{total}(y_i)$ the

[10] The need for applying this regression models in this study is shown in chapter 5.

combined instrument uncertainty as calculated in equation (3.33).

The sensitivity coefficients is calculated by

$$\frac{\partial}{\partial y_i}\left(y(x)\right)=\sum_{k=0}^{m}\left(x_i^k\sum_{j=0}^{m}\left(\varepsilon_{k,j}x^j\right)\right) \tag{3.49}$$

3.7 Summary

The conservation laws explained in this chapter serve as the foundation upon which this study is based. Furthermore, the most commonly used concepts in this field of study was discussed and explained. Seeing that the implementation and comparison of different *Nu* number correlations form the basis of this study, each correlation was discussed in detail. For data reduction purposes, the methods used to address uncertainty and non-linear regression were explained in detail.

In the chapter to follow, the practical layout of the test facility as well as the broad structure of the theoretical analysis model will be discussed.

Chapter 4 EXPERIMENTAL PROCEDURE AND TEST FACILITY

This chapter describes the experimental procedure used in this study. Firstly, the test bench facility will be discussed with elaboration on the following:

- The general layout.
- Construction details.
- Main components installed.
- Instrumentation.

The second part of this chapter will describe the analysis model used to compare theoretical generated data with experimentally captured data.

4.1 Test bench

4.1.1 General layout

A trans-critical carbon dioxide heat pump system forms the basic layout of the test bench facility. As shown in Figure 2, the test bench consists of four basic components namely:

1. Compressor.
2. Gas cooler.
3. Expansion valve.
4. Evaporator.

These components are the basis of any refrigeration cycle, whether designed for heating or cooling purposes. The test bench is further equipped with:

- Mass flow meters on the water and gas sides.

- Temperature transmitters on the water and gas sides.
- Pressure transmitters on the gas sides.
- Motorized automation on the expansion valve.
- Variable Frequency Drive (VFD) on the compressor.
- Thermal insulation on all piping and heat exchangers.
- Data logging equipment.
- Water pumps, flow switches and hand valves to control water flows.

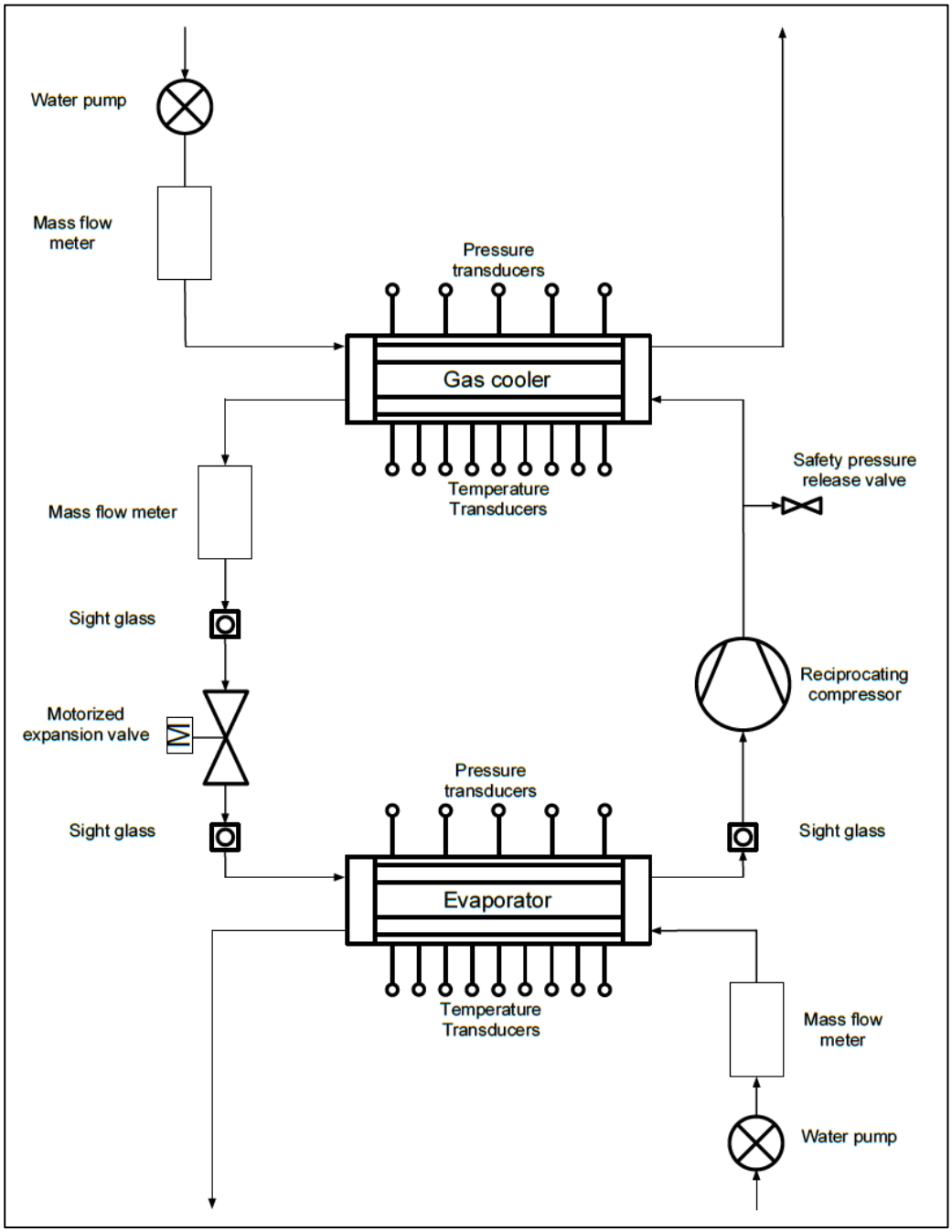

Figure 2: Basic test bench layout.

Figure 3: Trans-critical carbon dioxide heat pump test bench facility.

This fully functional heat pump test bench shown in Figure 3 is a well-equipped experimental facility where numerous studies can be done on different components. Such studies may include an analysis of the evaporator and compressor or the performance of the overall heat pump system.

In the section to follow the components used will be described in more detail.

4.1.2 Main components

Compressor and VFD control

The Bitzer 4KTC-15K semi hermetic, reciprocating compressor is specifically designed for carbon dioxide refrigeration systems. The compressor has four cylinders and is powered by a 17kW 3-phase induction motor. The maximum pressure on the outlet is rated at 13.0MPa, with a fluid displacement of 9.2 m^3/h (Bitzer, 2010). Power consumption and cooling capacities at different operating conditions are summarised in Table 3.

Table 3: Compressor characteristic table (Bitzer, 2010).

Gas cooler outlet temperature [°C]	High Pressure [MPa]	Evaporating Temperature		
		5°C	**0°C**	**-5°C**
15	7.5	Q_c = 49.3 P_e = 8.94	Q_c = 40.7 P_e =9.17	Q_c = 33.55 P_e =9.29
25	7.5	Q_c = 41.9 P_e = 8.94	Q_c = 34.65 P_e =9.17	Q_c = 28.6 P_e =9.29
30	7.5	Q_c = 35.85 P_e =8.94	Q_c = 29.7 P_e =9.17	Q_c = 24.5 P_e =9.29
35	9.0	Q_c = 32.25 P_e =11.10	Q_c = 26.65 P_e =11.05	Q_c = 21.95 P_e =10.89
40	10.0	Q_c = 28.15 P_e =12.34	Q_c = 23.25 P_e =12.12	Q_c = 19.11 P_e =11.81
Q_c = Cooling Capacity [kW] P_e = Power Consumption [kW]				

The Danfoss AKD 102 VFD (Danfoss, 2008) regulates the electrical supply to the compressor. This lends flexibility in the capacity control of the compressor, enabling the operator to easily vary the mass flux by setting the electrical phase frequency at the desired value between 30 – 70 Hz.

Gas cooler and evaporator

A tube-in-tube configuration was used to construct the heat exchangers. Carbon dioxide flows in the inner tube with water in the annular section between the inner and the outer tube.

Figure 4 visually illustrates this configuration.

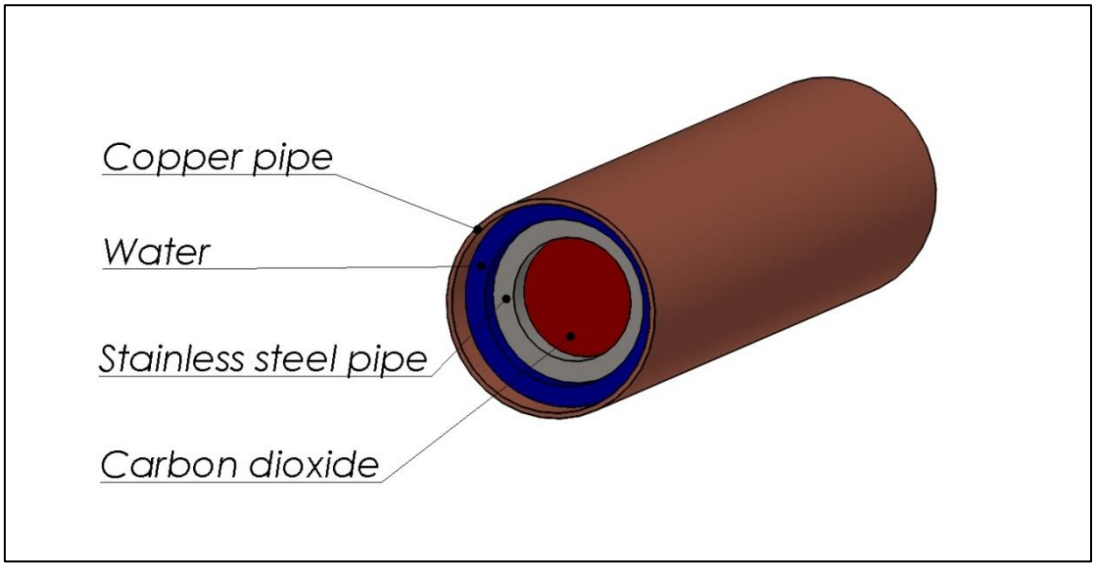

Figure 4: Heat exchange flow channels.

Bends were constructed by using copper T-pieces and 90° stainless steel elbows as shown in Figure 5. The stacked configuration, as shown in Figure 3, comprised of several pipe sections on both heat exchangers. The gas cooler has twelve sections of 2m each giving a total gas cooler length of 24m. The evaporator consists of eight sections of the same length, resulting in a total length of 16m.

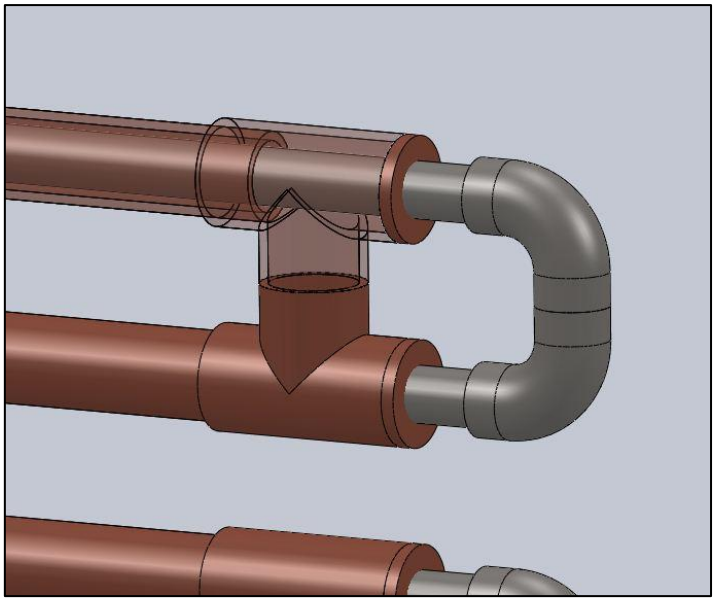

Figure 5: Copper T-pieces and elbows used to connect section.

Due to the high pressure of supercritical carbon dioxide, precaution was taken to ensure that all components are certified and capable to work under high pressure. These components are described in Table 4.

Table 4: Heat exchanger component properties

Component	Dimension	Material
High pressure gas piping	16mm inner diameter	AISI 304 stainless steel, seamless, schedule 40
Low pressure water piping	26mm inner diameter	Class 0 copper tube
Tube Insulation	12.5mm thick	Low density foam type

Expansion valve

The test bench was equipped with a Danfoss motorized expansion valve which is electronically controlled by a programmable logic controller (PLC), specifically developed for high pressure carbon dioxide refrigeration systems. The controller regulates the system pressure by using input signals from two pressure transducers upstream and downstream from the valve. Automatic regulation can also be bypassed to manual operation, where the operator specifies the opening degree of the valve. By selecting the desired opening degree, precise gas cooler pressures can be obtained and varied with the required intervals. This method was used during this study to obtain experimental data.

Water circuit

Water was circulated through the two heat exchangers to cool the gas cooler and heat the evaporator. Two 5000 liter water tanks served as reservoirs for the test facility. Flexible hose piping which connects the test facility to the reservoirs enabled the operator to switch the water supply hoses between the evaporator and gas cooler. This allows the operator to take control of the tank temperature which is prone to over heating / chilling when the facility is operating for extended periods of time. Flow switches with fault signals were installed on the water circuit to ensure the presence of water flowing through the system. Zero water flow will

result in over heating of the gas cooler or freezing of the evaporator.

4.1.3 Instrumentation

The test facility has been fitted with extensive instrumentation equipment to evaluate real time data and store it for further processing. Instrumentation fitted to the test bench will be discussed in the following paragraphs.

Digital pressure sensor / transmitter

Six AKS 2050 pressure transmitters supplied by Danfoss (Danfoss, 2011c) were installed at specific positions (Figure 2) on the gas cooler to measure the carbon dioxide pressure. Moreover, six pressure sensors were also installed along the length of the evaporator. These sensors convert the measured pressure into a linear output signal which is proportional to the supply voltage. This is a disadvantage to a system where the supply voltage fluctuates between different supply units, as was the case on the test bench. This problem can easily be overcome if voltage fluctuations are recorded. The pressure sensor also has a built-in voltage stabilizer which rectifies noise from the power supply. The accuracy is rated at ±0.3% of the measured value (including linearity, hysteresis and repeatability analysis).

Digital temperature transmitter

MBT 3270 temperature transmitters supplied by Danfoss (2010) were installed in two meter increments on both heat exchangers to measure the carbon dioxide temperature. The sensor screws into a socket which is welded onto the inner tubing elbow. A thermal pocket that forms part of the sensor brings the Pt1000 element in contact with the bulk fluid in the centre of the tube (Figure 6).

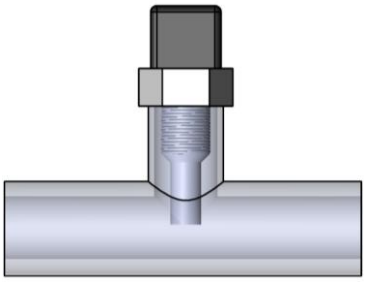

Figure 6: Danfoss MBT 3270 temperature transmitter shown in the mounted position with the Pt1000 element in direct contact with the bulk fluid.

The accuracy is rated at a tolerance of t and can be calculated by:

$$t = \pm\left(0.3 + 0.005 \times T_m\right) \tag{4.1}$$

where T_m denotes the measured fluid temperature.

The water temperature was measured in two meter increments in both heat exchangers with the AKS 12 temperature sensor from Danfoss which contains a Pt1000 resistive measuring element (Danfoss, 2011b). These sensors were installed with the measuring element in direct contact with the bulk fluid. The accuracy is similar to the MBT 3270 sensor described above and can be calculated by equation (4.1).

Mass flow instrumentation

The carbon dioxide mass flow is measured by the Promass 80M coriolis mass flow meter supplied by Endress

& Hauser (Endress & Hauser, 2010b). The measuring principle is based on the generation of controlled coriolis forces by superimposing oscillation on the moving fluid, perpendicular to the flow direction. The phase of the superimposed oscillation will be accelerated at the inlet of the meter, and decelerated at the outlet. This difference in phase provides a direct measure of mass flow rate and the inertia of the fluid provides a direct measure for density (Endress & Hauser, 2010b). The Promass 80M flow meter is suitable for measurements of high pressure carbon dioxide. The accuracy for gas measurements is rated at ± 0.5% of the reading.

Water flow is measured on both the gas cooler and the evaporator by two Promag 50P magnetic mass flow meters supplied by Endress & Hauser (Endress & Hauser, 2010a). The measuring principle is based on Faraday's law of induction which states that a voltage is induced in a conductor when the conductor moves through a magnetic field (Endress & Hauser, 2010a). Water is a conductor and the induced voltage is proportionate to the volume flow through the measuring duct (Endress & Hauser, 2010a). The accuracy for water measurements is rated at ± 0.5% of the reading.

Data logging

All instrumentation installed on the test bench gives a linear voltage output signal related to the measured value. These signals are interpreted by the AK-SC255 system controller supplied by Danfoss (Danfoss, 2011a) and logged into the internal memory of the unit. A personal computer can be connected to the AK-SC255 via a standard Ethernet connection where a history log containing measured data of all 47 data points can be downloaded. Measured data can be logged in specified increments as short as five seconds between two consecutive values. For this study temperature data were logged every 30 seconds or 0.033 Hertz. These measured data points are stored into a comma separated data file for further interpretation.

The test bench components discussed are summarized in Table 5.

Table 5: Test bench component specifications.

Component	Fabricate and description	Technical Specification
Compressor	Bitzer 4KTC-15K Semi hermetic reciprocating compressor	Power consumption: 17kW 13.0MPa maximum output pressure, Suitable for operating at 30 -70 Hz
Expansion valve	Danfoss ICMTS expansion valve	Working pressure up to 14.0MPa
	Danfoss ICAD 900 actuator	Manual operation / automated by Danfoss controller
Variable Frequency Drive	Danfoss AKD 102	Input 380 – 500V 3 phase, output 0 – 100% of supply voltage and frequency from 30 – 70 Hz
Gas mass flow meter	Endress & Hauser Promass 80 M Coriolis flow meter	Operating pressure up to 35.0MPa Operating temperature up to 150°C Accurate flow measurement from 0 – 610 kg/s

Component	Fabricate and description	Technical Specification
Water mass flow meter	Endress & Hauser Promag 50 P15 Electromagnetic flow meter	Operating pressure up to 4.0MPa Operating temperature up to 180°C Accurate flow measurement from 0 – 2600 kg/s
Water pumps	Zilmet CMB 100 M	Flow: 100 – 250 l/min Total head: 14 – 16m
Data logging system	Danfoss AK-SC 255	Accommodate up to 60 sensor inputs Store measured value every 5 sec Export values in comma separated text file format via Ethernet connection
Temperature transmitter	Danfoss AKS 12 PT 1000 type	Temperature range: -50 – 150°C Used on gas side
	Danfoss MBT 3270 PT 1000 type	Temperature range: -40 – 100°C Used on water side
Pressure transmitter	Danfoss AKS 2050 Ratiometric	Pressure range: -1 – 15.9MPa Output signal is a function of supply voltage

4.2 Data acquisition procedure

To obtain useful experimental results, a systematic experimental procedure was followed. This procedure was necessary to ensure that tests done on the system were well thought through, planned and consistent. In the following paragraphs, detail regarding the method on how tests were performed at the test facility will be discussed.

4.2.1 Controlled variables for desired operating conditions

Due to the closed cycle heat pump layout of this test facility, it is impossible to vary certain test parameters independently of others. For instance, one cannot vary the carbon dioxide mass flow without affecting the inlet gas temperature. These parameters might be independent of each other when external control is applied to the fluid condition with additional heaters, coolers and bypassing valves, but this however, is not the case with the closed cycle heat pump test bench used in this study.

In order to acquire test results over a spectrum of operating conditions, it was decided to use the gas cooler pressure as the independent variable. Tests were conducted at 0.5MPa increments with gas cooler pressures ranging from 8.0MPa to 11.0MPa. This pressure range also covers a wide range of pressures as specified in the chosen correlations to be verified. It was found that the inlet gas temperature and gas mass flux range are in general agreement to the specified ranges found in the papers on heat transfer correlations as discussed in Chapter 2.

Control of gas cooler pressure is obtained by adjusting the following:

- Expansion valve opening degree.
- Compressor frequency.

- Total carbon dioxide charge in the system.
- Water mass flow in the gas cooler.

The first step in varying the operating pressure is to change the expansion valve opening degree together with the compressor frequency. A choked expansion valve with higher compressor frequency will result in the gas cooler pressure (and temperature) to rise. This method of pressure change is limiting due to the mass flux range limits of 600 – 900 kg/m^2.s and subsequent lowering evaporator temperature (with possible ice formation on the water side) due to the high pressure drop over the expansion valve. To gain more control over the gas cooler pressure, the carbon dioxide charge within the system can be varied by letting some of the gas out, or charging the system with more gas. The more refrigerant present in the system, the higher the obtainable pressure in the system will be. Water mass flow rate also has a slight effect on the gas cooler pressure due to the temperature profile of the gas being related to the mass flow of water and subsequently also effects the gas cooler pressure.

4.2.2 Test bench operation

Each time the test bench is operated to do experimental tests, the operator must adhere to the operating procedure and safety requirements as stated in the document found at the test bench. For the purpose of this study, a concise start-up procedure is given to provide an overview of the typical operation of the test bench.

Start-up procedure:

1) Switch on the main electrical supply, control circuit and the instrumentation circuit.
2) Switch on the crank case heater of the compressor and allow 8 hours to heat up.
3) Ensure that the water tanks supplying the gas cooler and evaporator are full and at ambient conditions of 20 – 23 °C.
4) Switch on both water pumps and check for adequate water flow through the system.
5) Ensure that the expansion valve is set to an opening degree of at least 50%.
6) Ensure that the VFD is set to 35 Hz for slow start-up.
7) Switch on the main compressor switch and wait for 15 minutes until the compressor starts.
8) Stand in front of the instrumentation display and ensure the following:
    - The compressor outlet temperature must not exceed 120°C.
    - The evaporator outlet condition should be well within the superheated phase to prevent liquid from entering the compressor.
    - Water flow in both the evaporator and gas cooler must initially be > 15 l/min

With the above mentioned points followed, tests can commence by varying the expansion valve, compressor frequency, gas charge and water mass flow until the desired gas cooler condition is reached. It may be required to repeat the process of adjusting certain variables numerous times, as each input will affect all other components in the system

Once the desired test condition is reached, the condition is maintained for 20 minutes to ensure steady state

operation. The standard deviation (σ) for temperature measurements was also evaluated after testing was completed to confirm steady state operation and validity of the captured data.

The Danfoss AK-CS255 controller logs all system data continuously throughout the experimental procedure from the moment it is switched on. It is thus required to take note of the exact time when steady state conditions are reached in order to capture the correct data set from the logging device.

4.3 Data processing procedure

To compare theoretical *Nu* numbers to the experimental *Nu* values, the approach towards the data processing should be carefully considered. There are two ways of comparing experimental data with theoretical data namely simulation and analysis. These two methods are briefly compared in the section to follow.

One way would be to calculate theoretical *Nu* values with a discretised heat exchanger simulation[11] program. In a simulation program, the outlet temperature per increment is calculated and used as the inlet temperature for the following increment. By employing different correlations parallel to each other for the same overall inlet condition, different temperature profiles (and fluid conditions) can be obtained for a particular increment. This would result in comparing the evaluated parameters from various correlations (such as *Nu*) at different fluid conditions for a specific increment (Figure 7). The validity of this method could be questioned if the simulation approach is employed to compare correlations to each other and with experimental test data due to different fluid conditions found per increment. This is visually illustrated in Figure 7.

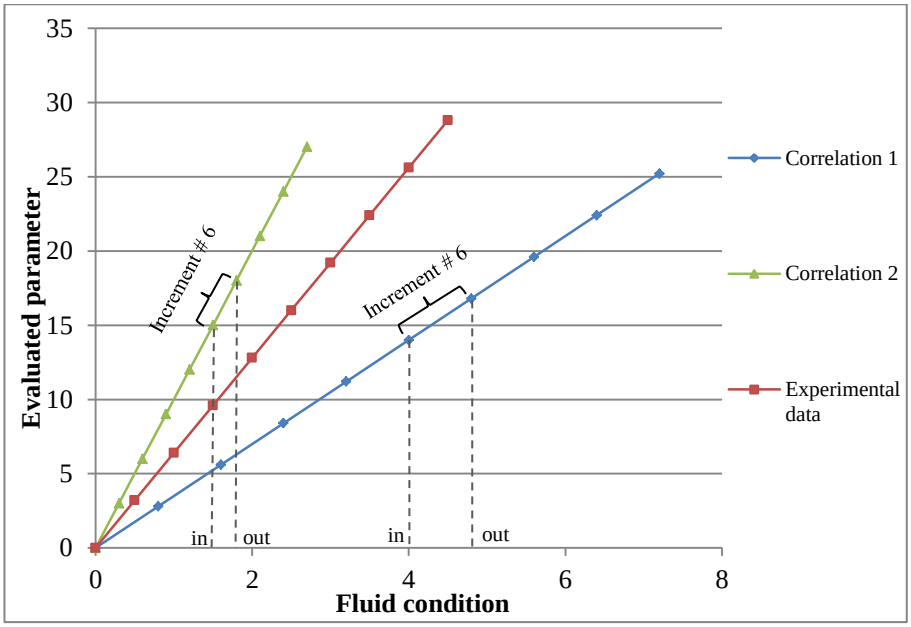

Figure 7: The resulting plot of the evaluated parameter *vs.* dependent parameter from a simulation model.

When comparing different *Nu* correlations with each other it is required to control the dependable parameter (or fluid condition) to create a basis on which comparison can take place impartially. The alternative data

[11] Simulation refers to a discretised heat transfer model which uses the previous increment outlet conditions as the inlet condition in the following increment.

processing procedure to a simulation model would be by an analysis[12]. An analysis model would use experimental test conditions as inlet and outlet for each increment in a discretised model, ensuring that each increment is compared to each other at the same fluid conditions as shown in Figure 8. When calculating the evaluated parameter (such as *Nu*), a viable comparison per increment can be done at common fluid conditions, determined by the experimental tests conditions.

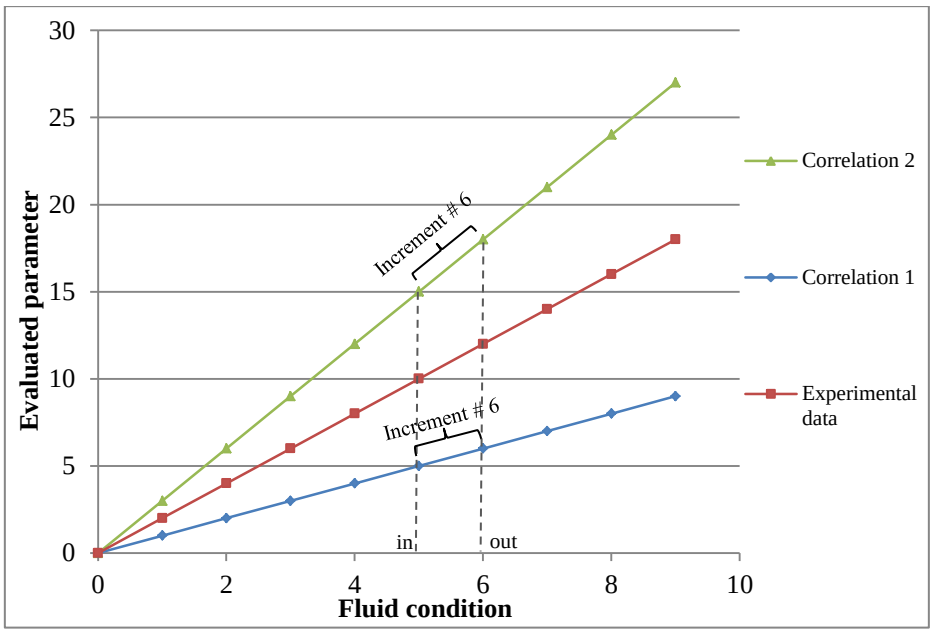

Figure 8: The resulting plot of the evaluated parameter *vs.* dependent parameter from an analysis model.

Details regarding the analysis procedure of experimental and theoretical data are discussed in detail in the following section.

4.3.1 Analysis of a supercritical gas cooler

The objective of the study is to compare different *Nu* correlations to experimental *Nu* values. It is therefore necessary to calculate values for Nu_{exp} as well as Nu_{theo} employing various *Nu* correlations for the exact same fluid conditions as observed in the experiments. The analysis therefore consists of two main sections namely

- Calculation of $Nu_{theo,}$
- Calculation of $Nu_{exp.}$

Analysis interface

The analysis code is written in the numerical equation solver program called Engineering Equation Solver or EES for short (Klein & Alvardo, 2009). This program is particularly suitable for thermo-fluid calculations because of its built-in thermodynamic and transport property database.

Methodology for determining Nu_{theo}

In this section the programming structure of the analysis program used to calculate the Nu_{theo}, values will be

[12] Analysis refers to a model using experimental measured flow conditions measured at each increment as the inlet and outlet condition for each increment in the theoretical calculations.

discussed. A flow diagram of the program is visually illustrated in Figure 9.

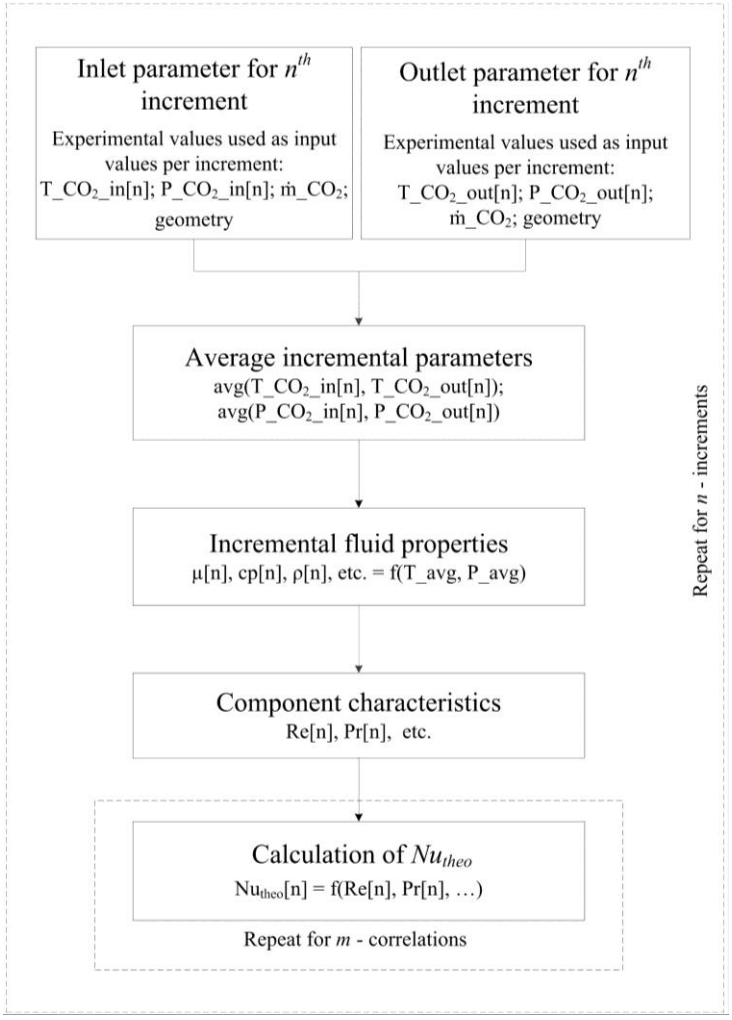

Figure 9: Calculation of Nu_{theo} - analysis program flow diagram.

The inlet and outlet parameters are fixed to the same values of the particular test condition for the increment under evaluation. Inlet conditions include the following basic measureable parameters:

- Temperature.
- Pressure.
- Mass flow rate.
- Channel geometry.

Once the inlet and outlet conditions are fixed, the averaged conditions per increment are calculated and used to determine fluid properties for each increment using property tables found in the software. These fluid properties are functions of the average incremental temperature and pressure, along with the applicable flow channel geometry. Fluid properties include:

- Viscosity.
- Specific heat capacity.
- Density.

- Velocity.
- Enthalpy.
- Entropy.

Component characteristics can be calculated once the fluid properties are known. Component characteristics include:

- Reynolds number.
- Prandtl number.
- Friction factor.

Once the component characteristics and fluid properties are known, the numerous *Nu* number correlations are employed to calculate Nu_{theo} values under the same conditions as measured on the test bench.

The complete analysis programming code is shown in APPENDIX A - EES program.

Methodology of determining Nu_{exp}

Nu_{exp} numbers cannot be measured and therefore must be calculated for each test section. This section explains the methodology of this calculation.

The path of heat transfer from the hot carbon dioxide to the cold water involves convection on the inner surface of the thick-walled stainless steel pipe, conduction in the radial direction through the stainless steel wall and convection from the stainless steel wall to the water in the annular area. Conduction heat transfer in the axial direction of the fluid and stainless steel pipe was assumed to be negligible (Pitla *et al.*, 2001).

Theoretically all the heat rejected by the carbon dioxide is transferred into the water due to the tube-in-tube configuration of the heat exchanger. It is however possible for some heat to be dissipated into the atmosphere through the insulation material from the water side. The difference between the carbon dioxide heat transfer and the water heat transfers is shown in the energy balance (5.1.1) and can therefore be ascribed to the heat loss through the insulation to the atmosphere. Hence it was argued that the calculation of the theoretical heat transfer coefficient of carbon dioxide should be based on the measured values of the carbon dioxide side of the heat exchanger due to the geometry of the system.

The Nu_{exp} number of carbon dioxide in each sub-section of the heat exchanger was calculated using the following procedure illustrated visually in Figure 10.

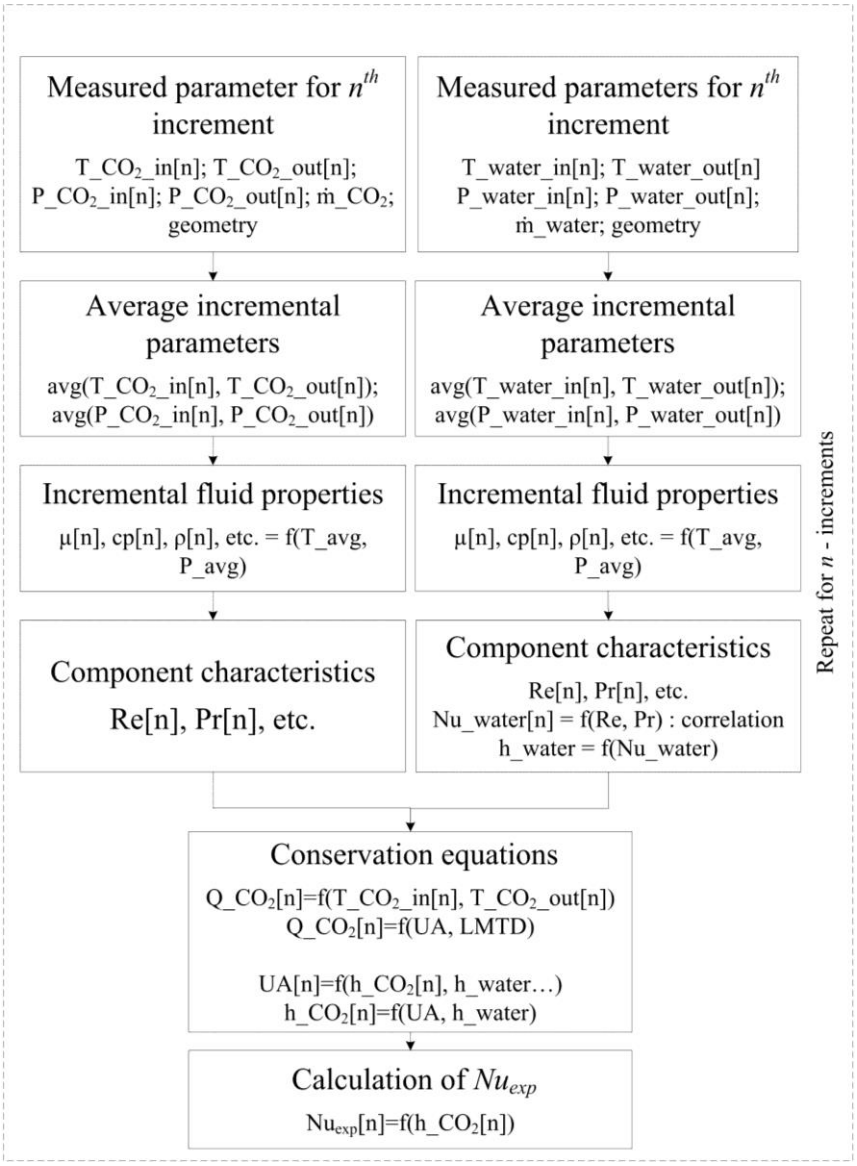

Figure 10: Calculation of Nu_{exp} - analysis program flow diagram.

The first steps in the program are similar to what was explained in the previous section up to the point of determining the component characteristics of an increment.

Using the conservation of energy, the heat transfer rate was calculated from the change in enthalpy in the CO_2 over a test section. Enthalpy of CO_2 was obtained from thermodynamic tables in EES with pressure and temperature values as input variables for these sub-routines.

$$\dot{Q}_{CO_2} = \dot{m}_{CO_2}(h_{CO_2,1} - h_{CO_2,0}) \tag{4.2}$$

Heat transfer rate between two fluids can also be calculated using equation (4.3)

$$\dot{Q} = U \cdot A \cdot LMTD \tag{4.3}$$

where U is the overall heat transfer coefficient and $LMTD$ the logarithmic mean temperature difference. The $LMTD$ value is calculated by equation (4.4)

$$LMTD = \frac{\Delta T_1 - \Delta T_0}{\ln \frac{\Delta T_1}{\Delta T_0}} \tag{4.4}$$

and the temperature differences are calculated by

$$\begin{aligned} \Delta T_1 &= T_{CO_2,1} - T_{water,1} \\ \Delta T_0 &= T_{CO_2,0} - T_{water,0} \end{aligned} \tag{4.5}$$

The overall heat transfer coefficient *(U)* in equation (4.6) defined by the sum of three terms of heat transfer: 1) forced convection heat transfer from carbon dioxide in the inner tube, 2) conduction heat transfer through the stainless steel tube and 3) convection heat transfer to the water.

$$\frac{1}{U \cdot A} = \frac{1}{h_{c,CO_2} A_i} + \frac{\ln(D_o/D_i)}{2\pi kL} + \frac{1}{h_{c,water} A_o} \tag{4.6}$$

After the energy balance is confirmed, the $\dot{Q}_{CO_2}$ value over each increment is used to calculate $U \cdot A$ from equation (4.3). The conduction term is easily calculated from the known thermal conductivity of stainless steel and dimensions of the tubes. The forced convection term on the water side can be calculated using a proven water heat transfer correlation. The correlation of Gnielinski (valid for $3000 \leq Re \leq 5 \text{ x } 10^6$) was chosen to accommodate Reynolds numbers ranging from 5000 to 12000 on the water side (Incropera *et al.*, 2011).

The $h_{c,CO2}$ value can be calculated since all other variables in equation (4.6) are known. Finally the Nu_{CO2} values can be calculated by relating $h_{c,CO2}$ with Nu_{CO2} by using equation (4.7):

$$Nu_{CO2} = \frac{h_{c,CO2} D_H}{k_b} \tag{4.7}$$

In summary the experimental convection coefficient of carbon dioxide can be calculated by using measured values from both the water and CO_2 side as input. The accuracy of this data reduction procedure is however dependent on the choice and validity of the correlation used to calculate the convection heat transfer coefficient of the water $\left(h_{c,water}\right)$ in the annular area.

Two different *Nu* correlations for internal flow were tested in the calculation of $h_{c,water}$. Results for $Nu_{CO2,exp}$ produced by employing Dittus & Boelter (1985) and Gnielinski (1976) correlations on the water side agreed within 1.5% with each other after data reduction as will be explained in the following chapter. Due to the larger *Re* validity range of the Gnielinski (1985) correlation, it was chosen for further use on the water side.

4.4 Summary

This chapter gave an overview of the test facility constructed and used to conduct the experimental phase of the project. The EES analysis program used for comparison studies were also discussed in detail. The comparison and interpretation of measured and theoretical data will be discussed in the chapter to follow.

Chapter 5 EXPERIMENTAL RESULTS

The purpose of this chapter is to compare and verify theoretical models with experimental results. The following points will be looked at:

- Experimental data reduction method.
- Uncertainty propagation analysis.
- Comparative study between theoretical data and experimental *Nu* values.
- Discussion on the findings.

5.1 Experimental data reduction

The first step in data reduction is to determine the validity of the dataset captured from the data logger.

5.1.1 Validation of data

To test the validity of each dataset, an energy balance between water and carbon dioxide is calculated. Significant differences (> 5%) between the two independently calculated values would raise the flag to a possible invalid dataset. The energy balance is shown in equations (5.1) - (5.3).

$$\dot{Q}_{CO_2} = \dot{m}_{CO_2}(h_{CO_2,0} - h_{CO_2,1}) \tag{5.1}$$

$$\dot{Q}_{water} = \dot{m}_{water}(h_{water,1} - h_{water,0}) \tag{5.2}$$

$$Q_{\%difference} = \frac{\dot{Q}_{water} - \dot{Q}_{CO_2}}{\dot{Q}_{CO_2}} \times 100 \tag{5.3}$$

Table 6 below shows the percentage difference between the water side and the gas side heat transfer expressed as a percentage of the gas side heat transferred over the entire length of the gas cooler.

Table 6: Energy balance results indicating the difference in heat transfer calculated from the CO_2 *vs.* heat transferred to the water.

Data set	$\dot{Q}_{water}$ [kW]	$\dot{Q}_{CO_2}$ [kW]	$Q_{\%difference}$
8.0 [MPa]	18.82	18.44	2.07
8.5 [MPa]	23.73	22.78	4.13
9.0 [MPa]	26.96	26.35	2.33
9.5 [MPa]	29.23	28.67	1.97
10.0 [MPa]	31.36	30.98	1.23
10.5 [MPa]	29.54	30.89	4.37
11.0 [MPa]	31.10	32.49	4.26

The difference between the energy transfer measured on the water side and the energy transfer on the CO_2 side can be ascribed to measurement inaccuracies and heat loss to the atmosphere. For the purpose of this study, the differences between the water and CO_2 sides are on an acceptable level.

5.1.2 Non-linear regression

When experimental readings are influenced by some constant external factor it is possible to use regression models to smooth out data.

The need to use non-linear regression to smooth saw-toothed experimental data was observed in a first iteration of experimental data processing[13]. It was proposed to use non-linear regression as a scientific tool to generate useful experimental data and keeping account of all possible uncertainties imposed on the data by the regression models.

It is important to be aware of the possibility to impose a weak trend on data due to the wrong mathematical model used for the type of data analysed when using regression to derive a smooth mathematical function. After considering various mathematical models, a fifth order polynomial was used to obtain a mathematical function for each of the CO_2 temperature data sets and a third order polynomial was used on the water side. To illustrate the positive effect that the regression has on data, the accumulative fluctuation and smoothing thereof is best shown when the difference between the inlet and outlet temperatures (ΔT) per increment is plotted against position. The accumulative fluctuations seen in Figure 11 is also seen throughout the calculations of Nu_{exp} due to the effective ΔT term's presence in equation (4.2).

In Figure 12 the raw experimental temperature data of the 85 bar test is shown together with the regression polynomials and uncertainty bands. The uncertainty bands include all the different components contributing to the total standard uncertainty value of measured values. The calculation thereof is discussed in section 5.1.2 to follow.

[13] Fluctuations were observed outside the instrumentation uncertainty band and were therefore ascribed to an external influence such as magnetic inductance from nearby electrical equipment.

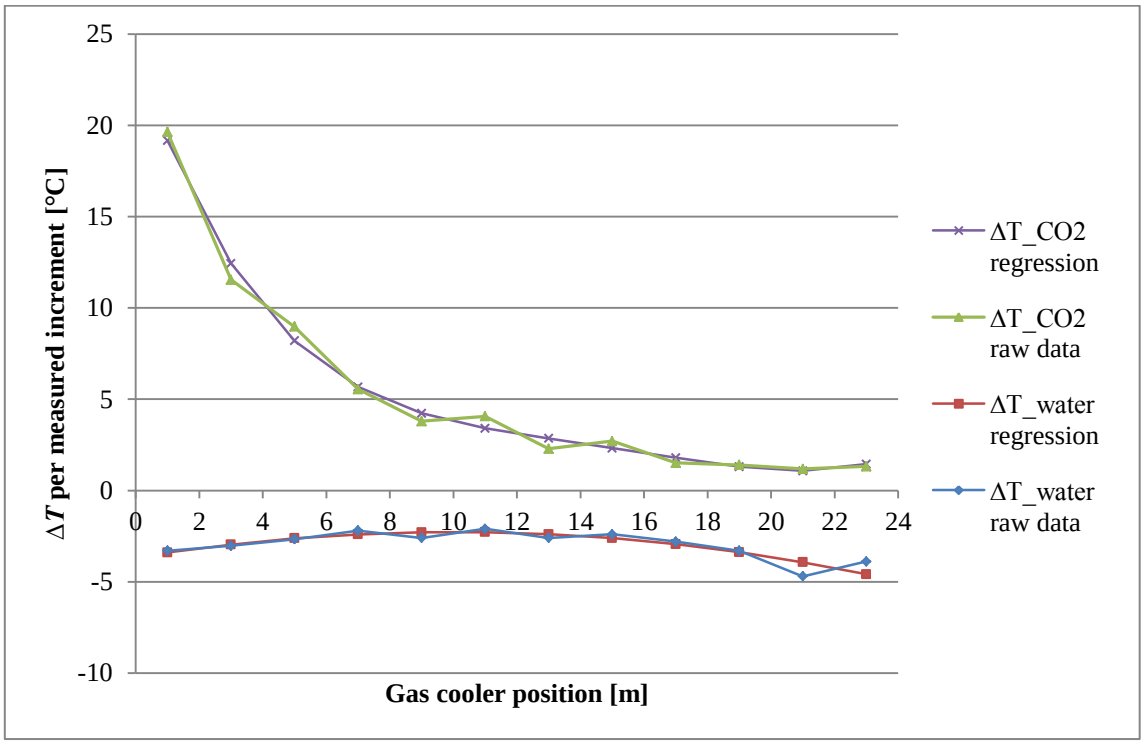

Figure 11: The positive effect of non-linear regression on the experimental test data when plotting ΔT values against gas cooler position.

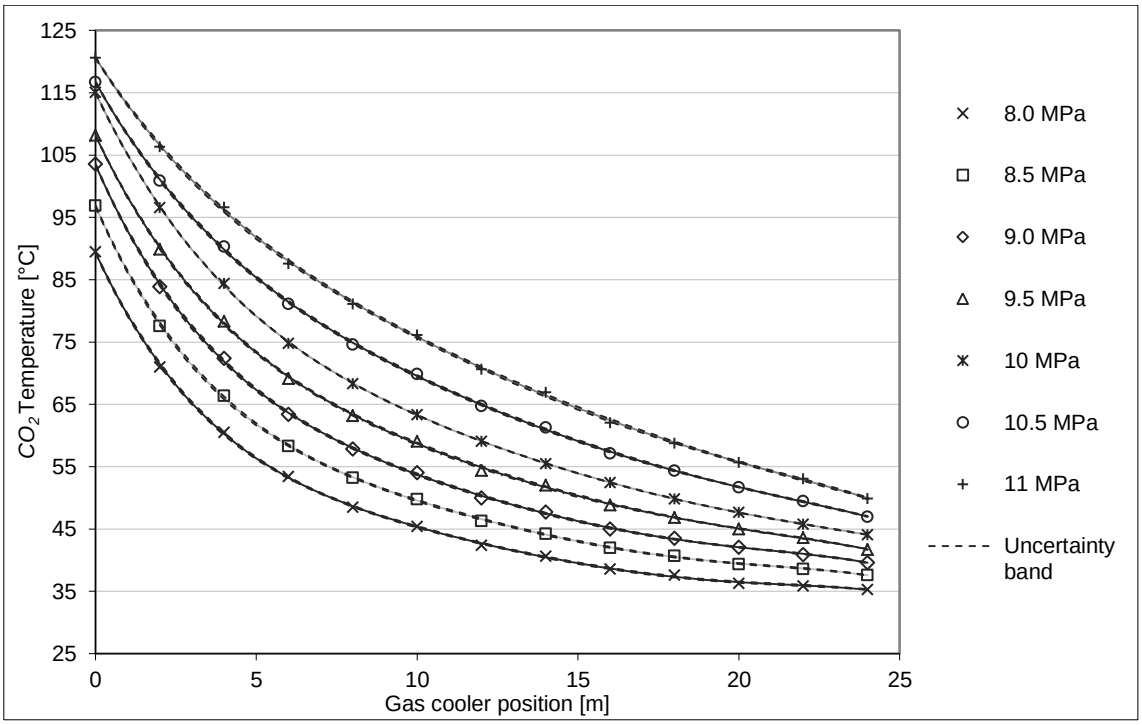

Figure 12: Experimental carbon dioxide temperatures along the gas cooler position.

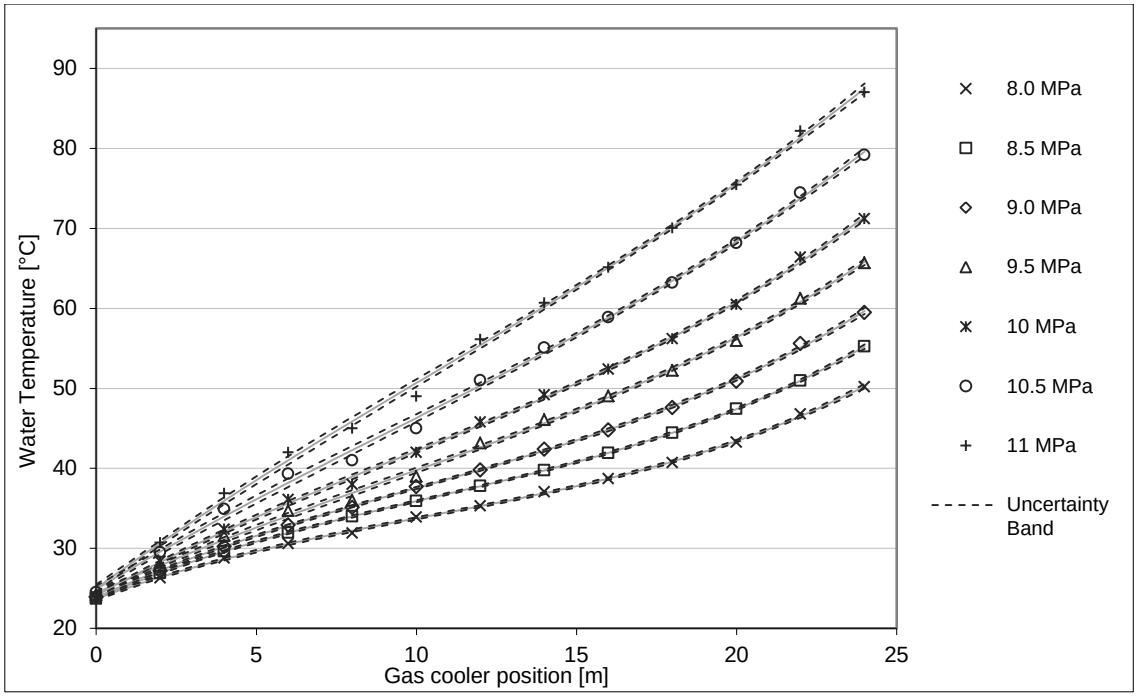

Figure 13: Experimental water temperature plotted along the position of the gas cooler.

With reference to the methodology described in section 3.6, the following $\bar{c}$ vectors were obtained for each set of data shown in Table 7.

Table 7: Non-linear regression $\bar{c}$ vectors for each data set.

	$\bar{c}_{80MPa}$	$\bar{c}_{85MPa}$	$\bar{c}_{90MPa}$	$\bar{c}_{95MPa}$	$\bar{c}_{100MPa}$	$\bar{c}_{105MPa}$	$\bar{c}_{110MPa}$
CO_2 temperature profile	$\begin{bmatrix}117.48\\-34.65\\7.32\\-0.85\\0.05\\-0.001\end{bmatrix}$	$\begin{bmatrix}126.13\\-36.02\\7.51\\-0.87\\0.051\\-0.001\end{bmatrix}$	$\begin{bmatrix}132.75\\-35.74\\7.22\\-0.83\\0.049\\-0.0011\end{bmatrix}$	$\begin{bmatrix}134.67\\-31.87\\5.97\\-0.65\\0.037\\-0.0008\end{bmatrix}$	$\begin{bmatrix}141.1\\-30.96\\5.39\\-0.55\\0.02\\-0.0006\end{bmatrix}$	$\begin{bmatrix}138.55\\-25.76\\4.34\\-0.46\\0.02\\-0.0006\end{bmatrix}$	$\begin{bmatrix}139.83\\-22.45\\3.6\\-0.39\\0.022\\-0.0005\end{bmatrix}$
Water temperature profile	$\begin{bmatrix}20.39\\3.6\\-0.34\\0.018\end{bmatrix}$	$\begin{bmatrix}19.86\\4.2\\-0.37\\0.02\end{bmatrix}$	$\begin{bmatrix}19.89\\4.27\\-0.33\\0.018\end{bmatrix}$	$\begin{bmatrix}21.45\\3.34\\-0.125\\0.01\end{bmatrix}$	$\begin{bmatrix}20.89\\3.81\\-0.13\\0.01\end{bmatrix}$	$\begin{bmatrix}21.03\\4.31\\-0.08\\0.007\end{bmatrix}$	$\begin{bmatrix}20.69\\4.87\\-0.031\\0.004\end{bmatrix}$

Once the formula which best describes each temperature profile was obtained, a new set of data was generated at the same increments as the raw data. The data obtained from the non-linear regression models were used for further analysis in computing the Nu_{exp} numbers.

For completeness the raw CO_2 pressure data is shown in Figure 14. No regression was needed on data, as the profile captured by the pressure transducers was smooth.

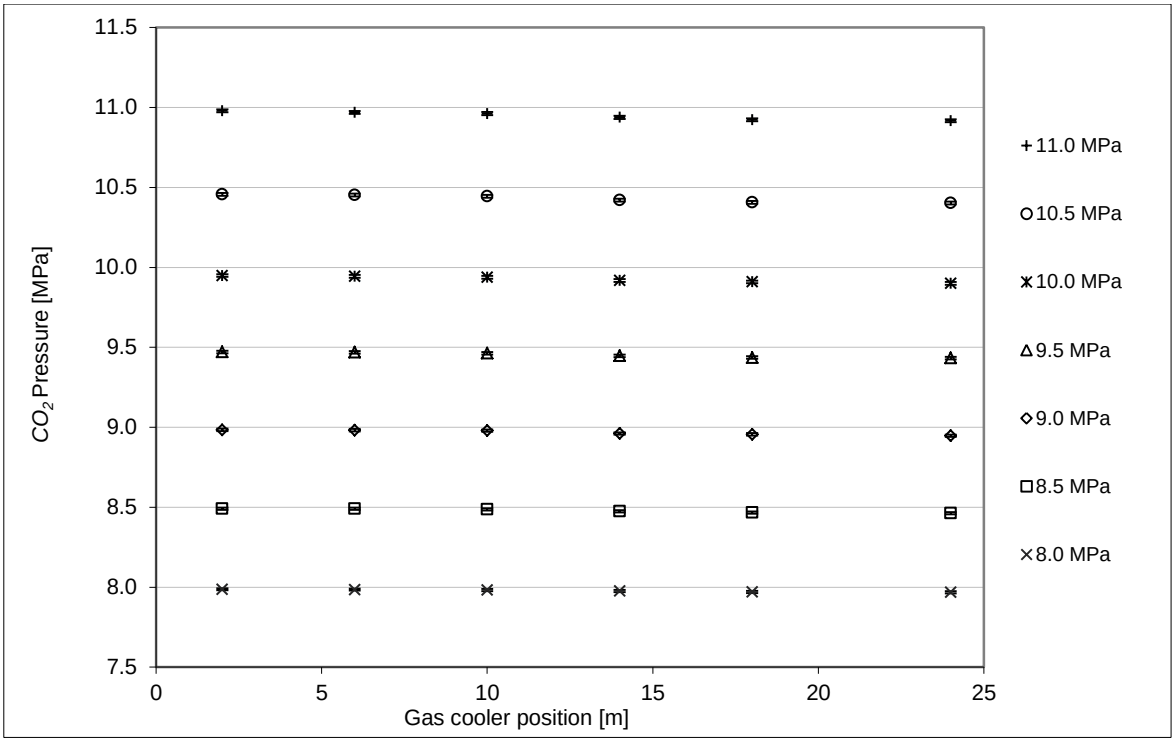

Figure 14: Experimental carbon dioxide pressures plotted against gas cooler position.

Any experimentally measured value has an intrinsic uncertainty associated with it. When further calculations are based on these experimental values, the uncertainty is propagated to the next calculation step. It is important to keep account of these uncertainties, and evaluate the end result together with the uncertainty propagated to this point. An uncertainty propagation analysis is shown in section 5.2.

5.2 Experimental uncertainty propagation analysis

For each temperature, pressure and mass flow data point captured, a total uncertainty value was calculated using the procedure explained in section 3.4. The raw temperature data was smoothed using a regression model where the total standard uncertainty of the mathematical function was derived while incorporating the instrumentation and statistical uncertainties in the calculation. The uncertainty due to instrumentation drift was not included in this study. The uncertainty band of all the regressed temperature data was shown in Figure 12 and Figure 13.

The propagation of uncertainty from measured values to calculated Nu_{exp} numbers were calculated for each position (data point) in the gas cooler. These uncertainty values of Nu_{exp} are shown in Figure 15.

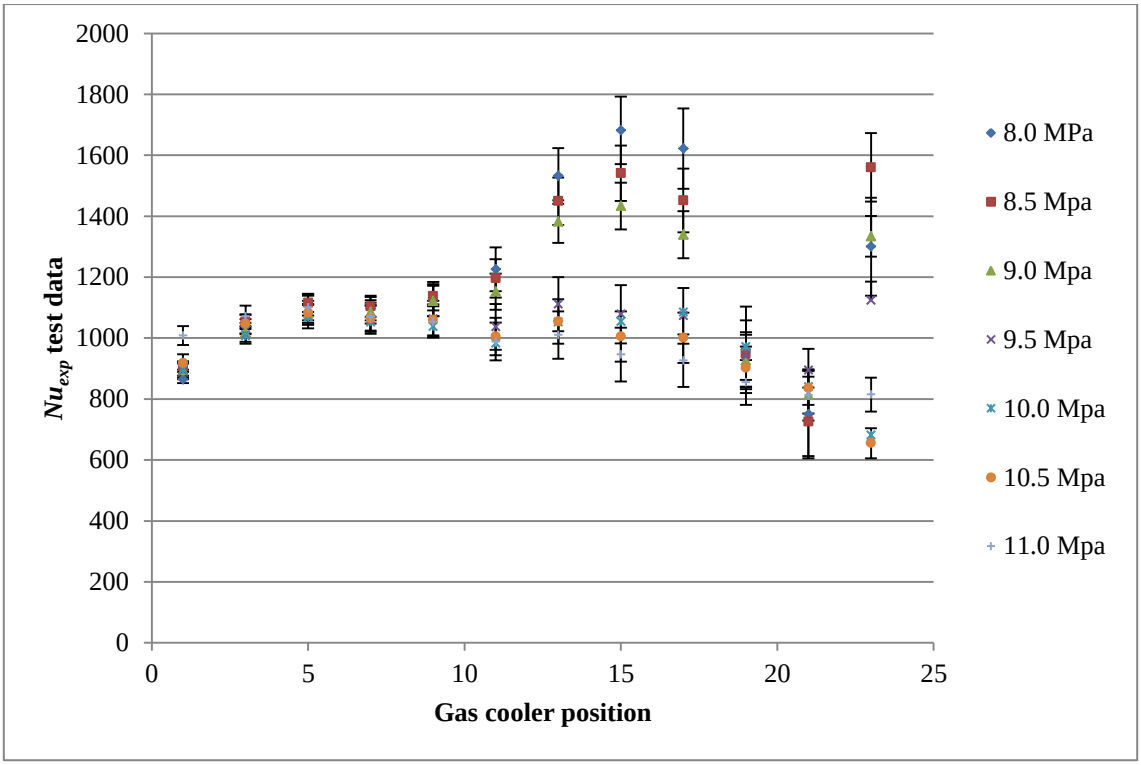

Figure 15: Nu_{exp} for each data set shown with each point's associated uncertainty.

The uncertainty of Nu_{exp} is expressed as percentages in Table 8. It is clear that the relative uncertainty of Nu_{exp} increases along the length of the gas cooler. This can be explained by the small value of ΔT between gas and water measured near the gas cooler exit as well as the decreasing ΔT measured between consecutive points on each fluid (also shown by Figure 11), allowing the total standard uncertainty of the temperature measurements to have a greater effect on the uncertainty of Nu_{exp}. This effect is the largest at lower pressures, where the ΔT values are the smallest.

Table 8: Experimental uncertainty values of Nu_{exp} expressed as percentages of Nu_{exp}.

	Pos. 1	Pos. 2	Pos. 3	Pos. 4	Pos. 5	Pos. 6	Pos. 7	Pos. 8	Pos. 9	Pos. 10	Pos. 11	Pos. 12
8.0 [MPa]	1%	2%	3%	4%	5%	6%	6%	7%	8%	15%	19%	12%
8.5 [MPa]	1%	2%	3%	3%	4%	5%	5%	6%	7%	12%	16%	7%
9.0 [MPa]	3%	3%	3%	4%	4%	5%	5%	5%	6%	9%	10%	5%
9.5 [MPa]	3%	3%	4%	4%	6%	7%	8%	9%	9%	8%	8%	5%
10.0 [MPa]	3%	3%	3%	4%	4%	5%	6%	7%	7%	7%	6%	7%
10.5 [MPa]	3%	3%	4%	4%	5%	6%	7%	8%	8%	8%	7%	7%
11.0 [MPa]	3%	3%	4%	4%	5%	6%	8%	9%	9%	9%	7%	7%

5.3 Comparison between experimental and theoretical data

5.3.1 Platform of comparison

When analysing the *Nu* correlations for a particular fluid over a range of conditions, it is worthwhile to put some thought into the comparison platform. It might be viable to plot the change of *Nu* over the entire length of the gas cooler for different operating conditions and compare the results with that of the theoretical values as obtained by the different correlations. This method of comparison will however only provide information

about the *Nu* at certain positions for a unique gas cooler. Another method might be to plot Nu_{exp} *vs.* Nu_{theo} values for each correlation. The shortcoming with this method would be that no dependent parameter is available to characterise the type of flow. It would only be useful for the unique test conditions and gas cooler of this study.

A better method of comparison would be to plot different *Nu* values against non-dimensional parameters such as the *Re* number or *Pr* number which not only provides a non-dimensional platform, but also reveals more about the type of flow at the specific point. By using non-dimensional parameters, conclusions made by this study may be applied to other heat exchangers by analysing the *Re* range within the gas cooler. It also allows us to combine all data sets on one single graph and effectively combining a wide operating range and making holistic conclusions.

5.3.2 Comparison

In this section the different *Nu* correlations are evaluated against the *Re* and *Pr* numbers as measured along the length of the gas cooler. All the different datasets measured at different pressures are combined here to get data over a wide spectrum of flow conditions.

Figure 16 and Figure 17 shows the experimental and theoretical data plotted against *Re* and *Pr* numbers. Each individual dataset in Figure 16 clearly follows a unique trend. The majority of correlations over-predict *Nu* for all *Re*, but to a lesser extent as the *Re* number increases. Figure 17 shows the same *Nu* data, but plotted against the *Pr* number. For the majority of data *Nu* is over-predicted compared to Nu_{exp}, increasingly as the *Pr* number increases. The percentage error of each correlation for different *Re* and *Pr* number ranges are shown in Table 9 and Table 10.

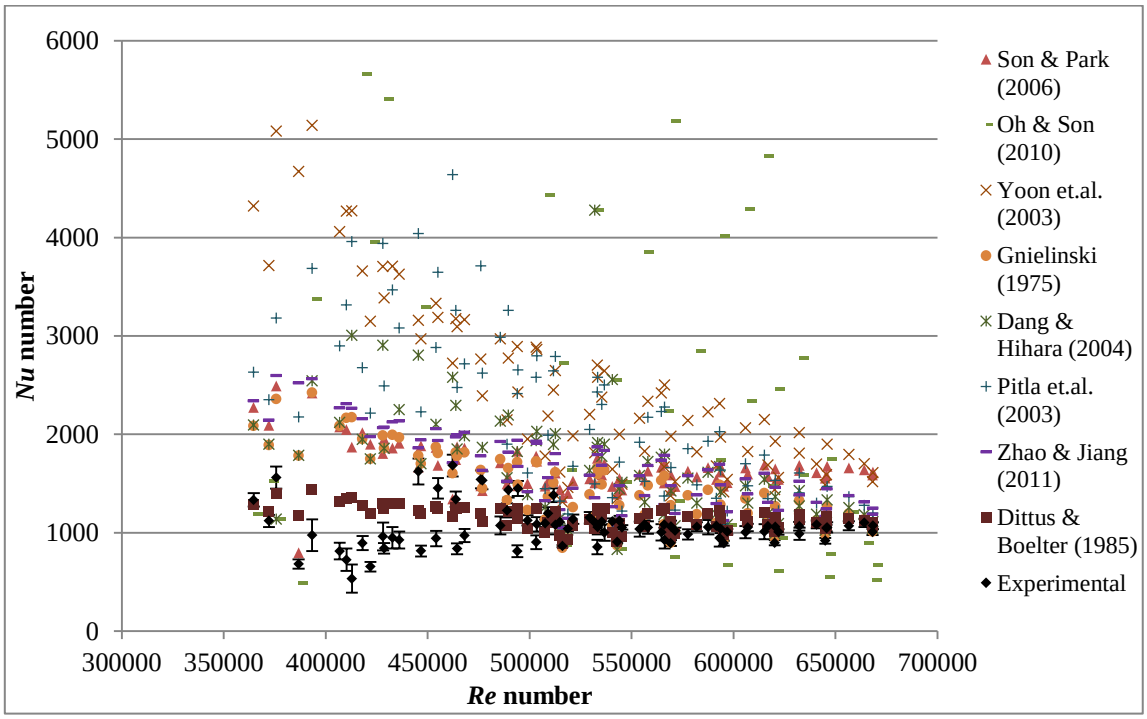

Figure 16: *Nu* numbers plotted against *Re* numbers. This plot combines all data sets (8MPa – 11MPa) by plotting against the non-dimensional *Re* number.

Table 9: Percentage error of each correlation compared with experimental values for various *Re* number bands.

Reynolds number	Dittus & Boelter (1985)	Son & Park (2006)	Yoon *et.al.* (2003)	Oh & Son (2010)	Gnielinski (1975)	Pitla *et.al.* (2003)	Dang & Hihara (2004)	Zhao & Jiang (2011)
350'000 - 400'000	28%	110%	300%	127%	97%	162%	95%	118%
400'000 - 450'000	59%	133%	346%	566%	138%	275%	173%	158%
450'000 - 5000'00	24%	46%	139%	1169%	42%	139%	75%	56%
500'000 - 550'000	12%	47%	99%	654%	28%	80%	98%	43%
550'000 - 600'000	11%	56%	91%	554%	24%	63%	37%	44%
600'000 - 650'000	9%	58%	75%	107%	15%	38%	23%	34%
650'000 - 700'000	4%	53%	56%	29%	4%	17%	8%	21%
Average	**20%**	**66%**	**143%**	**458%**	**45%**	**107%**	**73%**	**62%**

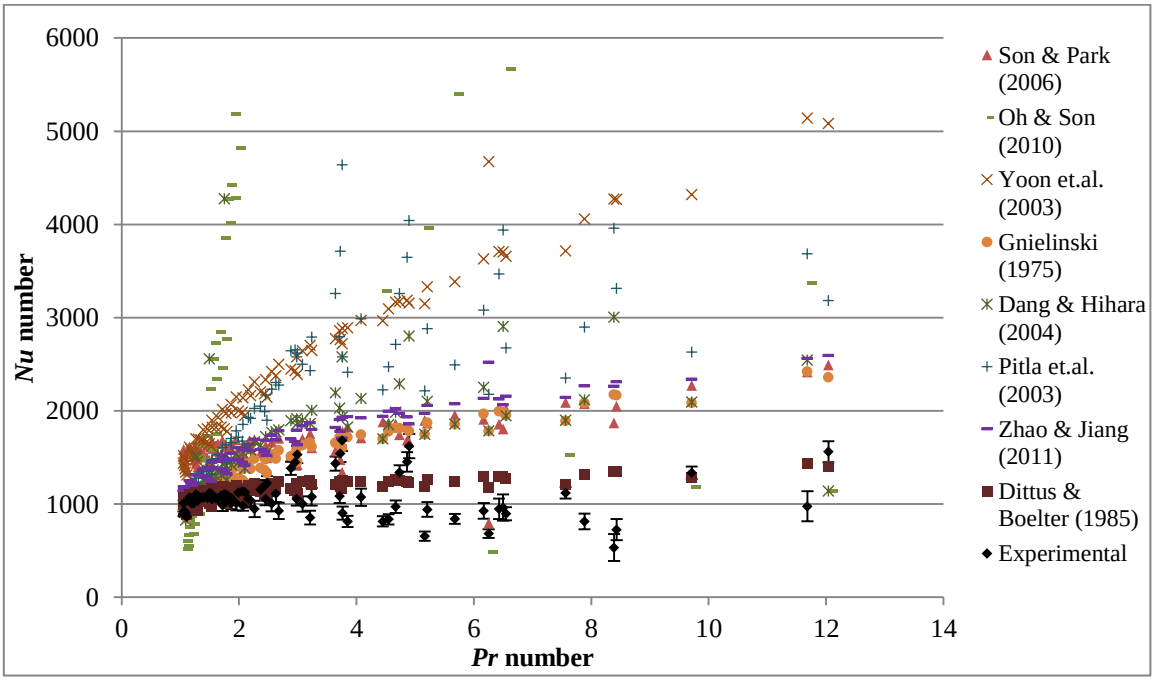

Figure 17: *Nu* numbers plotted against *Pr* numbers. This plot combines all data sets (8MPa – 11MPa) by plotting against the non-dimensional *Pr* number.

Table 10: Percentage error of each correlation for various *Pr* numbers.

Prandtl number	Dittus & Boelter (1985)	Son & Park (2006)	Yoon et.al. (2003)	Oh & Son (2010)	Gnielinski (1975)	Pitla et.al. (2003)	Dang & Hihara (2004)	Zhao & Jiang (2011)
0-2	6%	51%	63%	117%	9%	30%	28%	26%
2-4	21%	48%	127%	1322%	37%	127%	180%	54%
4-6	32%	77%	212%	750%	75%	184%	104%	94%
6-8	34%	103%	272%	689%	102%	198%	123%	120%
8-10	47%	112%	319%	996%	119%	228%	152%	135%
10-12	30%	115%	371%	138%	109%	210%	97%	127%
Average	**20%**	**66%**	**143%**	**458%**	**45%**	**107%**	**73%**	**62%**

Dittus & Boelter (1985) correlation

The Dittus & Boelter (1985) correlation compared well with experimental values with an average error of 9% at 350'000 < *Re* < 550'000. Substantial errors were seen at *Re* numbers in the range of 400'000 to 450'000, clearly indicating a fluid property variation in experimental data in this region of the gas cooler. From Table 10 the average error is only 6% from 0 < *Pr* < 2 ranging up to an average error of 30% for 8 < *Pr* < 10.

Son & Park (2006) correlation

This correlation generally over-predicted *Nu* over the entire range of *Re* numbers, compared to the experimental *Nu* values. For *Re* > 450'000 an average error of 52% was recorded. According to the literature, the correlation of Son & Park (2006) is valid for a mass flux range of 200 to 400 kg/m^2.s. These mass flux values will produce *Re* numbers of approximately[14] 50'000 < *Re* < 150'000 which is much lower than the *Re* numbers seen in experimental tests from this study. The same amount of deviation is seen from the *Nu vs. Pr* plot, where the average error increases as *Pr* increases.

Yoon *et.al.* (2003) correlation

The correlation by Yoon *et.al.* (2003) over-predicts *Nu* to a large extend over the entire range of *Re* numbers evaluated when compared to the experimental *Nu* values. This correlation was tested by the authors at mass fluxes of 225 to 450 kg/m^2.s. For the flow conditions specified in the literature, this translates to 60'000 < *Re* < 170'000. By applying this correlation for much higher *Re* numbers the over-prediction of *Nu* can be ascribed to the dominant effect of *Re* in the correlation as seen in equation (3.22). When looking at the *Pr* numbers, the Yoon *et.al.*(2003) correlation over-predicts *Nu* increasingly as *Pr* increases.

Oh & Son (2010) correlation

The correlation by Oh & Son (2010) shows the highest deviation from experimental values captured. This correlation also shows very large fluctuations in *Nu* numbers for the same region of *Re*. These large deviations may be ascribed to the use of inappropriate property parameter groups such as $c_{p,b} / c_{p,w}$ with negative exponents derived specifically for the study done by Oh & Son (2010). The *Re* numbers tested by the authors ranged from 40000 < Re < 210'000 which is lower than the *Re* numbers seen in experimental tests from this study. The volatility and high % errors of this correlation make it unsuitable for further analysis.

Gnielinski (1975) correlation

The correlation by Gnielinski (1975) compared relatively well with experimental data at *Re* numbers between 600'000 < *Re* < 700'000 with an average error value of 9.5% over this *Re* increment, making this correlation the second most accurate from the correlations analysed in this study. For lower *Re* numbers this correlation deviates up to 138%. For *Pr* < 2 the average error was 9% from where it increased over the *Pr* range up to 109% for 10 < *Pr* < 12.

[14] *Re* numbers can be calculated by using the stated inlet / outlet temperatures, pressures, mass flux and geometry found in the published literature for the particular correlation.

Pitla *et.al.* (2003) correlation

The correlation by Pitla *et.al.*(2003) shows increasingly larger deviations from experimental data as the *Re* number decreases. As seen in Table 9, the minimum error of this correlation was 17% at 650'000 < *Re* < 700'00 as opposed to the maximum error of 275% at 400'000 < *Re* < 450'000. The experimental tests by Pitla *et.al.* (2003) were done at *Re* numbers ranging from 95'000 < *Re* < 415'000. In Figure 16 and Figure 17 is clear that this correlation is not packed closely together, but scatters over the chart. The inaccuracy of this correlation may be ascribed to the different flow conditions and smaller tube geometries tested by Pitla *et.al.* (2003).

Dang & Hihara (2004) correlation

From the correlations developed specifically for supercritical CO_2, the correlation by Dang & Hihara (2004) performed second best with an average error of 15.5% for 600'000 < *Re* < 700'000 and an average error of 95.6% for 350'000 < *Re* < 600'000. The correlation deviates increasingly from the experimental values as *Re* decreases and *Pr* increases. The experimental tests done by Dang & Hihara (2004) were at *Re* numbers ranging from 15'000 < *Re* < 53'000. With reference to Figure 16, the Nu_{exp} numbers predicted by this correlation is quite unstable with a bit of scatter. The flow conditions and tube geometry used by the authors to analyse the radial distribution to derive equation (3.24) differed significantly from the flow conditions in this study, thus accounting for the large errors and scatter observed.

Zhao & Jiang (2011) correlation

The correlation by Zhao & Jiang (2011) showed an average error of 39.6% at 450'000 < *Re* < 700'000 and 138% from 350'000 < *Re* <450'000. Zhao & Jiang (2011) confirmed their correlation to be valid over a *Re* number range of 4000 < *Re* < 80'000, pressures from 4.5MPa < P_{co2} < 5.5MPa and *Pr* from 1.2 < *Pr* < 8.8. From all the correlations developed specifically for supercritical CO_2 this correlation compared the most accurate. This Gnielinski-based correlation, eq. (3.32), employs a property variation coefficient accounting for property variations in the radial and axial directions of the test section. By accounting for thermo-physical property variation in the axial direction (along the test section as cooling progresses), less emphasis is placed on the property changes in the radial direction. Due to the high *Re* numbers measured in the experimental facility, the velocity boundary layer is flatter and thus the property change in the radial direction would differ much from what was seen in most of the studies found in the literature. It was argued that this correlation therefor might be more suitable over a larger range of *Re* due to the twofold property variation coefficient employed.

5.3.3 Effect of the pseudo-critical point

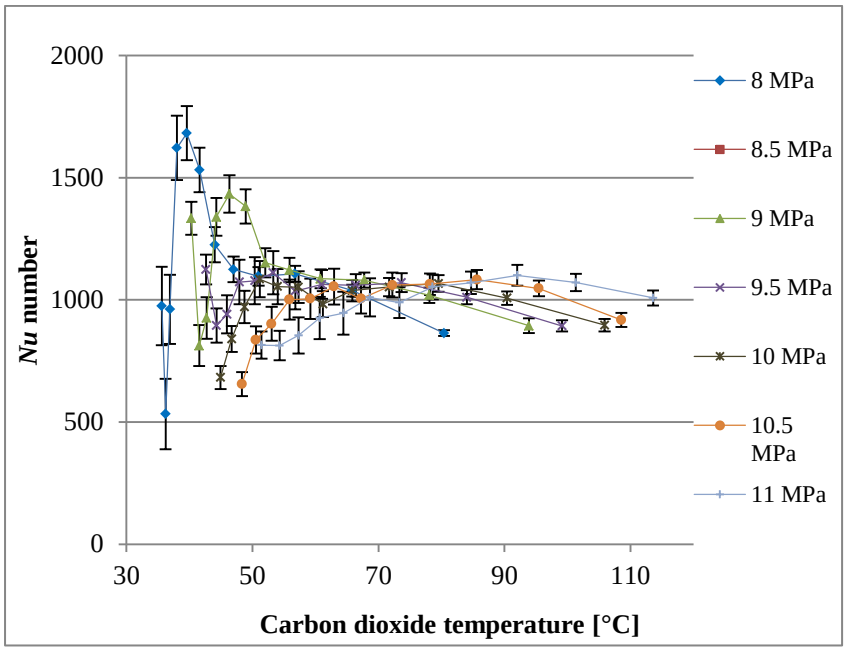

Figure 18: Nu_{exp} numbers plotted against CO_2 temperature to illustrate the effect of fluid property variations near the pseudo-critical region on *Nu* numbers.

Table 11: The pseudo-critical temperature of CO_2 at various pressures.

CO_2 pressure [MPa]	Pseudo-critical temperature [°C]
8	34.69
8.5	37.38
9	40.02
9.5	42.56
10	45.01
10.5	47.37
11	49.65

Table 11 shows the pseudo-critical temperature for each pressure shown in Figure 18.

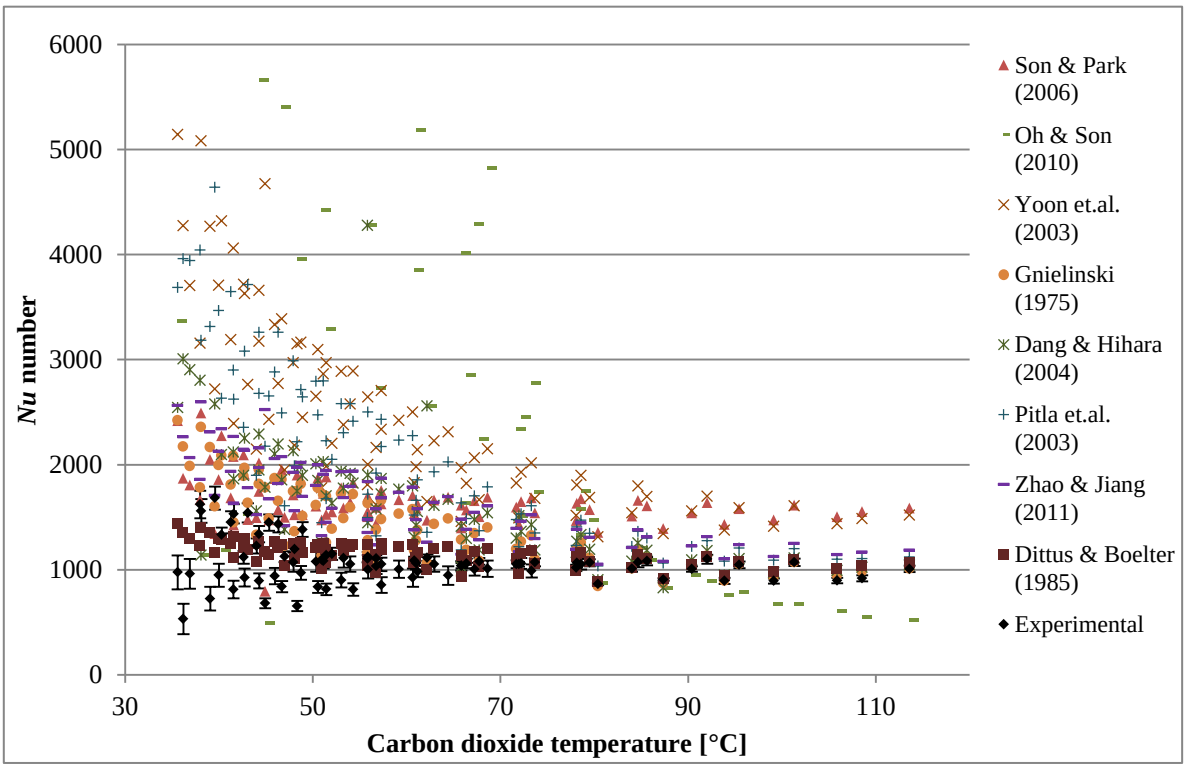

Figure 19: *Nu* numbers plotted against carbon dioxide temperature to illustrate the effect of fluid property variations near the pseudo-critical region.

As mentioned earlier, vast property changes occur when the pseudo-critical point is approached. It is therefore important to consider the effect of the pseudo-critical point in the temperature glide seen in a gas cooler and

the effect it has on the heat transfer and *Nu* correlations.

The Nu_{exp} numbers plotted against T_{CO2} are shown in Figure 18. Note that at lower pressures, a more prominent spike in Nu_{exp} is seen. This stands in agreement to the severity of thermo-physical property variations seen in Figure 1. The exact same experimental data seen in Figure 18 is also shown in Figure 19 together with Nu_{theo} numbers as calculated by the different correlations and scaled accordingly. It becomes clear that the thermo-physical property variations near the pseudo-critical point have a much larger effect on the correlated values than on the experimental data.

With reference to Figure 19, the following observations were made regarding some correlations described in the previous section:

- It can clearly be seen that Dittus & Boelter (1985) is the only correlation remaining relatively stable throughout the pseudo-critical region due to the absence of thermo-physical property ratios in the correlation.
- The correlations by Son & Park (2006) and Yoon *et.al.* (2003) over-predicts the *Nu* numbers increasingly as the carbon dioxide temperature approaches the pseudo-critical region. The effort in minimizing the effect of thermo-physical property change by introducing a specific heat ratio to the Dittus & Boelter-type equation has a negative impact on the accuracy of the correlation at higher *Re* numbers and larger tube geometries than what were analysed by the developers of these correlations.
- When considering the Gnielinski (1975) correlation, it is seen that high deviations exist near the pseudo-critical region as the gas cools down. It is also interesting to note that the Gnielinski (1975) correlation serves as the basis equation for numerous other heat transfer correlations including the correlation of Pitla *et.al* (2003), Dang & Hihara (2004) and Zhao & Jiang (2011), all of which over-predicts the *Nu* value near the pseudo-critical region.

Thus, for the flow conditions analysed in this experimental study, the correlations specifically developed for supercritical cooling of CO_2 over emphasise the factors addressing the variations seen in the thermo-physical properties. The *Re* number band analysed in this study vastly exceeded the *Re* numbers of other studies. Conclusively, at higher *Re* numbers the property variations near the pseudo-critical region has a lesser effect on *Nu* numbers.

5.3.4 Convective heat transfer mechanism

Thus far, all *Nu* correlations evaluated were functions of *Re*, *Pr* and fluid property ratios of some sort, implying that the dominant heat transfer mechanism present is forced convection (as opposed to the presence of the *Gr* number in free convection correlations). According to the publication of Du *et.al.*(2010), free convection may be considered as a heat transfer mechanism in the cooling of supercritical CO_2 as discussed in section 2.3.6 This statement was investigated by calculating the ratio between *Gr* and Re^2 and plotting experimental values against CO_2 temperatures. The combined effects of free convection and forced convection must be considered when $Gr \approx Re^2$. Furthermore, free convection may be neglected when $Gr \ll Re^2$

(Incropera *et.al*, 2011). As seen in Figure 20, forced convection is the dominant convective heat transfer mechanism observed in the experimental results with all $Gr/Re^2 < 0.04$ and the mean value equal to *0.009*. It is however noted that the ratio of relative importance (Gr/Re^2) of free convection becomes larger as carbon dioxide temperature approaches the pseudo-critical region.

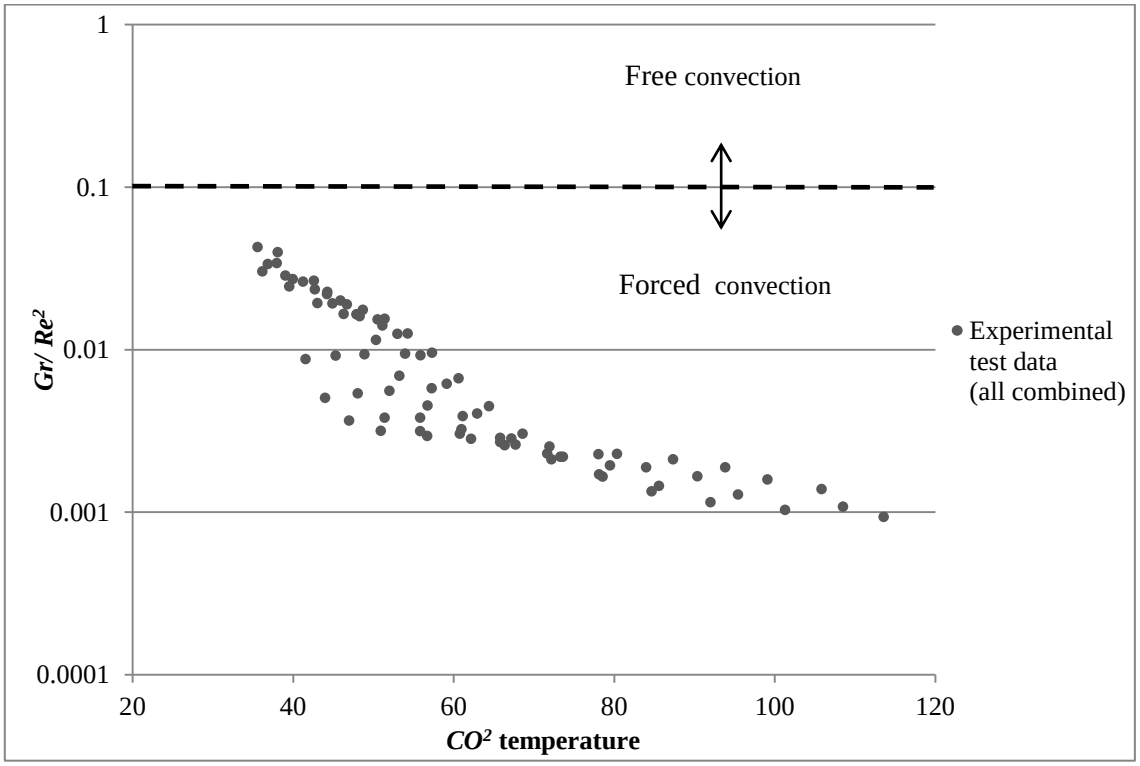

Figure 20: The ratio between *Grashof* number and the squared *Reynolds* number gives indication of the relative roles of free convection *vs.* forced convection in convective heat transfer. Free convection becomes dominant when this ratio is larger than 0.1 (Incropera *et.al.*, 2011).

5.4 Conclusions

In this chapter the eight correlations from the literature review were critically compared to experimental data obtained from the trans-critical carbon dioxide test bench. Table 12 shows a summary of the average relative errors made by each correlation.

Table 12: Summary of results obtained in chapter 5.

Nu Correlation	Average relative error (%)
Dittus & Boelter (1985)	20%
Son & Park (2006)	66%
Yoon *et al.* (2003)	143%
Oh & Son (2010)	458%
Gnielinski (1975)	45%
Pitla *et al.* (2002)	107%
Dang & Hihara (2004)	73%
Zhao & Jiang (2011)	62%

In section 5.1 the method of data reduction was explained. This included the validation of data and the explanation of the non-linear regression applied to the data. Section 5.2 elaborated on the propagation of

uncertainty in the calculation of Nu_{exp}. A comparison between experimental and theoretical data was further shown in section 5.3.

The following conclusions were made when comparing experimental Nu_{exp} to Nu_{theo}:

- The Dittus & Boelter (1985) correlation predicts *Nu* values the best with an average relative error of 20% over the entire *Re* range and with an average of 9% at 350'000 < *Re* < 550'000. The second best performance was seen by the correlation of Gnielinski (1975) with an average relative error of 45% over the entire *Re* range and 9.5% for *Re* numbers between 600'000 < *Re* < 700'000.
- *Nu* values are generally over-predicted by most correlations.
- At temperatures close to the pseudo-critical point theoretical Nu_{theo} values responds very volatile to the change in fluid properties whereas Nu_{exp} remains relative constant. This phenomenon was observed especially in correlations where complex fluid property ratios are used.
- It is notable that the two correlations with the highest accuracies (Dittus & Boelter (1985) and Gnielinski (1975)) are the only two correlations not specifically developed for supercritical carbon dioxide cooling and therefor does not contain any property ratios as an additional factor in the correlation.
- In general the correlations evaluated in this study were developed for much lower *Re* number ranges than what were measured in the experimental tests. This allowed for the conclusion to be made that the thermo-physical property variations plays a larger role in the *Nu* numbers for flow conditions with lower *Re* numbers, as found by numerous studies in the literature.

Chapter 6 CONCLUSION AND RECOMMENDATIONS

The research question of this study was to test and validate *Nu* correlations for cooling heat transfer of supercritical carbon dioxide by specifically using a larger tube diameter (16mm) than was generally used (1mm to 7.75mm) in published experimental studies.

A comprehensive literature survey (chapter 2) was done on previous studies to identify relevant *Nu* correlations to be validated. Relevant theoretical concepts, laws and correlations quoted in the literature study were discussed in chapter 3. Detailed information regarding the choice of experimental methods used to answer the research question was discussed in chapter 4.

It was shown in chapter 5 how data reduction was done with the incorporation of uncertainty propagation throughout. The *Re* and *Pr* numbers were used as common parameters to compare experimental and theoretical data. Relative errors between experimental and theoretical values were calculated and specific trends were observed:

- Nu_{exp} numbers are generally over-predicted by Nu_{theo} at all test conditions by the correlations specifically developed for the supercritical cooling of carbon dioxide. An increasing over-prediction was seen as *Re* decreased.
- The correlation by Dittus & Boelter (1985) correlated the best with experimental data with an average relative error of 9% between 350’000 < *Re* < 550’000 and 20% over the entire range of 350’000 < *Re* < 700’000.
- For the correlations specifically developed for supercritical carbon dioxide cooling, it was calculated that the *Re* range tested by the previous experimental studies were generally much lower than the range tested in the current study. From these correlations the lowest relative errors were achieved with the correlation by Zhao & Jiang (2011) with a relative error of 39% for 450’000 < *Re* < 7000’000 and an average error of 68% over the entire range of *Re* tested.

- At higher *Re* numbers, the effect of property variations near the pseudo-critical region seems to be much lower on the experimental data than what was seen in the theoretical predictions. The need to address these thermo-physical property variations with property ratio correction factors seems to have a negative effect on the accuracy of the correlations. The weight attributed to the property ratios should be reduced when applying the correlations at higher *Re* numbers.
- None of the correlations specifically developed for carbon dioxide were regarded as valid for design purposes for a gas cooler with larger tube geometries and high *Re* numbers.

Conclusion

The experimental results were most accurately predicted by the Dittus & Boelter (1985) correlation, which unlike specialized supercritical carbon dioxide correlations do not employ complex fluid property ratios.

Due to the simplicity of this correlation, it is very convenient for use when simulating or designing a supercritical carbon dioxide gas cooler with larger diameters.

The statement by Andresen (2006) and Mitra (2005) that property correction coefficients must be introduced due to the dissimilarity of wall and bulk temperatures, must be quantified in terms of *Re* number ranges. It was concluded from this study that these property correction coefficients have a negative impact on the prediction of *Nu* numbers for the conditions tested by this study.

Recommendations for further work

The following points can be seen as positive inputs to further studies relating the characterization and analysis of trans-critical carbon dioxide heat pump systems:

- It has been concluded that correlations developed specifically for supercritical carbon dioxide cooling are invalid for the test conditions evaluated in the experimental setup. Further tests should include conditions at lower *Re* numbers in large geometry tubes as well as high *Re* numbers in smaller geometry tubes. This would further clarify the validity of use of some of the correlations designed specifically for supercritical cooling of carbon dioxide.
- For further work done on the gas cooler of the test bench at the NWU facility it is recommended that the root cause of instrumentation fluctuations be found and corrected to ensure that highly reliable raw data can be captured. The accuracy of the temperature sensors should also be re-evaluated and possibly be replaced with devices of higher accuracy.

BIBLIOGRAPHY

ALDANA, J.P., GEORGIADIS, J. and JACOBI, A. 2002. Critical heat flux of CO_2 in a microchannel at elevated subcritical pressures. Air Conditioning and Refrigeration Center. College of Engineering. University of Illinois at Urbana-Champaign

ANDRESEN, U.C. 2006. Supercritical gas cooling and near-critical-pressure condensation of refrigerant blends in microchannels. Ph.D. thesis. Department of Mechanical Engineering, Georgia Institute of Technology.

AUSTIN, B.T. and SUMATHY, K. 2011. Transcritical carbon dioxide heat pump systems: A review. *Renewable and Sustainable Energy Reviews* 10, 15(8), 4013-4029.

BASKOV, V., KURAEVA, I. and PROTOPOPOV, V. 1977. Heat transfer with the turbulent flow of a liquid at supercritical pressure in tubes under cooling conditions. *Teplofizika Vysokikh Temperatur*, 15(1), 96-102.

BITZER. 2010. *Data Sheet: 4JTC-15K*. Bitzer. 2010/07/19, Available from: https://www.bitzer.de/eng/productservice/p3/127.

BRINGER, R. and SMITH, J. 1957.Heat transfer in the critical region. *AIChE Journal*, 3(1), 49-55.

CALM, J.M. 2008.The next generation of refrigerants-historical review, considerations, and outlook. *International Journal of Refrigeration*, 31(7), 1123-1133.

CHENG, C., MA, W. and HUANG, W., 1994. Numerical Predictions of Entropy Generations for Mixed Convective Flows in a Vertical Channel with Transverse Fin Array. *International Communications in Heat and Mass Transfer*, 21, 4, 519-530.

CHENG, L., RIBATSKI, G. and THOME, J.R. 2008.Analysis of supercritical CO_2 cooling in macro- and micro-channels. *International Journal of Refrigeration* 12, 31(8), 1301-1316.

COLEMAN, H.W. & STEELE, W.G.2009. *Experimentation, Validation, and Uncertainty Analysis for Engineers*. John Wiley & Sons.

DANFOSS. 2011a. *AK2-SC 255 Quick Reference Guide*. 2011/10/31, Available from: http://www.danfoss.com/BusinessAreas/RefrigerationAndAirConditioning/Products/Literature/RA/Electronic

-Controls/Electronic-Controls-System-Management/System-Controller/AK-SC-255-System-Controller/52d52d61-c5c3-4889-8c91-adb04387eba3.html.

DANFOSS. 2011b. *AKS 12, PT 1000 Temperature Sensor*. 2011/12/09, Available from: http://www.danfoss.com/BusinessAreas/RefrigerationAndAirConditioning/Products/Literature/RA/Electronic-Controls-Sensors-Transmitters/AKSEKS-Temperature-sensors/AKS-12-PT-1000-Temperature-Sensor/dcd58815-b99b-49d0-8537-7754413b8151.html.

DANFOSS. 2011c. *AKS 2050, Ratiometric Output Signal*. 2011/08/19, Available from: http://www.danfoss.com/Products/Categories/Photos/RA/Electronic-Controls-Sensors-Transmitters/AKS-pressure-transmitters/AKS-2050-ratiometric-output-signal/56b6273e-3ccd-499b-9fa0-f6cf8ef26aa2.html.

DANFOSS. 2010.*MBT 3270, Temperature Sensors*.2010/04/13, Available from: http://www.danfoss.com/BusinessAreas/IndustrialAutomation/Products/List/IA/Temperature-Monitoring-and-Control/Temperature-sensors/MBT-3270-Temperature-sensors/0f6a30a7-6d79-4919-ba95-a20ed2afb9fe.html.

DANFOSS. 2008. *AKD 102, Variable Speed Drives*. 2008/09/26, Available from: http://www.danfoss.com/Products/Categories/Literature/RA/Electronic-Controls/Electronic-Controls-Speed-control-of-Compressors-Condensers-and-Fans/Variable-Speed-Drives/AKD-102-Variable-Speed-Drives-200-240V/3ee18c9f-60d3-438c-9ff5-0342cb905409.html.

DANG, C. and HIHARA, E. 2004. In-tube cooling heat transfer of supercritical carbon dioxide. Part 1. Experimental Measurement. *International Journal of Refrigeration*, 27(7), 736-747.

DANG, C., IINO, K., FUKUOKA, K. and HIHARA, E. 2007. Effect of lubricating oil on cooling heat transfer of supercritical carbon dioxide. *International Journal of Refrigeration*, 30(4), 724-731.

DITTUS, F.W. and BOELTER, L.M.K. 1985. Heat transfer in automobile radiators of the tubular type. *International Communications in Heat and Mass Transfer*, 12(1), 3-22.

DU, Z., LIN, W. and GU, A., 2010. Numerical Investigation of Cooling Heat Transfer to Supercritical CO2 in a Horizontal Circular Tube. *The Journal of Supercritical Fluids*, 11(55), 116-121.

ENDRESS & HAUSER. 2010a. *Promag 50P*. 2010/02/01, Available from: http://www.br.endress.com/#product/50P?open.

ENDRESS & HAUSER. 2010b. *Promass 80M*. 2010/04/01, Available from: http://www.br.endress.com/#product/80M.

FANG, X., BULLARD, C.W. and HRNJAK, P.S. 2001. Heat transfer and pressure drop of gas coolers. *ASHRAE Trans*, 107(1), 255-266.

GHAJAR, A. and ASADI, A. 1986. Improved forced convective heat-transfer correlations for liquids in the near-critical region. *AIAA Journal*, 24, 2030-2037.

GNIELINSKI, V. 1975. New equations for heat and mass transfer in the turbulent flow in pipes and channels. *NASA STI/Recon Technical Report A*, 752, 22028.

HIROAKI, T., NIICHI, N., MASARU, H. and AYAO, T. 1971.Forced convection heat transfer to fluid near critical point flowing in circular tube. *International Journal of Heat and Mass Transfer*, 14(6), 739-750.

HUAI, X.L., KOYAMA, S. and ZHAO, T.S. 2005. An experimental study of flow and heat transfer of supercritical carbon dioxide in multi-port mini channels under cooling conditions. *Chemical Engineering*

Science 6, 60(12), 3337-3345.

INCROPERA, F.P., BERGMAN, T.L., LAVINE, A.S. and DEWITT, D.P. 2011. *Fundamentals of Heat and Mass Transfer*. Wiley.

JING, W., TAO, T., XIYUAN, L. and YIFEI, P. 2012. Analysis on Influence of Gravity on Convection Heat Transfer in Manned Spacecraft during Terrestrial Test. *World Academy of Science, Engineering and Technology*, 69, 661 - 666.

KIM, M., PETTERSEN, J. and BULLARD, C.W. 2004. Fundamental process and system design issues in CO_2 vapor compression systems. *Progress in Energy and Combustion Science*, 30(2), 119-174.

KLEIN, S. and ALVARDO, F. 2009. EES – Engineering Equation Solver. User's manual for Microsoft Windows Operating Systems, Version 8.609. *F-Chart Software, Madison, WI, USA*.

KRASNOSHCHEKOV, E., KURAEVA, I. and PROTOPOPOV, V. 1970. Local heat transfer of carbon dioxide at supercritical pressure under cooling conditions. *Teplofizika Vysokikh Temperatur*, 7(5), 922-930.

KRASNOSHCHEKOV, E. and PROTOPOPOV, V. 1966. Experimental study of heat exchange in carbon dioxide in the supercritical range at high temperature drops (heat transfer in turbulent carbon dioxide pipeflow at supercritical region). *High Temperature*, 4, 375-382.

LIAO, S. 2002. Measurements of heat transfer coefficients from supercritical carbon dioxide flowing in horizontal mini/micro channels. *Journal of Heat Transfer*, 124, 413.

MCADAMS, W.H. 1954. *Heat transmission.* McGraw-Hill New York.

MITRA, B. 2005. Supercritical gas cooling and condensation of refrigerant R410A at near-critical pressures. Georgia Institute of Technology.

MONTREAL PROTOCOL. 1987. Montreal Protocol on substances that deplete the ozone layer. *Washington, DC: US Government Printing Office*, 26.

MORI, K., SHIMAOKA, H., ONISHI, J., FUJIMOTO, K., YAMAMOTO, N. and NAKANISHI, S. 2003. Heat transfer characteristics of CO_2 and CO_2-oil mixtures in cooling stage at supercritical pressure conditions. *Proceedings of the Eurotherm seminar no. 72, March 30–April 2; Valencia, Spain*.

MUNSON, B.R., YOUNG, D.F. and OKIISHI, T.H. 1999. *Fundamentals of fluid mechanics.* John Wiley & Sons, Inc.

OH, H. and SON, C. 2010. New correlation to predict the heat transfer coefficient in-tube cooling of supercritical CO_2 in horizontal macro-tubes. *Experimental Thermal and Fluid Science* 11, 34(8), 1230-1241.

PEARSON, A. 2005. Carbon dioxide—new uses for an old refrigerant. *International Journal of Refrigeration*, 28(8), 1140-1148.

PETROV, N. and POPOV, V. 1985. Heat transfer and resistance of carbon dioxide being cooled in the supercritical region. *Thermal Engineering*, 32(3), 131-134.

PETTERSEN, J., RIEBERER, R., MUNKEJORD, ST 2000. *Heat transfer and pressure drop for flow of supercritical and subcritical CO_2 in microchannel tubes*. Norwegian University of Science and Technology Trondheim Department of Refrigeration and Air Conditioning.

PETUKHOV, B., KRASNOSHCHEKOV, E. and PROTOPOPOV, V. 1961. An Investigation of heat transfer to fluids flowing in pipes under supercritical conditions. *ASME International Developments in Heat Transfer Part*, 3, 569-578.

PETUKHOV, B. 1974. *Turbulent Heat transfer in tubes with variable fluid properties.* Heat exchangers: design and theory sourcebook. Scripta Book Co.

PITLA, S.S., GROLL, E.A. and RAMADHYANI, S. 2001. Convective heat transfer from in-tube cooling of turbulent supercritical carbon dioxide: part 2—experimental data and numerical predictions. *HVAC&R Research*, 7(4), 367-382.

PITLA, S.S., ROBINSON, D.M., GROLL, E.A. and RAMADHYANI, S. 1998. heat transfer from supercritical carbon dioxide in tube flow: a critical review. *Hvac&R Research*, 4(3), 281-301.

PITLA, S.S., GROLL, E.A. and RAMADHYANI, S. 2002. New correlation to predict the heat transfer coefficient during in-tube cooling of turbulent supercritical CO_2. *International Journal of Refrigeration* 11, 25(7), 887-895.

ROUSSEAU, P.G. 2011. Thermal-Fluid Systems Modelling II: Course Notes 2011. Potchefstroom: Platinum Press.

ROUSSEAU, P.G., C. DU TOIT, W. VAN ANTWERPEN and H. VAN ANTWERPEN. 2012. Separate Effects Tests to Determine the Effective Thermal Conductivity in the PBMR HTTU Test Facility, *HTR2012-6-022, Tokyo, Japan*

RICE, J.A. 2007. *Mathematical Statistics and Data Analysis.* Duxbury press.

SHITSMAN, M. 1963. Impairment of the heat transmission at supercritical pressures (heat transfer process examined during forced motion of water at supercritical pressures). *High Temperature*, 1, 237-244.

SON, C. and PARK, S. 2006. An experimental study on heat transfer and pressure drop characteristics of carbon dioxide during gas cooling process in a horizontal tube. *International Journal of Refrigeration* 6, 29(4), 539-546.

SONNTAG, R.E., BORGNAKKE, C. and VAN WYLEN, G.J. 2003. *Fundamentals of Thermodynamics*. Wiley.

UNFCOCC (UNITED NATIONS FRAMEWORK CONVENTION ON CLIMATE CHANGE). 1997. Kyoto Protocol. Kyoto.

VENTER, P. 2010. A supercritical R-744 heat transfer simulation implementing various Nusselt number correlations. M. Ing. dissertation. School for Mechanical and Nuclear Engineering, North-West University, Potchefstroom campus.

YOON, S.H., KIM,J.H., HWANG, Y.W., KIM, M.S., MIN, K. and KIM,Y. 2003. Heat Transfer and pressure drop characteristics during the in-tube cooling process of carbon dioxide in the supercritical region. *International Journal of Refrigeration* 12, 26(8), 857-864.

ZHAO, C. and JIANG, P. 2011. Experimental study of in-tube cooling heat transfer and pressure drop characteristics of R134a at supercritical pressures. *Experimental Thermal and Fluid Science* 10, 35(7), 1293-1303.

APPENDIX A - EES program

```
"Analysis of a supercritical carbon dioxide gas cooler – 85 Bar test condition"
"Programming code for Engineering Equation Solver"
"by Marius Harris"

{Procedure Nusselt number Son and Park}

Procedure Nu_sp(rho_co2_sp, rho_co2_w_sp,Re_Co2_SP,
Pr_co2_sp,Cp_co2_sp,Cp_co2_w_sp,T_co2_sp,T_co2_pc:Nu_co2_sp)

If (T_co2_sp > T_co2_pc) then
    Nu_co2_sp =Re_CO2_SP^0.55*Pr_CO2_SP^0.23*(Cp_CO2_SP/Cp_co2_w_SP)^0.15
else
    Nu_co2_sp =Re_CO2_SP^0.35*Pr_CO2_SP^1.9*((rho_co2_sp/rho_co2_w_sp)^(-
    1.6))*(Cp_CO2_SP/Cp_co2_w_SP)^(-3.4)
endif

END {procedure}

{Procedure Nusselt number Yoon}

Procedure Nu_yn(Re_co2_yn,Pr_co2_yn,rho_co2_yn, rho_co2_pc,T_co2_gem_yn,T_co2_pc:Nu_co2_yn)
if (T_co2_gem_yn > T_co2_pc) then
    Nu_CO2_YN = 0.14*Re_co2_YN^0.69*Pr_CO2_YN^0.66
else
    Nu_co2_yn = 0.013*Re_co2_yn*Pr_co2_yn^(-0.05)*(rho_co2_pc/rho_co2_yn)^1.6
endif

END

{Procedure Nusselt number Oh and Son}

Procedure
Nu_OS(Re_CO2_OS,Pr_Co2_OS,rho_co2_OS,rho_co2_w_OS,Cp_CO2_OS,CP_CO2_w_OS,T_co2_gem_os,T_co2_pc
:Nu_co2_os)
If (T_co2_gem_os>T_co2_pc) then
    Nu_CO2_OS = 1*(0.023*Re_CO2_OS^0.7*Pr_Co2_OS^2.5*(Cp_CO2_OS/CP_CO2_w_OS)^(-3.5)) +
    0.0*(Re_CO2_os^0.55*Pr_CO2_os^0.23*(Cp_CO2_os/Cp_co2_w_os)^0.15)
else
    Nu_CO2_OS
```

```
    =0.023*Re_CO2_OS^0.6*Pr_Co2_OS^3.2*(rho_co2_OS/rho_co2_w_OS)^3.7*(Cp_CO2_OS/CP_CO2_w_OS)^(-
    4.6)
endif
END {Procedure}

{Procedure Nusselt number Dang and Hihara}
Procedure
Nu_Dh(f_f_f_dh,Re_co2_dh,cp_co2_dh,mu_co2_dh,k_co2_dh,cpint_co2_dh,mu_co2_f_dh,k_co2_f_dh:nu_co2_dh)

if (cp_co2_dh > cpint_co2_dh) then
Pr_co2_dh = cp_co2_dh*mu_co2_dh/k_co2_dh
else
    if ((cp_co2_dh < cpint_co2_dh) and ( mu_co2_dh/k_co2_dh >= mu_co2_f_dh/k_co2_f_dh)) then
    Pr_co2_dh = cpint_co2_dh*mu_co2_dh/k_co2_dh
    else
      if ((cp_co2_dh < cpint_co2_dh) and ( mu_co2_dh/k_co2_dh < mu_co2_f_dh/k_co2_f_dh)) then
      Pr_co2_dh = cpint_co2_dh*mu_co2_f_dh/k_co2_f_dh
      endif
    endif
endif
Nu_co2_dh = (f_f_f_DH /8)*(Re_co2_DH - 1000)*Pr_CO2_DH*(1.07+12.7*sqrt(f_f_f_dh/8)*(Pr_co2_DH^(2/3)-1))^(-
1)
END {Procedure}

{Procedure Nusselt number Zhao and Jiang}
Procedure
nu_zj(f_f_zj,Re_co2_zj,Pr_co2_zj,Pr_co2_w_zj,ID_inner,L,T_co2_gem_zj,T_co2_pc,cpmean_co2_zj,cp_co2_zj,rho_co
2_zj,rho_co2_w_zj,T_co2_w_zj:nu_co2_zj)
if (T_co2_gem_zj<=T_co2_pc) then
    C_vp = 0.93*((Pr_co2_w_zj/Pr_co2_zj)^(-
    0.11))*((cpmean_co2_zj/cp_co2_zj)^0.96)*((rho_co2_w_zj/rho_co2_zj)^1.06)
else
    C_vp = 1.07*((T_co2_w_zj/T_co2_gem_zj)^(-
    0.45))*((cpmean_co2_zj/cp_co2_zj)^0.61)*((rho_co2_w_zj/rho_co2_zj)^(-0.18))
endif

Nu_co2_zj = (f_f_ZJ/8)*(Re_Co2_ZJ - 1000)*(Pr_co2_ZJ)*((1.07+12.7*sqrt(f_f_ZJ/8)*(Pr_co2_ZJ^(2/3)-1))^(-
1))*(1+(ID_inner/L)^(2/3))*C_vp
END {Procedure}

"Procedure to import test data from CSV file containing test data"
Procedure TESTDATA_85(row,col:value)
    value = Lookup('testdata_85.csv',row,col)
end
filename$ = 'D:\...\export_from_ees_85.csv'

{============================MAIN PROGRAM============================}
"=========================Import Test data 85 BAR ========================="

Call TESTDATA_85 (1,26:T_w_TD[0])
Call TESTDATA_85(1,25:T_w_TD[1])
Call TESTDATA_85(1,24:T_w_TD[2])
Call TESTDATA_85(1,23:T_w_TD[3])
Call TESTDATA_85(1,22:T_w_TD[4])
Call TESTDATA_85(1,21:T_w_TD[5])
Call TESTDATA_85(1,20:T_w_TD[6])
Call TESTDATA_85(1,19:T_w_TD[7])
Call TESTDATA_85(1,18:T_w_TD[8])
Call TESTDATA_85(1,17:T_w_TD[9])
Call TESTDATA_85(1,16:T_w_TD[10])
```

Call TESTDATA_85(1,15:T_w_TD[11])
Call TESTDATA_85(1,14:T_w_TD[12])

{gas side}
Call TESTDATA_85(1,1:T_CO2_TD[0])
Call TESTDATA_85(1,2:T_CO2_TD[1])
Call TESTDATA_85(1,3:T_CO2_TD[2])
Call TESTDATA_85(1,4:T_CO2_TD[3])
Call TESTDATA_85(1,5:T_CO2_TD[4])
Call TESTDATA_85(1,6:T_CO2_TD[5])
Call TESTDATA_85(1,7:T_CO2_TD[6])
Call TESTDATA_85(1,8:T_CO2_TD[7])
Call TESTDATA_85(1,9:T_CO2_TD[8])
Call TESTDATA_85(1,10:T_CO2_TD[9])
Call TESTDATA_85(1,11:T_CO2_TD[10])
Call TESTDATA_85(1,12:T_CO2_TD[11])
Call TESTDATA_85(1,13:T_CO2_TD[12])

Call TESTDATA_85(1,27:P_CO2_TD[0]/100)
Call TESTDATA_85(1,27:P_CO2_TD[1]/100)
Call TESTDATA_85(1,28:P_CO2_TD[2]/100)
Call TESTDATA_85(1,28:P_CO2_TD[3]/100)
Call TESTDATA_85(1,29:P_CO2_TD[4]/100)
Call TESTDATA_85(1,29:P_CO2_TD[5]/100)
Call TESTDATA_85(1,30:P_CO2_TD[6]/100)
Call TESTDATA_85(1,30:P_CO2_TD[7]/100)
Call TESTDATA_85(1,31:P_CO2_TD[8]/100)
Call TESTDATA_85(1,31:P_CO2_TD[9]/100)
Call TESTDATA_85(1,32:P_CO2_TD[10]/100)
Call TESTDATA_85(1,32:P_CO2_TD[11]/100)
Call TESTDATA_85(1,32:P_CO2_TD[12]/100)

{Test data mass flow and compressor work}
Call TESTDATA_85(1,59:m_dot_CO2_TD)
Call TESTDATA_85(1,58:m_dot_w_TD)
Call TESTDATA_85(1,63:W_comp_TD)

{Temperature uncertainties}
Call TESTDATA_85(1,68:U_T_co2_i[1])
Call TESTDATA_85(1,69:U_T_co2_i[2])
Call TESTDATA_85(1,70:U_T_co2_i[3])
Call TESTDATA_85(1,71:U_T_co2_i[4])
Call TESTDATA_85(1,72:U_T_co2_i[5])
Call TESTDATA_85(1,73:U_T_co2_i[6])
Call TESTDATA_85(1,74:U_T_co2_i[7])
Call TESTDATA_85(1,75:U_T_co2_i[8])
Call TESTDATA_85(1,76:U_T_co2_i[9])
Call TESTDATA_85(1,77:U_T_co2_i[10])
Call TESTDATA_85(1,78:U_T_co2_i[11])
Call TESTDATA_85(1,79:U_T_co2_i[12])
Call TESTDATA_85(1,80:U_T_co2_o[12])

Call TESTDATA_85(1,93:U_T_w_i[1])
Call TESTDATA_85(1,92:U_T_w_i[2])
Call TESTDATA_85(1,91:U_T_w_i[3])
Call TESTDATA_85(1,90:U_T_w_i[4])
Call TESTDATA_85(1,89:U_T_w_i[5])
Call TESTDATA_85(1,88:U_T_w_i[6])
Call TESTDATA_85(1,87:U_T_w_i[7])
Call TESTDATA_85(1,86:U_T_w_i[8])

```
 Call TESTDATA_85(1,85:U_T_w_i[9])
Call TESTDATA_85(1,84:U_T_w_i[10])
Call TESTDATA_85(1,83:U_T_w_i[11])
Call TESTDATA_85(1,82:U_T_w_i[12])
Call TESTDATA_85(1,81:U_T_w_o[12])

Duplicate n =1,12
    T_w_i_TD[n] = T_w_TD[n]
    T_w_o_TD[n] = T_w_TD[n-1]
    T_w_gem_TD[n] = (T_w_i_TD[n] + T_w_o_TD[n])/2
    P_w_gem_TD[n] = 250
end

"================================================================="
"Input Parameters"
    m_dot_w = m_dot_w_td
    m_dot_CO2 = m_dot_co2_td
    G_dot_co2 = m_dot_co2/A_inner
    "1/2`` ID inner pipe & 1`` ID outer pipe"
    ID_inner = 0.016                                    [m]
    ID_outer = 0.026035                                 [m]
    OD_inner = ID_inner + (2 * wall_inner)
    wall_inner =0.00275                                 [m]
    Epsilon_stainless = 1.5 * 10^(-6)
    T_co2_pc =37
    rho_co2_pc = density(r744,T=T_co2_pc,P=P_co2_i_TD[1])
    "Calculate hydaulic diameter for annular area"
    Dh_annulus = ID_outer - OD_inner
    "Cross sectional area"
    A_annulus = (pi*(ID_outer/2)^2) - (pi*(OD_inner/2)^2)
    A_inner = pi*(ID_inner/2)^2
    "Relative roughness"
    RR_inner = epsilon_stainless / ID_inner
    RR_outer = epsilon_stainless / ID_outer
    "Surface area of pipe"
    A_w = pi*L*OD_inner
    A_CO2 = pi*L*ID_inner
    L = 2
    Length[0] = 0

"=======================Loop================================="
Duplicate n = 1, 12
length[n] = Length[n-1] + L

"Input values"
    T_CO2_i_TH[n] = T_CO2_i_TD[n]
    T_w_i_TH[n] = T_w_i_TD[n]
    P_CO2_i_TH[n] = P_CO2_i_TD[n]
    P_w_i_TH[n] = 250
    T_CO2_o_TH[n] = T_CO2_o_td[n]
    T_w_o_TH[n] = T_w_o_td[n]
    P_CO2_o_TH[n] = P_CO2_i_td[n]
    P_w_o_TH[n] = P_w_i_TH[n]
"Average values"
    T_CO2_gem_TH[n] = (T_co2_i_TH[n] + T_co2_o_TH[n])/2
    T_w_gem_TH[n] = (T_w_i_TH[n] + T_w_o_TH[n])/2
    P_CO2_gem_TH[n] = (P_co2_i_TH[n] + P_co2_o_TH[n])/2
    P_w_gem_TH[n] = (P_w_i_TH[n] + P_w_o_TH[n])/2

" Water side"
```

```
"Fluid properties"
    cp_w_TH[n] =Cp(Water,T=T_w_gem_TH[n],P=P_w_gem_TH[n])
    k_w_TH[n] =Conductivity(Water,T=T_w_gem_TH[n],P=P_w_gem_TH[n])/1000
    Re_w_TH[n] = (rho_w_TH[n] * v_w_TH[n] * dh_annulus)/mu_w_TH[n]
    rho_w_TH[n] =Density(Water,T=T_w_gem_TH[n],P=P_w_gem_TH[n])
    v_w_TH[n] = m_dot_w/(rho_w_TH[n] * A_annulus)
    mu_w_TH[n] =Viscosity(Water,T= T_w_gem_TH[n],P=P_w_gem_TH[n])
    Pr_w_TH[n] = Prandtl(water,T=T_w_gem_TH[n],P=P_w_gem_TH[n])
"Co2"
"Fluid properties"
    cp_CO2_TH[n] = Cp(R744, T=T_CO2_gem_TH[n], P=P_CO2_gem_TH[n])
    k_CO2_TH[n] = Conductivity(R744,T=T_CO2_gem_TH[n],P=P_CO2_gem_TH[n])/1000
    Re_CO2_TH[n] = (rho_CO2_TH[n] * v_CO2_TH[n] * ID_inner)/mu_CO2_TH[n]
    Pr_CO2_TH[n] = Prandtl(R744, T = T_CO2_gem_TH[n], P = P_CO2_gem_TH[n])
    rho_CO2_TH[n] =Density(R744,T=T_CO2_gem_TH[n],P=P_CO2_gem_TH[n])
    v_Co2_TH[n]  = m_dot_co2/(rho_co2_TH[n] * A_inner)
    mu_CO2_TH[n] = Viscosity(R744,T=T_CO2_gem_TH[n], P = P_CO2_gem_TH[n])
    Nu_CO2_TH[n] = h_co2_th[n]*ID_inner/k_CO2_TH[n]
    Nu_co2_TH[n] = 0.023 * Re_CO2_TH[n]^(4/5) * Pr_CO2_TH[n]^(0.3)

    Gr_co2_th[n] = (9.81*(ID_inner^3)*rho_CO2_TH[n]*(rho_co2_w_th[n] - rho_CO2_TH[n]))/(mu_co2_th[n]^2)
    GRRe_verh[n] = Gr_co2_th[n] / (Re_co2_th[n]^2)
    q_th_flux[n] = q_th[n] /A_CO2

    rho_co2_w_TH[n] = Density(R744,T=T_CO2_w_TH[n],P=P_CO2_gem_TH[n])
    cp_CO2_w_TH[n] = Cp(R744,T=T_CO2_w_TH[n], P = P_co2_gem_TH[n])
    mu_CO2_w_TH[n] = Viscosity(R744,T=T_CO2_w_TH[n], P = P_CO2_gem_TH[n])
    k_CO2_w_TH[n] = Conductivity(R744,T=T_CO2_w_TH[n],P=P_CO2_gem_TH[n])/1000
    Re_CO2_w_TH[n] = (rho_CO2_w_TH[n] * v_CO2_TH[n] * ID_inner)/mu_CO2_w_TH[n]
    Pr_CO2_w_TH[n] = Prandtl(R744, T = T_CO2_w_TH[n], P = P_CO2_gem_TH[n])

    cpint_co2_TH[n] = (h_enth_co2_TH[n] - h_enth_co2_w_TH[n])/(T_co2_gem_TH[n] - T_co2_w_TH[n])
    k_co2_f_TH[n] = Conductivity(R744,T=T_CO2_w_TH[n],P=P_CO2_gem_TH[n])/1000
    rho_CO2_f_TH[n] = density(R744, T=t_co2_f_TH[n], P=P_co2_gem_TH[n])
    Re_co2_f_TH[n] = (rho_CO2_f_TH[n] * v_CO2_TH[n] * ID_inner)/mu_CO2_f_TH[n]
    T_co2_f_TH[n] = (T_co2_w_TH[n] + T_co2_gem_TH[n])/2
    h_enth_co2_TH[n] = enthalpy(r744,T=T_co2_gem_TH[n],P=P_co2_gem_TH[n])
    h_enth_co2_w_TH[n] = enthalpy(r744,T=T_co2_w_TH[n],P=P_co2_gem_TH[n])
     cv_CO2_TH[n] =Cv(R744,T=T_CO2_gem_TH[n], P = P_co2_gem_TH[n])
    mu_CO2_f_TH[n]=Viscosity(R744,T=T_CO2_f_TH[n], P = P_CO2_gem_TH[n])
    h_enth_co2_in_TH[n] = enthalpy(r744,T=t_co2_i_TH[n],P=P_co2_i_TH[n])
    h_enth_co2_out_TH[n] = enthalpy(r744,T=t_co2_o_TH[n],P=P_co2_o_TH[n])
    cpmean_co2_TH[n] = (h_enth_co2_in_TH[n] - h_enth_co2_out_TH[n])/(T_co2_i_TH[n]  - T_co2_o_TH[n])
    f_f_TH[n] = (1.82*log10(Re_co2_TH[n]) - 1.64)^(-2)
    f_f_f_TH[n] = (1.82*log10(Re_co2_f_TH[n]) - 1.64)^(-2)
    f_f_w_TH[n] = (1.82*log10(Re_co2_w_TH[n]) - 1.64)^(-2)

"Calculate stainless steel properties"
    k_stainless_TH[n] =k_('Stainless_AISI304', T_pipe_TH[n])/1000
    T_pipe_TH[n] = (T_w_gem_TH[n] + T_CO2_gem_TH[n])/2

"Calculate wall temperature of CO2"
    q_TH[n] = (T_co2_gem_TH[n] - T_co2_w_TH[n])/(1/(pi*ID_inner*L*h_co2_TH[n]))
"Calculate heat transfer"
    q_TH[n] = m_dot_CO2*cp_co2_TH[n]*(T_CO2_i_TH[n] - T_CO2_o_TH[n])
"Dittus-Boelter CO2 side"
    Nu_CO2_DB[n] = 0.023 * Re_CO2_TH[n]^(4/5) * Pr_CO2_TH[n]^(0.3)
"Son and Park"
    Call Nu_SP(rho_co2_TH[n], rho_co2_w_TH[n],Re_Co2_TH[n],
    Pr_co2_TH[n],Cp_co2_TH[n],Cp_co2_w_TH[n],T_co2_gem_TH[n],T_co2_pc:Nu_co2_sp[n])
```

```
"Yoon"
    call
    Nu_YN(Re_co2_TH[n],Pr_co2_TH[n],rho_co2_TH[n],rho_co2_pc,T_co2_gem_TH[n],T_co2_pc:nu_co2_yn[n])
"Oh & Son"
    Call
    Nu_OS(Re_CO2_TH[n],Pr_Co2_TH[n],rho_co2_TH[n],rho_co2_w_TH[n],Cp_CO2_TH[n],CP_CO2_w_TH[n],T_c
    o2_gem_TH[n],T_co2_pc: Nu_co2_os[n])
"Gnielinski"
    Nu_CO2_GN[n] = (f_f_TH[n]/8)*(Re_Co2_TH[n]
    )*(Pr_co2_TH[n])*(1.07+12.7*sqrt(f_f_TH[n]/8)*(Pr_co2_TH[n]^(2/3)-1))^(-1)
"Pitla"
    Nu_CO2_PLA[n] =((Nu_gn_w[n] + Nu_gn[n])/2)*(k_co2_w_TH[n]/k_co2_TH[n])
    Nu_GN_w[n] = (f_f_w_TH[n]/8)*(Re_Co2_w_TH[n] -
    1000)*(Pr_co2_w_TH[n])*(1.07+12.7*sqrt(f_f_w_TH[n]/8)*(Pr_co2_w_TH[n]^(2/3)-1))^(-1)
    Nu_GN[n] = (f_f_TH[n]/8)*(Re_Co2_TH[n] -
    1000)*(Pr_co2_TH[n])*(1.07+12.7*sqrt(f_f_TH[n]/8)*(Pr_co2_TH[n]^(2/3)-1))^(-1)

"Dang and Hihara"
    Call Nu_DH
    (f_f_f_TH[n],Re_co2_TH[n],cp_co2_TH[n],mu_co2_TH[n],k_co2_TH[n],cpint_co2_TH[n],mu_co2_f_TH[n],k_co2
    _f_TH[n]:nu_co2_dh[n])
"Zhao & Jiang"
    call
    nu_ZJ(f_f_TH[n],Re_co2_TH[n],Pr_co2_TH[n],Pr_co2_w_TH[n],ID_inner,L,T_co2_gem_TH[n],T_co2_pc,cpmean
    _co2_TH[n],cp_co2_TH[n],rho_co2_TH[n],rho_co2_w_TH[n],T_co2_w_TH[n]:nu_co2_ZJ[n])

    $export filename$ T_co2_i_TH[n], T_co2_i_TH[1..12]
    $export /A filename$ T_co2_o_TH[n], T_co2_o_TH[1..12]
    $export /A filename$ T_co2_gem_TH[n], T_co2_gem_TH[1..12]
    $export /A filename$ T_w_i_TH[n], T_w_i_TH[1..12]
    $export /A filename$ T_w_o_TH[n], T_w_o_TH[1..12]
    $export /A filename$ T_w_gem_TH[n], T_w_gem_TH[1..12]
    $export /A filename$ q_TH[n], q_TH[1..12]
    $export /A filename$ Nu_CO2_DB[n], Nu_CO2_DB[1..12]
    $export /A filename$ Nu_CO2_SP[n], Nu_CO2_SP[1..12]
    $export /A filename$ Nu_CO2_YN[n], Nu_CO2_YN[1..12]
    $export /A filename$ Nu_CO2_OS[n], Nu_CO2_OS[1..12]
    $export /A filename$ Nu_CO2_GN[n], Nu_CO2_GN[1..12]
    $export /A filename$ Nu_CO2_PLA[n], Nu_CO2_PLA[1..12]
    $export /A filename$ Nu_CO2_DH[n], Nu_CO2_DH[1..12]
    $export /A filename$ Nu_CO2_ZJ[n], Nu_CO2_ZJ[1..12]
end {Duplicate}

"====================-======TEST DATA============================="
"======================Calculate Test data Nu values======================"
Duplicate n = 1,12
"Put temperatures in right arrays"
    T_CO2_i_TD[n] = T_CO2_TD[n-1]
    T_CO2_o_TD[n] = T_CO2_TD[n]
    T_CO2_gem_TD[n] = (T_CO2_i_TD[n] + T_CO2_o_TD[n])/2
    P_CO2_i_TD[n] = P_CO2_TD[n-1]
    P_CO2_o_TD[n] = P_CO2_TD[n]
    P_co2_gem_TD[n] = (P_CO2_i_TD[n] + P_CO2_o_TD[n])/2

"LMTD"
    DELTA_TD1[n] = (T_CO2_o_td[n] - T_w_i_td[n])
    DELTA_TD2[n] = (T_CO2_i_td[n] - t_w_o_td[n])
    LMTD_TD[n] = (DELTA_TD1[n] - DELTA_TD2[n])/(ln(delta_td1[n]/delta_td2[n]))

"Fluid properties"
```

```
    mu_CO2_TD[n] = Viscosity(R744,T=T_co2_gem_TD[n], P = P_co2_gem_TD[n])
    cp_CO2_TD[n] = Cp(R744,T=T_co2_gem_TD[n], P = P_co2_gem_TD[n])
    k_co2_td[n]=  Conductivity(R744,T=T_co2_gem_TD[n], P = P_co2_gem_TD[n])/1000
    v_Co2_TD[n]  = m_dot_co2/(rho_co2_TD[n] * A_inner)
    Re_CO2_TD[n] = (rho_CO2_TD[n] * v_CO2_TD[n] * ID_inner)/mu_CO2_TD[n]
    Pr_CO2_TD[n] = Prandtl(R744, T = T_CO2_gem_TD[n], P = P_CO2_gem_TD[n])
    rho_CO2_TD[n] =Density(R744,T=T_CO2_gem_TD[n],P=P_CO2_gem_TD[n])

    k_w_TD[n] = Conductivity(Water,T=T_w_gem_TD[n],P=P_w_gem_TD[n])/1000
    cp_w_TD[n] = Cp(water, T=T_w_gem_TD[n], P = P_w_gem_TD[n])
    v_w_TD[n] = m_dot_w_TD/(rho_w_TD[n] * A_annulus)
    Re_w_TD[n] = (rho_w_TD[n] * v_w_TD[n] * dh_annulus)/mu_w_TD[n]
    rho_w_TD[n] =Density(Water,T=T_w_gem_TD[n],P=P_w_gem_TD[n])
    mu_w_TD[n] =Viscosity(Water,T= T_w_gem_TD[n],P=P_w_gem_TD[n])
    Pr_w_TD[n]= Prandtl(Water,T= T_w_gem_TD[n],P=P_w_gem_TD[n])

    f_f_td[n] = (1.82*log10(Re_w_td[n]) - 1.64)^(-2)
    k_stainless_TD[n] = k_('Stainless_AISI304', T_stainless_TD[n])/1000
    T_stainless_TD[n] = (T_CO2_gem_TD[n] + T_w_gem_TD[n])/2
end

Duplicate n =1, 12
    h_ent_co2_i_TD[n] = enthalpy(R744, T=T_CO2_i_TD[n],P=P_CO2_i_TD[n])
    h_ent_co2_o_TD[n] = enthalpy(R744, T=T_CO2_o_TD[n],P=P_CO2_o_TD[n])
    h_ent_w_i_td[n] = enthalpy(water,T=t_w_i_td[n],P=P_w_gem_TD[n])
    h_ent_w_o_td[n] = enthalpy(water,T=t_w_o_td[n],P=P_w_gem_TD[n])
end

Duplicate n =1, 12
"Calculate Q, UA, Convection coeffisient etc"
    Q_CO2_TD[n] = m_dot_CO2_TD*( h_ent_CO2_i_TD[n] - h_ent_co2_o_TD[n])
    Q_CO2_TD[n] = UA_TD[n]*LMTD_td[n]_
    1/UA_TD[n] = 1/(h_w_td[n]*A_w) + (ln(OD_inner/ID_inner))/(2*pi*k_stainless_td[n]*L) +
    1/(h_co2_td[n]*A_CO2)
    Nu_w_TD[n] = (h_w_TD[n] *Dh_annulus) / k_w_TD[n]
    Nu_w_TD[n] = 0.023*(Re_w_TD[n])^(0.82)*Pr_w_TD[n]^0.4
    {Nu_w_td[n] = (f_f_td[n]/8)*(Re_w_td[n]-1000 )*(Pr_w_td[n])*(1+12.7*sqrt(f_f_td[n]/8)*(Pr_w_td[n]^(2/3)-1))^(-
1)}"Gnielinski Correlation"
    Nu_co2_TD[n] = h_co2_td[n]*ID_inner/k_co2_td[n]

    $export /A filename$ q_co2_TD[n], q_co2_TD[1..12]
    $export /A filename$ Nu_w_TD[n], Nu_w_TD[1..12]
    $export /A filename$ Nu_co2_TD[n], Nu_co2_TD[1..12]

“Energy Balance”
    Q_w_TD[n] = m_dot_w_TD*( h_ent_w_o_TD[n] - h_ent_w_i_TD[n])
    Q_%_Loss[n] = ((Q_co2_td[n] - Q_w_TD[n])/Q_CO2_TD[n])*100

end
    Q_w_TD = m_dot_w_TD*( h_ent_w_o_TD[1] - h_ent_w_i_TD[12])
    Q_CO2_TD = m_dot_co2_TD*( h_ent_co2_i_TD[1] - h_ent_co2_o_TD[12])
    Q_total_%_loss=((Q_co2_TD-Q_w_TD)/(Q_CO2_TD)) *100

{============================Uncertainty analysis==============================}
{=================calculate the uncertainty of measured variables=====================}
duplicate n = 1,11
"uncertainties of measured temps"
    U_T_co2_o[n] =U_T_co2_i[n+1]
    U_T_w_o[n] = U_T_w_i[n+1]
end
```

```
duplicate n = 1,12
    U_T_co2_gem[n] = (U_T_co2_o[n] +U_T_co2_i[n])/2
    U_T_w_gem[n] = (U_T_w_o[n] +U_T_w_i[n])/2
    U_T_stainless[n] = (0.3 +(0.005*T_stainless_TD[n]))/sqrt(3)

"uncertainties of measured pressures"
    U_P_co2_i[n] =( 0.003*P_co2_i_td[n])/sqrt(3)
    U_P_co2_o[n] = (0.003*P_co2_o_td[n])/sqrt(3)
    U_P_co2_gem[n] = (0.003*P_co2_gem_td[n])/sqrt(3)
end

"uncertainties of measured mass flow"
    U_m_dot_co2_TD= (0.0005*m_dot_co2_td)/sqrt(3)
    U_m_dot_w_TD = (0.0005*m_dot_w_td)/sqrt(3)

“============Calc Partial derivitives using pertatation analysis=================”
"note: values were exported just for convenient use in excel at later stage"
Duplicate n =1, 12
"Partial derivitives:k_co2"
    k_co2_td1[n]=  Conductivity(R744,T=T_co2_gem_TD[n]+0.5, P = P_co2_gem_TD[n])/1000
    k_co2_td2[n]=  Conductivity(R744,T=T_co2_gem_TD[n]-0.5, P = P_co2_gem_TD[n])/1000
    dk_co2_dt_co2[n] = (k_co2_td1[n]-k_co2_td2[n])

    k_co2_td3[n]=  Conductivity(R744,T=T_co2_gem_TD[n], P = P_co2_gem_TD[n]+0.5)/1000
    k_co2_td4[n]=  Conductivity(R744,T=T_co2_gem_TD[n], P = P_co2_gem_TD[n]-0.5)/1000
    dk_co2_dp_co2[n] = (k_co2_td3[n]-k_co2_td4[n])

"Partial derivitives: k_stainless"
    k_stainless_TD1[n] = k_('Stainless_AISI304', T_stainless_TD[n]+0.5)/1000
    k_stainless_TD2[n] = k_('Stainless_AISI304', T_stainless_TD[n]-0.5)/1000
    dk_stainless_dt_stainless[n] = (k_stainless_td1[n]-k_stainless_td2[n])

"Partial derivitives: Pr_water"
    Pr_w_TD1[n]= Prandtl(Water,T= T_w_gem_TD[n]+0.5,P=P_w_gem_TD[n])
    Pr_w_TD2[n]= Prandtl(Water,T= T_w_gem_TD[n]-0.5,P=P_w_gem_TD[n])
    dpr_w_dt_w[n]=Pr_w_TD1[n]-Pr_w_TD2[n]

"Partial derivitives:mu_w"
    mu_w_TD1[n] =Viscosity(Water,T= T_w_gem_TD[n]+0.5,P=P_w_gem_TD[n])
    mu_w_TD2[n] =Viscosity(Water,T= T_w_gem_TD[n]-0.5,P=P_w_gem_TD[n])
    dmu_w_dt_w[n] = mu_w_td1[n] - mu_w_td2[n]

"Partial derivitives: k_water"
    k_w_TD1[n] = Conductivity(Water,T=T_w_gem_TD[n]+0.5,P=P_w_gem_TD[n])/1000
    k_w_TD2[n] = Conductivity(Water,T=T_w_gem_TD[n]-0.5,P=P_w_gem_TD[n])/1000
    dk_w_dt_w[n] = (k_w_td1[n]-k_w_td2[n])

"Partial derivitives: enthalpy CO2 inlet "
    h_ent_co2_i_TD1[n] = enthalpy(R744, T=T_CO2_i_TD[n]+0.5,P=P_CO2_i_TD[n])
    h_ent_co2_i_TD2[n] = enthalpy(R744, T=T_CO2_i_TD[n]-0.5,P=P_CO2_i_TD[n])
    dh_ent_co2_i_dt_co2_i[n] = h_ent_co2_i_td1[n]-h_ent_co2_i_td2[n]

    h_ent_co2_i_TD3[n] = enthalpy(R744, T=T_CO2_i_TD[n],P=P_CO2_i_TD[n]+0.5)
    h_ent_co2_i_TD4[n] = enthalpy(R744, T=T_CO2_i_TD[n],P=P_CO2_i_TD[n]-0.5)
    dh_ent_co2_i_dp_co2_i[n] = h_ent_co2_i_td3[n]-h_ent_co2_i_td4[n]

"Partial derivitives: enthalpy CO2 outlet "
    h_ent_co2_o_TD1[n] = enthalpy(R744, T=T_CO2_o_TD[n]+0.5,P=P_CO2_o_TD[n])
    h_ent_co2_o_TD2[n] = enthalpy(R744, T=T_CO2_o_TD[n]-0.5,P=P_CO2_o_TD[n])
```

```
    dh_ent_co2_o_dt_co2_o[n] = h_ent_co2_o_td1[n]-h_ent_co2_o_td2[n]

    h_ent_co2_o_TD3[n] = enthalpy(R744, T=T_CO2_o_TD[n],P=P_CO2_o_TD[n]+0.5)
    h_ent_co2_o_TD4[n] = enthalpy(R744, T=T_CO2_o_TD[n],P=P_CO2_o_TD[n]-0.5)
    dh_ent_co2_o_dp_co2_o[n] = h_ent_co2_o_td3[n]-h_ent_co2_o_td4[n]

"Partial derivitives: dUA_dT( )"
    UA_T_co2_i_1[n] =  m_dot_co2_TD*( h_ent_CO2_i_TD[n] - h_ent_co2_o_TD[n] )*ln((T_CO2_o_td[n] -
    T_w_i_td[n])/((T_CO2_i_td[n]+0.5) - t_w_o_td[n]))/((T_CO2_o_td[n] - T_w_i_td[n])-((T_CO2_i_td[n]+0.5) -
    t_w_o_td[n]))
    UA_T_co2_i_2[n] =  m_dot_co2_TD*( h_ent_CO2_i_TD[n] - h_ent_co2_o_TD[n] )*ln((T_CO2_o_td[n] -
    T_w_i_td[n])/((T_CO2_i_td[n]-0.5) - t_w_o_td[n]))/((T_CO2_o_td[n] - T_w_i_td[n])-((T_CO2_i_td[n]-0.5) -
    t_w_o_td[n]))
    dUA_dT_co2_i_pert[n] = UA_T_co2_i_1[n]-UA_T_co2_i_2[n]

    UA_T_co2_o_1[n] =  m_dot_co2_TD*( h_ent_CO2_i_TD[n] - h_ent_co2_o_TD[n] )*ln(((T_CO2_o_td[n]+0.5) -
    T_w_i_td[n])/(T_CO2_i_td[n] - t_w_o_td[n]))/(((T_CO2_o_td[n]+0.5) - T_w_i_td[n])-(T_CO2_i_td[n] -
    t_w_o_td[n]))
    UA_T_co2_o_2[n] =  m_dot_co2_TD*( h_ent_CO2_i_TD[n] - h_ent_co2_o_TD[n] )*ln(((T_CO2_o_td[n]-0.5) -
    T_w_i_td[n])/(T_CO2_i_td[n] - t_w_o_td[n]))/(((T_CO2_o_td[n]-0.5) - T_w_i_td[n])-(T_CO2_i_td[n] -
    t_w_o_td[n]))
    dUA_dT_co2_o_pert[n] = UA_T_co2_o_1[n]-UA_T_co2_o_2[n]

    UA_T_w_i_1[n] =  m_dot_co2_TD*( h_ent_CO2_i_TD[n] - h_ent_co2_o_TD[n] )*ln((T_CO2_o_td[n] -
    (T_w_i_td[n]+0.5))/(T_CO2_i_td[n] - t_w_o_td[n]))/((T_CO2_o_td[n] - (T_w_i_td[n]+0.5))-(T_CO2_i_td[n] -
    t_w_o_td[n]))
    UA_T_w_i_2[n] =  m_dot_co2_TD*( h_ent_CO2_i_TD[n] - h_ent_co2_o_TD[n] )*ln((T_CO2_o_td[n] -
    (T_w_i_td[n]-0.5))/(T_CO2_i_td[n] - t_w_o_td[n]))/((T_CO2_o_td[n] - (T_w_i_td[n]-0.5))-(T_CO2_i_td[n] -
    t_w_o_td[n]))
    dUA_dT_w_i_pert[n] = UA_T_w_i_1[n]-UA_T_w_i_2[n]

    UA_T_w_o_1[n] =  m_dot_co2_TD*( h_ent_CO2_i_TD[n] - h_ent_co2_o_TD[n] )*ln((T_CO2_o_td[n] -
    T_w_i_td[n])/(T_CO2_i_td[n] - (t_w_o_td[n]+0.5)))/((T_CO2_o_td[n] - T_w_i_td[n])-(T_CO2_i_td[n] -
    (t_w_o_td[n]+0.5)))
    UA_T_w_o_2[n] =  m_dot_co2_TD*( h_ent_CO2_i_TD[n] - h_ent_co2_o_TD[n] )*ln((T_CO2_o_td[n] -
    T_w_i_td[n])/(T_CO2_i_td[n] - (t_w_o_td[n]-0.5)))/((T_CO2_o_td[n] - T_w_i_td[n])-(T_CO2_i_td[n] -
    (t_w_o_td[n]-0.5)))
    dUA_dT_w_o_pert[n] = UA_T_w_o_1[n]-UA_T_w_o_2[n]

"Partial derivitive: dNu_co2_dh_co2"
    Nu_co2_TD1[n] = (h_co2_td[n]+h_co2_td[n]/100)*ID_inner/k_co2_td[n]
    Nu_co2_TD2[n] = (h_co2_td[n]-h_co2_td[n]/100)*ID_inner/k_co2_td[n]
    dNu_co2_dh_co2[n] =(Nu_co2_TD1[n]-Nu_co2_TD2[n])/(( h_co2_td[n]+h_co2_td[n]/100)-(h_co2_td[n]-
    h_co2_td[n]/100))
    dNu_co2_dk_co2[n] = h_co2_td[n]*ID_inner/k_co2_td[n]^2

end

"Calc Partial derivitives analytically and implement in Uncertainty propagation where applicable"
Duplicate n =1, 12
"U(Nu_co2) and derivitives"
    U_Nu[n] = sqrt((dNu_co2_dh_co2[n]*u_h_co2[n])^2 + (dNu_co2_dk_co2[n]*U_k_co2[n])^2
"U(k_co2)"
    U_k_co2[n] = sqrt((dk_co2_dt_co2[n]*U_T_co2_gem[n])^2 + (dk_co2_dp_co2[n]*U_P_co2_gem[n])^2)

"U(h_co2) and derivitives"
    U_h_co2[n] = sqrt((dh_co2_dh_w[n]*U_h_w[n])^2 + (dh_co2_dUA[n]*U_UA_pert[n])^2 +
    (dh_co2_dk_stainless[n]*U_k_stainless[n])^2)
    dh_co2_dh_w[n] = -(A_w/A_co2)
    dh_co2_dUA[n]=-1/A_co2
```

```
    dh_co2_dk_stainless[n]= -(ln(OD_inner/ID_inner))/(2*pi*L*k_stainless_TD[n] ^2)

"U(k_stainless)"
    u_k_stainless[n] = dk_stainless_dt_stainless[n] * U_T_stainless[n]

"U(h_w) and derivatives"
    U_h_w[n] = sqrt((dh_w_dPr_w[n]*u_Pr_w[n])^2 + (dh_w_dmu_w[n]*u_mu_w[n])^2
    +(dh_w_dk_w[n]*u_k_w[n])^2 + (dh_w_dm_w[n]*U_m_dot_w_TD)^2)
    dh_w_dPr_w[n]=(0.4/Dh_annulus)*(0.023*((m_dot_w_TD*Dh_annulus/(A_annulus*mu_w_TD[n]))^0.82) *
    k_w_td[n]*Pr_w_TD[n]^(-0.6))
    dh_w_dmu_w[n]=(-
    0.82)*(0.023)*(m_dot_w_td^0.82)*(dh_annulus^0.82)*(Pr_w_td[n]^0.4)*k_w_td[n]*(A_annulus^(-
    0.82))*dh_annulus^(-1)*mu_w_td[n]^(-1.82)
    dh_w_dk_w[n] = (0.023*(m_dot_w_td*dh_annulus/(A_annulus*mu_w_td[n]))^(0.82)*Pr_w_td[n]^0.4)/dh_annulus
    dh_w_dm_w[n] = (0.023*dh_annulus^0.82*Pr_w_td[n]^0.4*k_w_td[n]*0.82*m_dot_w_td^(-
    0.18))/(A_annulus^0.82*mu_w_td[n]^0.82*dh_annulus)

"U(Pr_w)"
    U_Pr_w[n] = dpr_w_dt_w[n]*U_T_w_gem[n]
"U(mu_w)"
    U_mu_w[n] = dmu_w_dt_w[n]*U_T_w_gem[n]
"U(k_w)"
    u_k_w[n] = dk_w_dt_w[n]*U_T_w_gem[n]

"U(UA) and derivatives"
    U_UA_pert[n] = sqrt((dUA_dm_dot_co2[n]*u_m_dot_co2_TD)^2 +
    (dUA_dh_ent_co2_i[n]*u_h_ent_co2_i[n])^2+(dUA_dh_ent_co2_o[n]*u_h_ent_co2_o[n])^2+(dUA_dT_co2_i_pert[
    n]*U_T_Co2_i[n])^2+(dUA_dT_co2_o_pert[n]*U_T_Co2_o[n])^2+(dUA_dT_w_i_pert[n]*U_T_w_i[n])^2+(dUA_
    dT_w_o_pert[n]*U_T_w_o[n])^2)

    dUA_dm_dot_co2[n] = (h_ent_co2_i_td[n] - h_ent_co2_o_td[n])/  ((T_co2_o_td[n] - T_w_i_TD[n] - T_co2_i_td[n]
    + T_w_o_TD[n])/ln((T_co2_o_td[n] - T_w_i_TD[n])/( T_co2_i_td[n] - T_w_o_TD[n] )) )

    dUA_dh_ent_co2_i[n] = m_dot_co2_TD / ((T_co2_o_td[n] - T_w_i_TD[n] - T_co2_i_td[n] +
    T_w_o_TD[n])/ln((T_co2_o_td[n] - T_w_i_TD[n])/( T_co2_i_td[n] - T_w_o_TD[n] )))
    dUA_dh_ent_co2_o[n] = -m_dot_co2_TD /  ((T_co2_o_td[n] - T_w_i_TD[n] - T_co2_i_td[n] +
    T_w_o_TD[n])/ln((T_co2_o_td[n] - T_w_i_TD[n])/( T_co2_i_td[n] - T_w_o_TD[n] )))

“========Q uncertainty=========”
"U(h_ent_CO2)"
    u_h_ent_co2_i[n] = sqrt((dh_ent_co2_i_dt_co2_i[n]*U_T_co2_gem[n])^2 +
    (dh_ent_co2_i_dP_co2_i[n]*U_P_co2_gem[n])^2)
    u_h_ent_co2_o[n] = sqrt((dh_ent_co2_o_dt_co2_o[n]*U_T_co2_gem[n])^2 +
    (dh_ent_co2_o_dP_co2_o[n]*U_P_co2_gem[n])^2)

"U(Q)"
    U_Q[n] = sqrt((dQ_dh_ent_o[n]*U_h_ent_co2_o[n])^2 + (dQ_dm_co2[n]*U_m_dot_co2_TD)^2 +
    (dQ_dh_ent_co2_i[n]*U_h_ent_co2_i[n])^2)
    dQ_dh_ent_o[n]=m_dot_co2_
    dQ_dh_ent_co2_i[n]=-m_dot_co2
    dQ_dm_co2[n]=(h_ent_co2_o_TD[n] - h_ent_co2_i_TD[n])

"% uncertainty of Nu"
    Uncertainty_%_Nu_TD[n] = (U_nu[n]/Nu_co2_td[n])*100
    $export /A filename$ U_Nu[n], U_Nu[1..12]
    $export /A filename$ Uncertainty_%_Nu_TD[n], Uncertainty_%_Nu_TD[1..12]
    $export /A filename$ Re_CO2_TD[n], Re_CO2_TD[1..12]
    $export /A filename$ Pr_CO2_TD[n], Pr_CO2_TD[1..12]
    $export /A filename$ Q_total%_loss, Q_total_%_loss
    $export /A filename$ Q_co2_TD1, Q_co2_TD
```

```
    $export /A filename$ Q_w_TD1, Q_w_TD
    $export /A filename$ G_flux_co2, G_dot_co2
    $export /A filename$ T_PC, T_co2_PC
    $export /A filename$ U_Q, U_Q[1..12]
    $export /A filename$ U_Q_CO2_tot U_Q_co2
    $export /A filename$ U_Q_w_tot U_Q_w
    $export /A filename$ P_CO2_TD[n], P_CO2_TD[1..12]
    $export /A filename$ U_P_co2_TD[n], U_P_co2_gem[1..12]
    $export /A filename$ Gr_co2_TH[n], Gr_co2_TH[1..12]
    $export /A filename$ GrRe_verh[n], GrRe_verh[1..12]
    $export /A filename$ q_th_flux[n], q_th_flux[1..12]
End

{======== Q uncertainty (outside loop)==============}
    U_Q_co2 = sqrt((dQ_co2_dh_ent_o*U_h_ent_co2_o)^2 + (dQ_co2_dm_co2*U_m_dot_co2_TD)^2 +
    (dQ_co2_dh_ent_co2_i*U_h_ent_co2_i)^2)

    dQ_co2_dh_ent_o = m_dot_co2
    u_h_ent_co2_o = sqrt((dh_ent_co2_o_dt_co2_o[12]*U_T_co2_gem[12])^2 +
    (dh_ent_co2_o_dP_co2_o[12]*U_P_co2_gem[12])^2)
    dQ_co2_dm_co2 = (h_ent_co2_o_td[12] - h_ent_co2_i_td[1])
    dQ_co2_dh_ent_co2_i = -m_dot_co2
    U_h_ent_co2_i = sqrt((dh_ent_co2_i_dt_co2_i[1]*U_T_co2_gem[1])^2 +
    (dh_ent_co2_i_dP_co2_i[1]*U_P_co2_gem[1])^2)

"U_Q_W_total"
    U_Q_w = sqrt((dQ_w_dh_ent_o*U_h_ent_w_o)^2 + (dQ_w_dm_w*U_m_dot_w_TD)^2 +
    (dQ_w_dh_ent_w_i*U_h_ent_w_i)^2)

    dQ_w_dh_ent_o = m_dot_w
    u_h_ent_w_o = sqrt((dh_ent_w_o_dt_w_o[1]*U_T_w_gem[1])^2 + (dh_ent_w_o_dP_w_o[1]*U_P_w_gem[1])^2)
    dQ_w_dm_w = (h_ent_w_o_td[12] - h_ent_w_i_td[1])
    dQ_w_dh_ent_w_i = -m_dot_w
    U_h_ent_w_i = sqrt((dh_ent_w_i_dt_w_i[12]*U_T_w_gem[12])^2 +
    (dh_ent_w_i_dP_w_i[12]*U_P_w_gem[12])^2)

"Partial derivitives: enthalpy W inlet "
    h_ent_w_i_TD1[12] = enthalpy(R744, T=T_W_i_TD[12]+0.5,P=P_W_i_TH[12])
    h_ent_w_i_TD2[12] = enthalpy(R744, T=T_W_i_TD[12]-0.5,P=P_W_i_TH[12])
    dh_ent_w_i_dt_w_i[12] = h_ent_w_i_td1[12]-h_ent_w_i_td2[12]

    h_ent_w_i_TD3[12] = enthalpy(R744, T=T_W_i_TD[12],P=P_W_i_TH[12]+0.5)
    h_ent_w_i_TD4[12] = enthalpy(R744, T=T_W_i_TD[12],P=P_W_i_TH[12]-0.5)
    dh_ent_w_i_dp_w_i[12] = h_ent_w_i_td3[12]-h_ent_w_i_td4[12]

"Partial derivitives: enthalpy W outlet "
    h_ent_w_o_TD1[1] = enthalpy(R744, T=T_W_o_TD[1]+0.5,P=P_W_o_TH[1])
    h_ent_w_o_TD2[1] = enthalpy(R744, T=T_W_o_TD[1]-0.5,P=P_W_o_TH[1])
    dh_ent_w_o_dt_w_o[1] = h_ent_w_o_td1[1]-h_ent_w_o_td2[1]

    h_ent_w_o_TD3[1] = enthalpy(R744, T=T_W_o_TD[1],P=P_W_o_TH[1]+0.5)
    h_ent_w_o_TD4[1] = enthalpy(R744, T=T_W_o_TD[1],P=P_W_o_TH[1]-0.5)
    dh_ent_w_o_dp_w_o[1] = h_ent_w_o_td3[1]-h_ent_w_o_td4[1]
    U_P_w_gem[12]=( 0.003*P_w_i_th[12])/sqrt(3)
    U_P_w_gem[1]=( 0.003*P_w_o_th[1])/sqrt(3)
```